MULTI-PORT DC-DC POWER CONVERTER

FOR

RENEWABLE ENERGY APPLICATION

A Thesis

by

HUNG-MING CHOU

Submitted to the Office of Graduate Studies of
Texas A&M University
in partial fulfillment of the requirements for the degree of

MASTER OF SCIENCE

August 2009

Major Subject: Electrical Engineering

MULTI-PORT DC-DC POWER CONVERTER

FOR

RENEWABLE ENERGY APPLICATION

A Thesis

by

HUNG-MING CHOU

Submitted to the Office of Graduate Studies of
Texas A&M University
in partial fulfillment of the requirements for the degree of

MASTER OF SCIENCE

Approved by:

Chair of Committee,   Mehrdad Ehsani
Committee Members,   Shankar Bhattacharyya
                                    Karen Butler-Purry
                                    Won-jong Kim
Head of Department,   Costas N. Georghiades

August 2009

Major Subject: Electrical Engineering

ABSTRACT

Multi-port DC-DC Power Converter

for Renewable Energy Application. (August 2009)

Hung-ming Chou, B.S., National Chiao Tung University

Chair of Advisory Committee: Dr. Mehrdad Ehsani

In recent years, there has been lots of emphasis put on the development of renewable energy. While considerable improvement on renewable energy has been made, there are some inherent limitations for these renewable energies. For example, for solar and wind power, there is an intermittent nature. For the fuel cell, the dynamics of electro-chemical reaction is quite slow compared to the electric load. This will not be acceptable for modern electric application, which requires constant voltage of constant frequency.

This work proposed and evaluated a new power circuit that can deal with the problem of the intermittent nature and slow response of the renewable energy.

The proposed circuit integrates different renewable energy sources as well as energy storage. By integrating renewable energy sources with statistical tendency to compensate each other, the effect of the intermittent nature can be greatly reduced. This integration will increase the reliability and utilization of the overall system. Moreover, the integration of energy storage solves the problem of the slow response of renewable energy. It can provide the extra energy required by load or absorb the excessive energy provided by the energy sources, greatly improving the dynamics of overall system.

To better understand the proposed circuit, "Dual Active Bridge" and "Triple Active Bridge" were reviewed first. The operation principles and the modeling were

presented. Analysis and design of the overall system were discussed. Controller design and stability issues were investigated. Furthermore, the function of the central controller was explained. In the end, different simulations were made and discussed.

Results from the simulations showed that the proposed multi-port DC-DC power converter had satisfactory performance under different scenarios encountered in practical renewable energy application. The proposed circuit is an effective solution to the problem due to the intermittent nature and slow response of the renewable energy.

To my beloved family

ACKNOWLEDGMENTS

I would like to express my sincerest appreciation to Dr. M. Ehsani for his inspiring guidance, constant encouragement, and stimulating suggestions throughout the course of my graduate studies. I also deeply appreciate the members of my committee, Dr. Shankar Bhattacharyya, Dr. Karen L. Butler-Purry, and Dr. Won-jong Kim for their valuable comments and interest in this project. My thanks are extended to the past and present lab members at Texas A&M University: Alex Skorcz, Hugo E. Mena, Billy Yancey, Guadalupe Gonzalez, Ronald Y. Barazarte, Ali Eskandari, Sriram Emani, and Richard Smith.

Without my family's sacrifice and support, this work would not have been possible. I would like to affirm my indebtedness to my parents, my younger sister, and my girl friend for their unconditional love, care, support, and encouragement.

TABLE OF CONTENTS

LIST OF TABLES

LIST OF FIGURES

FIGURE   Page

FIGURE   Page

CHAPTER I

INTRODUCTION

A.   Introduction

Due to the environmental problem, e.g., climate change, and political and eco-
nomical reasons, e.g., less dependence on the foreign energy import, high oil price,
renewable energy has attracted enormous attention. Investment worldwide in renew-
able energy has gone from below $10 billion in 1995 to over $70 billion in 2007 [1],
shown in Fig. 1. Since 2000, renewable electricity installations in the U.S., excluding
hydro power, have nearly doubled, and in 2007 there is 33 GW of installed capacity.
Wind power and solar power are the fastest growing renewable energy sectors. In
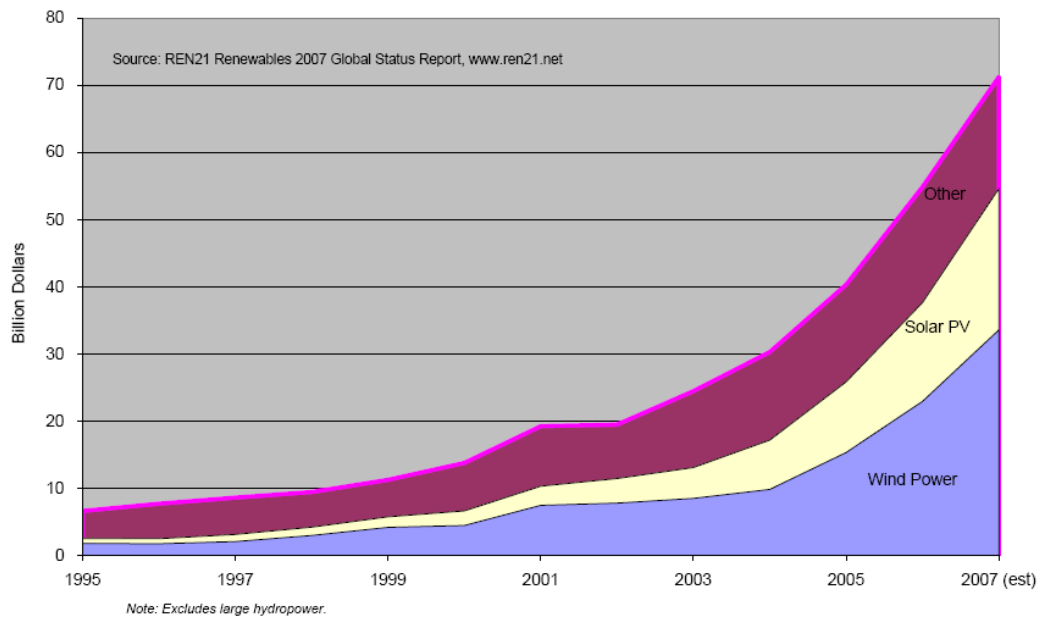
Fig. 1. Annual investment in new renewable energy capacity [1]

The journal model is *IEEE Transactions on Automatic Control.*

2007, wind capacity installations grew 45% and solar PV grew 40% from the previous year [2]. Fig. 2 shows the increase of renewable energy from 2000 to 2007.

	Hydro	Solar PV	CSP	Wind	Geothermal	Biomass	Advanced Water Power	Total (without Hydropower)	Total U.S.
2000	76,946 0%	139 18.8%	354 0%	2,578 2.6%	2,798 2.2%	10,676 2.6%	0 0%	16,545 -1.1%	93,491 -0.3%
2001	76,911 0%	168 20.9%	354 0%	4,275 65.8%	2,798 0%	10,576 0.9%	0 0%	18,171 9.8%	95,082 1.7%
2002	77,047 0.2%	212 26.5%	354 0%	4,686 9.6%	2,798 0%	10,867 2.8%	0 0%	18,917 4.1%	95,964 0.9%
2003	77,020 0%	275 29.7%	354 0%	6,353 35.6%	2,798 0%	10,856 0.1%	0 0%	20,636 9.1%	97,656 1.8%
2004	77,130 0.1%	365 32.7%	354 0%	6,725 5.9%	2,798 0%	11,034 1.6%	0 0%	21,276 3.1%	98,406 0.8%
2005	77,354 0.3%	479 31.2%	354 0%	9,121 35.6%	2,828 1.1%	11,222 1.7%	0 0%	24,004 12.8%	101,358 3.0%
2006	77,419 0.1%	624 30.3%	355 0.3%	11,575 26.9%	2,831 0.1%	11,554 3.0%	0 0%	26,939 12.2%	104,358 3.0%
2007	77,432 0%	874 40.1%	419 18%	16,818 45.3%	2,937 3.7%	11,738 1.6%	0 0%	32,786 21.7%	110,218 5.6%

− annual decrease   annual increase +

Fig. 2. Renewable electricity nameplate capacity(MW) and percent cumulative increase from previous year [2]

As great advance in renewable energy has been made, the price for electricity produced with renewable energy drops. The national average electricity price is about 10 cents per kWh. From Fig. 3, the price for certain kinds of renewable energy is lower than 10 cents per kWh [2]. As the cost of conventional energy resources is increasing every year, the receding trend in the cost of renewable technologies is encouraging, making renewable energy an economical means of power generation in the near future.

Renewable energy technologies not only can solve the climate change and reduce the dependence on foreign energy import, it is also suitable for distributed power generation. In remote areas, where there are no transmission lines or the cost of building new transmission lines is high, renewable energy can provide power without expensive and complicated grid infrastructure. Distributed power generation system
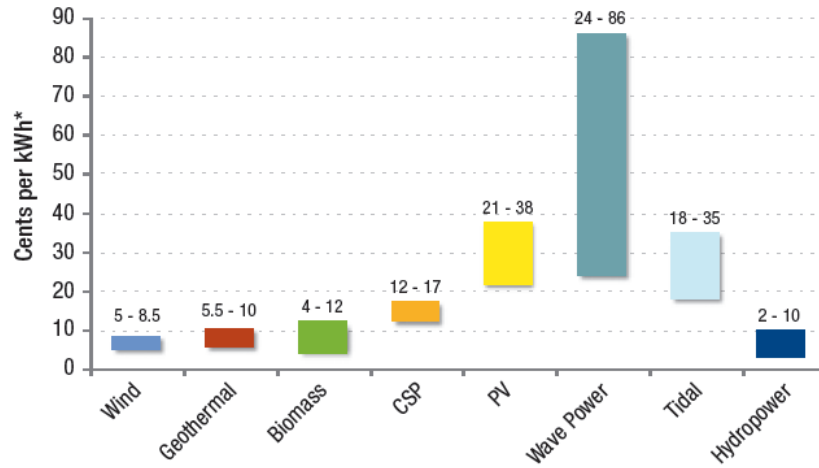
Fig. 3. Price range of renewable electricity by technology [2]

has several advantages [3].

- It can reduce or avoid the necessity to build new transmission/distribution lines or upgrade existing ones.

- It can be configured to meet peak power needs.

- It can diversify the energy sources and increase the reliability of the grid network.

- It can be configured to provide premium power, when coupled with uninterruptible power supply (UPS).

- It can be located close to the user and can be installed in small increments to match the load requirement of the customer.

B.   The Importance of Energy Storage

In spite of the advances made in renewable energy, there are some inherent problems. One is the intermittent nature. The output power from renewable energy sources is not constant. Another problem is slow response compared with electric load. Electric loads may change their power demand in very short time. However, it takes much longer time to change the output power from renewable energy sources.

A unique feature of renewable energy application is that renewable energy sources are operated in their optimal operating points. Since the cost of implementing renewable energy sources is high, it is desirable to get as much power as possible from the renewable energy sources. Maximum power points is tracked during the operation. Therefore, the power output from these sources tends to be constant, no matter how much the load power is. This concept is like hybrid vehicles. The engine, which provides power to a electric motor, is operated at its optimal operating point, no matter how much power the electric motor requires. The difference between the power coming from the engine and the power required by the motor is compensated by energy storage.

The following subsections will describe several examples and show the importance of energy storage in renewable energy applications.

1.   For Wind Power

Fig. 4 shows the characteristics of wind turbines for different wind speeds (v) [4]. The X-axis is the rotor speed of the wind turbine, while the Y-axis is the power extracted by the wind turbine. It can be seen that for a given wind speed, there is one operating point, where the power output is maximum. For example, if the wind speed is v_1, the rotor speed of the wind turbine is controlled to be ω_1 so that the power

from the wind turbine is maximum. This is the optimal operating point at which the wind turbine is controlled to operate. This is called maximum power tracking. There
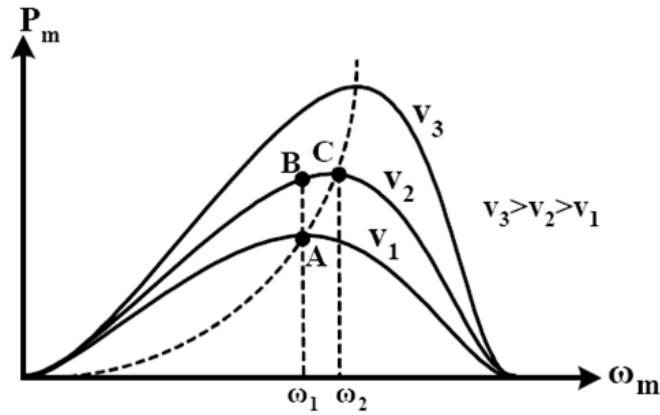
Fig. 4. Characteristics of wind turbines [4]

are two dynamics encountered in the wind power application. Firstly, if the wind speed is constant, the load power is changed , for example, from 1000 W to 500 W. Since the wind turbine is producing 1000 W, if there is no energy storage, the rotor speed had to be reduced such that the output power from the wind turbine is 500 W. However, it may take longer time for the wind turbine to adjust its rotor speed because of mechanical dynamics. Also if the rotor speed is changed, the operating point of the wind turbine would not be optimal, wasting the capability of the wind turbine. However, if there is energy storage installed in this system, the wind turbine can still produce 1000 W while the load power is 500 W. This extra 500 W will go to the energy storage. Therefore, with energy storage, the wind turbine can be operated at its optimal operating point even if the load requires different power.

Another dynamics is that the wind speed changes while the load power is constant. For example, when the wind speed changes from v_1 to v_2, the power from the wind turbine increases. If there is energy storage, this extra power will go into the

energy storage while the same power is supplied to the load. Therefore, with the energy storage, the load can be supplied constant power even if the wind speed is not constant.

2. For Solar Photovoltaics

Fig. 5 shows the characteristics for solar photovoltaics [4]. The X-axis is the terminal voltage of the photovoltaic cell while the Y-axis is the power output of the cell. It can be seen that for a given solar irradiance, there is one point, where the output power is maximum. The power electronics is controlled such that the terminal voltage of the solar photovoltaic is the voltage where the optimal operating point is. Just like wind turbine, the dynamics of the load and the photovoltaics require the
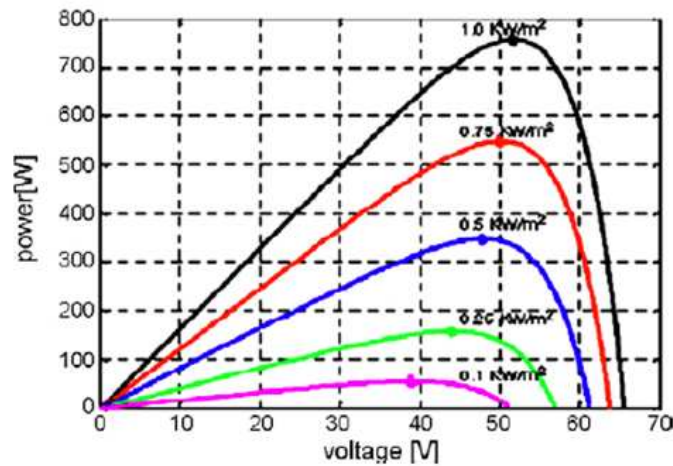
Fig. 5. Characteristics of photovoltaic [4]

usage of energy storage if we want to operate the solar photovoltaic in its optimal operating points. Then energy storage will provide the deficit power and absorb the excessive power of the system.

3. For Fuel Cell

Fig. 6 shows the characteristics for fuel cells [5]. It can be seen that there is a point where the efficiency is maximum. This is the operating point at which we want to operate the fuel cell. At this operating point, the output power from the fuel cell is fixed. If the load power is changed, the energy storage will compensate the power difference without changing the output power of the fuel cell.
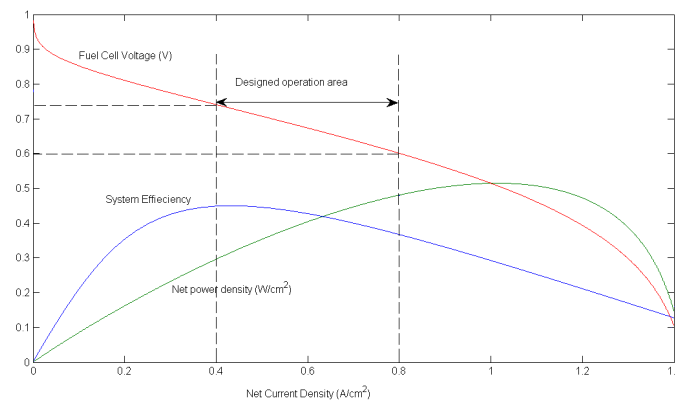
Fig. 6. Characteristics of fuel cell [5]

Because of the electrochemical reaction, the time to change the output power of the fuel cell is long compared to the dynamics of electric loads. Energy storage is needed to provide the rest of the load power. The usage of energy storage will increase the dynamics of overall system.

4. On Energy Storage

There are many different types of energy storage, including battery, super-capacitor, flywheel, SMES, hydrogen, compressed air, to name a few. In this work, instead of batteries, super-capacitors are used as energy storage because they have:

- higher power density

- linear relationship between its state-of-charge and its terminal voltage

- longer life

- faster response.

However, the price of super-capacitors is expensive. How to reduce the requirement of energy storage is vital to reduce the cost of the system. One way to reduce the requirement of energy storage is by integrating different renewable energy sources that can compensate with each other so that the energy storage does not need to provide the whole load power for a long time. This concept will be discussed in the next section.

C. Concept of Hybrid Distributed Generation System

Hybrid distributed generation system (HDGS) has gained attention in recent years. This system integrates different kinds of renewable energy sources to increase the overall stability and utilization [6].

A secure supply based on only one renewable energy source requires a substantial energy storage. The reason is that the renewable energy is not available during some period of time. For example, the photovoltaic cells produce zero power during the night or little power during the cloudy day. Wind energy may not be available if the wind speed is under certain speed, under which the wind turbine can not extract energy from the wind. If the system has to provide the power to load during the time when renewable energy source produces little power, the only way is to use the power from the energy storage.

If two or even more different renewable energy sources are integrated, the storage capacity requirement would be greatly reduced, since the fluctuations of these two

renewable energy sources may have a statistical tendency to compensate each other. For example, solar power is high during the day, while the wind power is high at night. Combining these two sources will approximately produce a constant power to the load during the entire day.

Another example of HDGS is the integration of photovoltaics and fuel cell. Since the output power of photovoltaics depends on the solar irradiance. Solar irrandiance varies during the day. In order to have a constant power output, the output power of fuel cell is adjusted according to the output power of photovoltaics. In this way, the total power from the photovoltaics and the fuel cell will be the same even though the solar irradiannce is not constant. Therefore, a combination of photovoltaic and fuel cell forms a good pair for HDGS application.

D.   Benefits of Multi-port Converter

There are two ways to integrate different renewable energy sources and energy storage. The conventional way is to use a common DC bus. Separated DC-DC power converters are used to connect different renewable energy sources to the DC bus. Fig. 7 shows the conventional structure.

However, there are several disadvantages for this structure. First, there are more power electronic devices, resulting in higher cost. For each renewable energy source, there has to be a DC-DC converter, which connects the renewable energy source to the DC bus. Also, there are more conversion steps. The power is transformed from DC to DC, then from DC to AC if the load is AC load. The efficiency is lower because of more conversion steps. Another problem is related to voltage levels of renewable energy sources. If the voltage levels for different renewable energy sources are quite different, and the DC bus voltage is much higher than that of the renewable energy
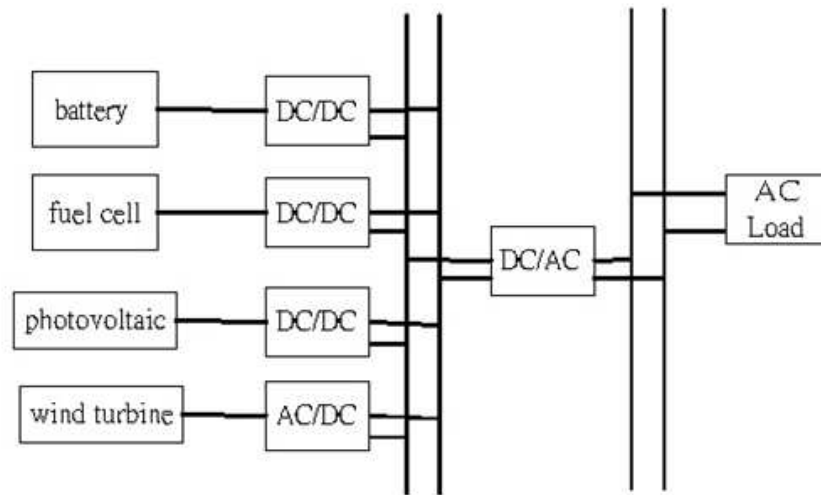
Fig. 7. Conventional structure of integrating renewable energy sources

sources, the DC-DC converters are operated in extreme case, where duty ratio is closed either to 1 or 0. In this operating point, the efficiency of the DC-DC converter is much lower than that when operating in normal case. The last issue is about control. In the conventional structure, the control is separated. The controller only controls the DC-DC converter without considering the overall system performance. Although this control is easy, there should be a central controller such that the power management can be achieved, and the interaction between the renewable energy sources, energy storage and load can be taken care of.

Another way of integration is by using multi-port power converters. The multi-port power converter will connect all renewable energy sources and energy storage. Some ports are bi-directional if they are connected with energy storage, while some are uni-directional if they are connected with energy source. Fig. 8 shows one of the applications of the multi-port DC-DC power converter. This converter integrates fuel cell, photovoltaic cells, energy storage and the load. If the load is AC, an extra

inverter is needed to convert the DC power into the AC power.
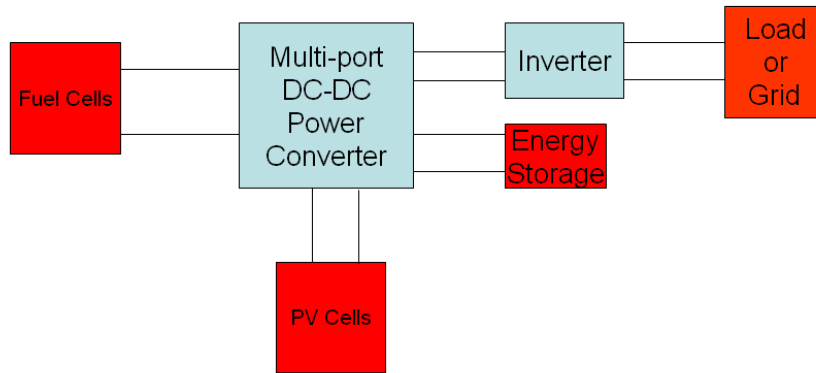
Fig. 8. Application of multi-port DC-DC power converter

In this multi-port DC-DC power converter, there will be fewer power devices, which means the cost of the power converter will be lower than that of the conventional one. Also, the conversion steps are minimized, resulting in higher efficiency. Due to the presence of the transformer in some circuits, electric isolation is available, which is important for safety. With the turn ratio of the transformer in certain topologies, it will be more efficient to integrate different renewable energy sources of different voltage levels. Finally, there is a central controller. The controller not only controls the individual switches, but also manages the whole system. For example, the controller may give the increase power command to the renewable energy source in order to charge the depleted energy storage. Another example is the controller can control the switch to perform the "Maximum Power Point (MPP)" tracking for the photovoltaic cell such that the output power is maximum at any operating points. The central controller will enhance the overall performance of the system.

E.   Previous Research Work

The concept of multi-port DC-DC converter has been discussed in several papers. Sachin Jain and Vivek Agarwal [6] and A. Di Napoli, et al., [7] connect different renewable energy sources in parallel across a common DC bus. Another method to connect different sources is by using series connection [8]. In this work, the AC voltage produced by the wind turbine is rectified by a uncontrolled rectifier. This DC voltage is connected in series with the DC voltage of PV generators. The combined DC voltage is the input to the PWM voltage source inverter to provide power to AC loads. Another method of integrating sources is by adding the flux in the multi-winding transformer [9]. In this circuit, there are two current-source input stage circuits, three-winding coupled transformer and a common output stage. These components are connected around the transformer. Magnetic flux addition is used to transfer power to the load.

However, the above topologies are uni-directional and suitable for low power application. For renewable energy application, the circuit has to be bi-directional to integrate energy storage. Also the circuit has to be for high power application. Therefore, there are some literatures proposing other topologies. There topologies is based on the two-port circuit proposed by Dr. Doncker [10], where the power transferred is controlled by phase difference of switching signals. This circuit consists of two sets of full-bridge circuits. Another version uses two sets of half-bridge circuits [11], where the number of switches is reduced. Based on two-port topologies, a three-port circuit, consisting of three sets of full-bridge circuits was proposed by M. Michon, J. L. Duarte, et al. [12]. H. Tao, A. Kotsopoulos et al. improved this circuit by duty ratio control to increase the soft-switching operation range and designed the controller to regulate the load voltage and the input power from renewable energy source. The

version of half-bridge was proposed by Danwei Liu and Hui Li, where there are three sets of half-bridge circuits [13]. The concept of the above circuit is quite similar. The leakage inductance of the transformer is used to transfer power and two phase differences are used to control the power flowing between the three ports.

However, these literatures didn't address how to change phase difference properly to avoid the un- symmetrical current flowing in the leakage inductance, which may result in the saturation of the inductor. Also, the controller was designed with trial and error. Some of the models were derived incorrectly for designing the controller. Moreover, there is no analysis on the stability issue. Moreover, the practical issues, such as starting of the circuit, influence of dynamic load, the current ripple of renewable energy sources, the variation of input power of renewable energy sources, and large load variance were not addressed in these literatures.

F.   Research Objective

In this work, a new kind of multi-port DC-DC power converter will be proposed in order to integrate different renewable energy sources and energy storage effectively and economically. The proposed circuit will be analyzed, modeled, designed, controlled, and simulated. Certain issues related to practical application will be discussed to verify the usefulness of the propose circuit. They will include the stability of the circuit under different operating points, how to start this circuit without external assistance, how to manage the power flow between the source, the load and the energy storage, how to control to circuit to regulate or control the load voltage while keeping the input power from the renewable energy sources almost constant under the influence of the dynamic load, how to maintain a fixed load voltage under the influence of the variation of input voltage of renewable energy sources, and how to

integrate current-source like renewable energy sources.

G.   Thesis Outline

In Chapter I, the trend in the renewable energy will be discussed. The need for the multi-port DC-DC power converter will be explained. Previous research will be described and the research objective of this work will be presented.

Chapter II will review the dual active bridge (DAB). This circuit is the fundamental circuit of the proposed circuit. Some description and analysis will be made and some simulation and design will be performed on this circuit.

In Chapter III, triple active bridge (TAB) will be described. This circuit is an extension of DAB, and is the predecessor of the proposed circuit. The fundamental circuit operation will be describe and analysis will be made. Some simulation of this circuit will be presented.

In Chapter IV, the proposed circuit will be described. The analysis and design will be performed. The mathematical model of the circuit will be derived. Based on the model, with some techniques in control theories, the controller will be designed. Stability analysis will be performed. The central controller will be designed and some practical issues will be addressed.

In Chapter V, the simulation will be performed for different scenarios encounter in the context of renewable energy application. Performance evaluation and discussion will be made in this chapter.

Chapter VI will conclude the entire work and future work will be described.

CHAPTER II

REVIEW OF DUAL ACTIVE BRIDGE

A. Introduction

High-power-density DC-DC converters have been a hot topic recently, especially in power supply application, hybrid vehicle, hybrid energy storage system and renewable energy. In order to have higher power density, the size of the converter has to be small. One way to achieve it is by operating the converter at higher frequencies, which will reduce the size of reactive components, transformers and filters. However, when the switching frequency is high, the switching losses will be high. There are some ways of switching that will reduce switching losses. One of them is by soft-switching. Examples of soft-switched dc/dc converters are the parallel output SRC [14], the pseudo-resonant converter, the resonant pole [15] and quasi-resonant converters[16]. In this work, dual active bridge (DAB) [10], invented by Dr. De Doncker, will be used as a building block. Therefore, in this chapter, a brief review of the DAB operation and analysis will be made and the control and simulation will be performed.

B. Circuit Description

The DAB, shown in Fig. 9, is a DC-AC-DC converter which allows energy transfer between the source and the load. The source side and the load side both are full-bridge circuits, operated at a fixed frequency. Full bridge circuits have the following features: 1)minimal voltage and current stresses in the devices and 2)minimum VA rating of the transformer. The two full bridges are connected via a high frequency transformer. The transformer has several functions. It can integrate different voltage levels with the turn ratio of the transformer. Also, the transformer provides electrical

isolation, which may be required by the industry standard. Finally, the leakage inductor of the transformer can be used as an energy transfer element. In every cycle, a small fraction of energy from the source is stored in this leakage inductor before it is transfered to the load. The inductance can be added by using external inductors connected in series with the transformer.
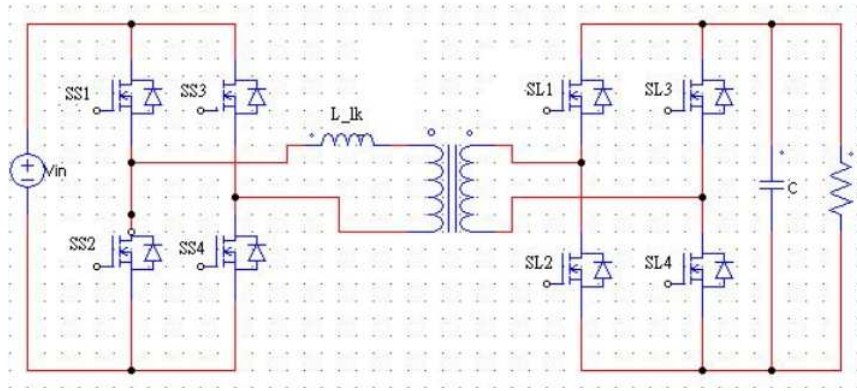
Fig. 9. Circuit representation of the DAB

The switches of the DAB circuit are operated at a constant frequency. The switching sequence of the switches on the source side is $S_{S1}S_{S4}$, $S_{S2}S_{S3}$, $S_{S1}S_{S4}$ while the switching sequence on the load side is $S_{L1}S_{L4}$, $S_{L2}S_{L3}$, $S_{L1}S_{L4}$. The switches are operated at a fixed frequency and with a fixed duty cycle of 50%. These two switching sequences do not need to be synchronized. As will be explained later, the phase difference between these two switching sequences is the important control variable which can be used to control the power transferred between the source side and the load side. The switching signal for these switches is shown in Fig. 10.

The equation of the power transferred between these two ports was derived in Appendix A. Equation (2.1) was obtained by averaging the current flowing out of the
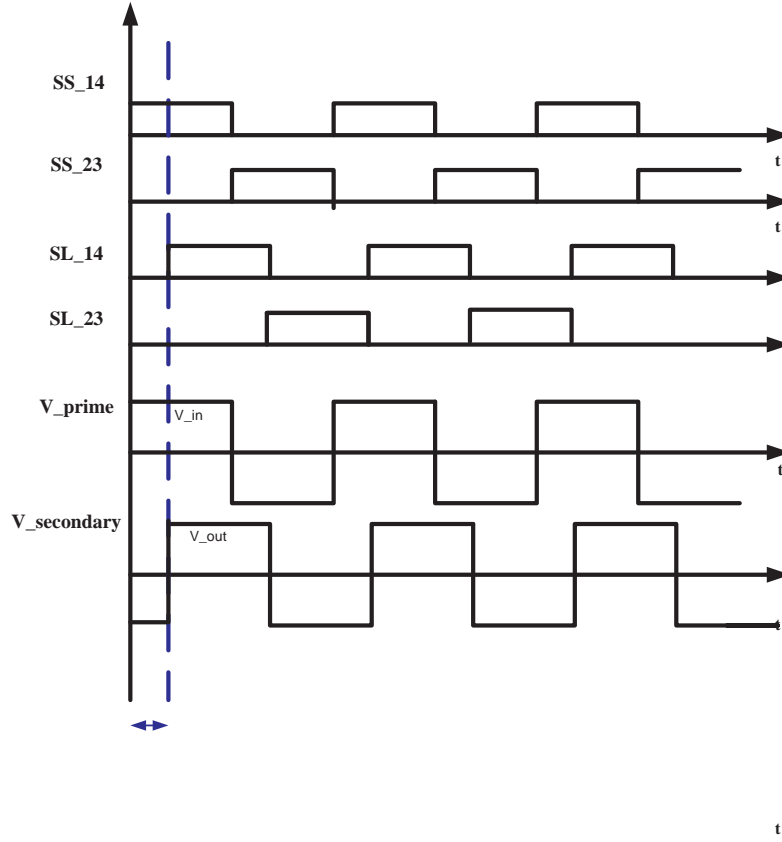
Fig. 10. Switching signal for the switches in the DAB

source.

$$P = \frac{V_{in}V_{out}}{N\omega L_{lk}}\phi(1 - \frac{\mid \phi \mid}{\pi}) \tag{2.1}$$

where ϕ is the phase difference between the two ports.

From this equation, it is clear that the equation is like the power equation in power systems, where the power transferred is related to source voltage V_{in}, the load voltage V_{out}, the inductor L_{lk} and the phase difference. Since the switches on both sides are switched with 50% duty cycle, the voltage across the primary side and

secondary side of the transformer are square waves. These two square waves have different phases and magnitudes. If we disregard the magnetizing inductance of the transformer, the transformer can be represented as a leakage inductor connecting these two ports. The following equivalent circuit is shown in Fig 11. The equivalent circuit is quite similar to the equivalent circuit in power systems, except that the voltage in this case is square wave.
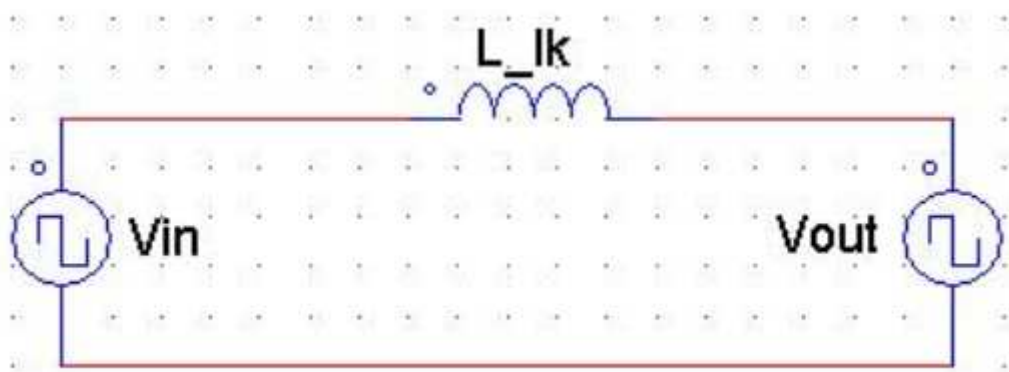
Fig. 11. Equivalent circuit of the DAB

If ϕ is positive, source side will lead the load side. From Equation (2.1), the power is positive, which means the power is transferred from the source side to the load side. If ϕ is negative, the source side will lag the load side. The power will be negative, which means the power is transferred back to source side from the load side.

From the Fig 12, which plots power versus phase angle, we can see that when the angle is 90 degrees, the power transferred is maximum.

C. Phase Shifting Technique

The equation (2.1) calculates the power transferred. Since in nominal cases, V_{in}, V_{out} and L_{lk} are constant, the power transferred can be controlled by the variation of
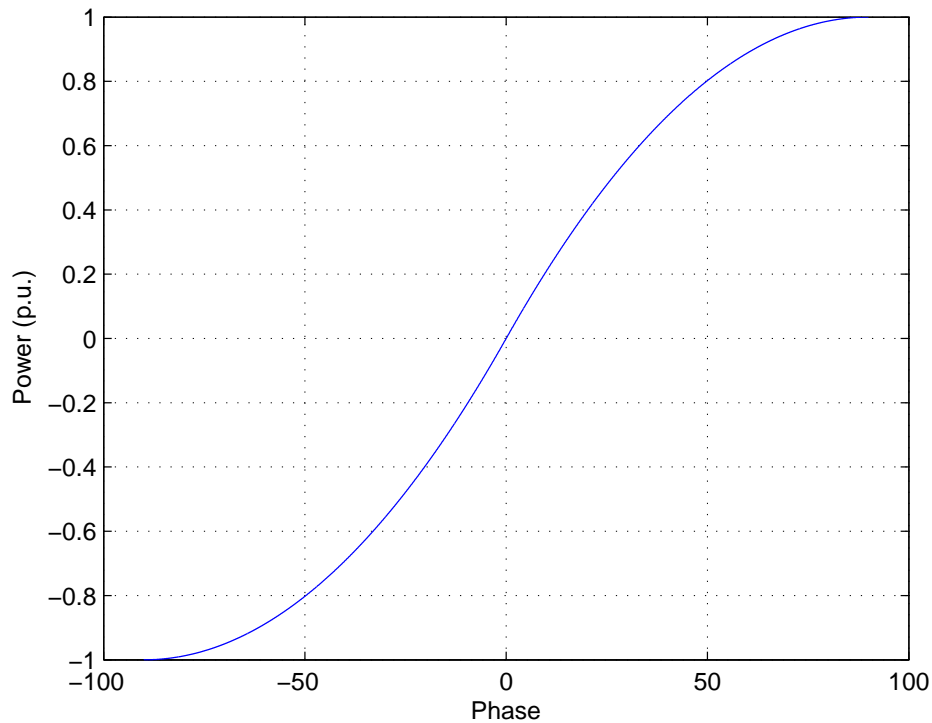
Fig. 12. Power transfer versus phase shift of DAB

phase difference ϕ between the two ports. The higher phase difference, the higher the power transferred. In typical operation, the output voltage is required to be constant even though the load changes. In order to regulate the output voltage under different loads, the phase difference needs to be changed accordingly. A PI controller is used to generate phase difference command. With this phase difference command, the gating signals can be generated.

The PI controller continuously generates phase difference command. If there is no special techniques by which the phase difference is changed, the current in the leakage inductor of the transformer will be un-symmetric. If this current is large enough, the transformer will be saturated.

Therefore, in order to change the phase difference properly, which is called phase shifting, some algorithm is needed to make the current of the leakage inductor symmetric, even though the phase difference command is continuously changing. This algorithm was invented by Dr. M. Ehsani, which was described in [17].

The shortest transient switching sequence for phase shifting in the DAB, without causing the leakage inductor current imbalance, has three-step. If a change of phase difference ϕ in time is Δt_ϕ, the three transient steps of the sequence are:

$$\Delta t_1^{(3)} = \Delta t_1 - \frac{\Delta t_\phi}{2} \tag{2.2}$$

$$\Delta t_2^{(3)} = \Delta t_1 - \frac{\Delta t_\phi}{2} \tag{2.3}$$

$$\Delta t_3^{(3)} = \Delta t_1 \tag{2.4}$$

where $\Delta t_1^{(3)}, \Delta t_2^{(3)}, \Delta t_3^{(3)}$ are the first, second and third steps of a three-step sequence and Δt_1 is the original switching time interval. The change of phase difference Δt_ϕ is divided and distributed in two switching sequences. Figure 13 shows an example where the phase difference ϕ is changed from 0° to 90°.

In the above example, the phase difference was changed from one value to another value. However, in the feedback control scheme, the phase difference command ϕ is always changing. The output of the PI controller depends on the controller's parameters and the difference between the actual value and the reference value. There are two problems.

First, since the phase difference command ϕ is always changing, the change in phase difference command $\Delta\phi$ exists even when the circuit is undergoing the procedure of the three-step transient switching sequence to change the phase difference.
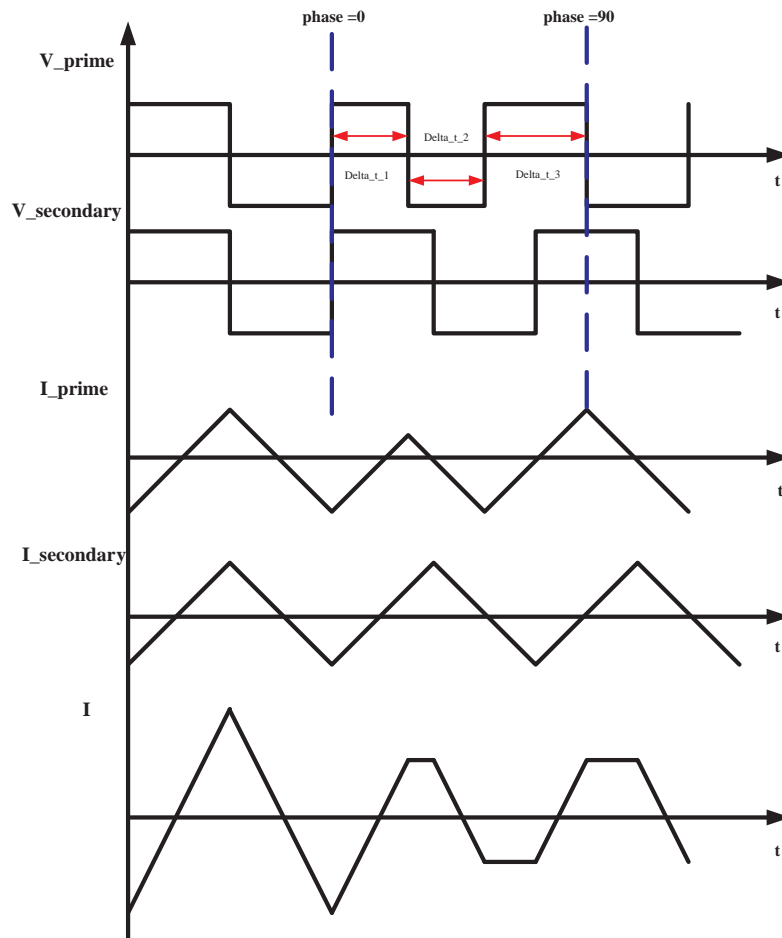
Fig. 13. 3 step phase shifting from $\phi = 0^o$ to 90^0 for DAB

Another problem is that even though it is not the right time to change the phase difference, the change in phase difference command $\Delta\phi$ still exists. For proper operation, the three-step transient switching sequence can not begin until the time is right. In the example shown in Fig. 13, the right time to begin the three-step transient switching sequence is when the gating signal is changing. The switching sequence starts when SS_{14} is turned on. In other words, the right time is when the voltage across the transformer changes its polarity. If the phase difference is not

changed at the right time, it will be hard to maintain the current balance of the transformer.

To solve these two problems, a specific program was designed. In this program, "TRANSITION" flag was used to tell the program when the system was undergoing the three-steps procedure. Another flag was "On-Time" flag. This flag told the program when was the right time to start the three-steps phase shifting procedure. The program is attached in Appendix B.
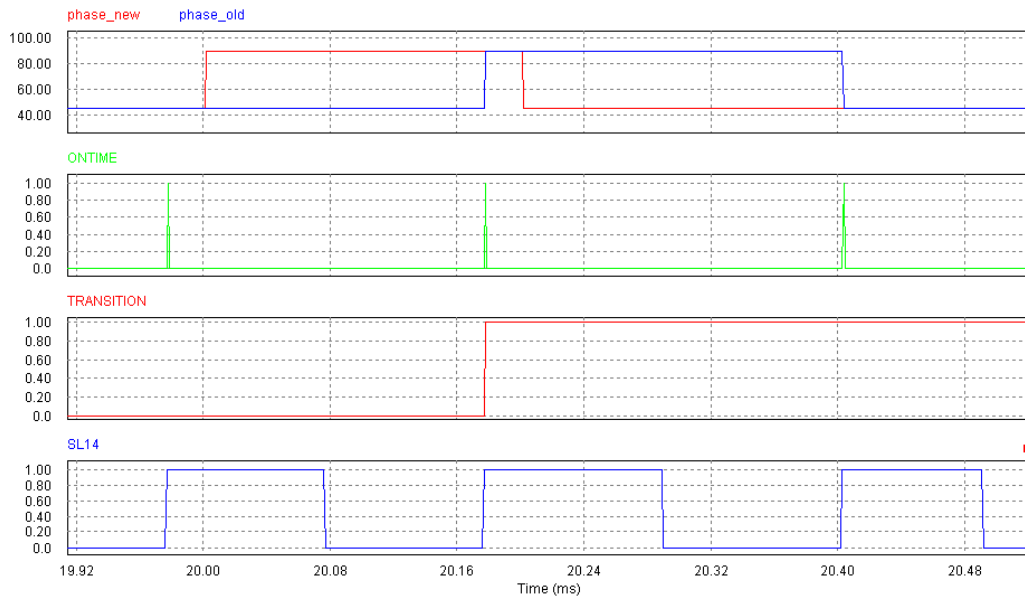
Fig. 14. Signal waveform of phase changing technique with several phase difference command (a)phase_old and phase_new [degree], (b)ONTIME flag (c)TRANSITION flag (d)SL14

In Fig 14 , there are two phase shiftings: from 45° to 90° and from 90° to 45°. In the waveforms, phase_old is the current phase difference while phase_new is the new phase difference. The correct time to change phase difference is when the ONTIME flag is equal to one. Only when the ONTIME flag is equal to one will phase_old become phase_new. In this case, phase_new is changed from 45° to 90° at 20ms.

Since the time is not right, the program will wait until the time is right. As soon as ONTIME flag becomes one, the program undergoes the three-step phase shifting procedure. During the transition from 45° to 90°, where TRANSITION flag is equal to one, the phase_new is again changed back to 45°. The program will block the change of phase_new since the system is undergoing the transition procedure. The program waits until the three-step phase shifting procedure is completed. When it completes the process, and the time is right, the phase_old becomes phase_new, and the system undergoes another three-step phase shifting procedure from 90° to 45°.

In Fig 15, it can be seen that the phase changing technique is successful even though the phase is continuously changing. Note that the current on the primary side and on the secondary side of the transformer is symmetric.
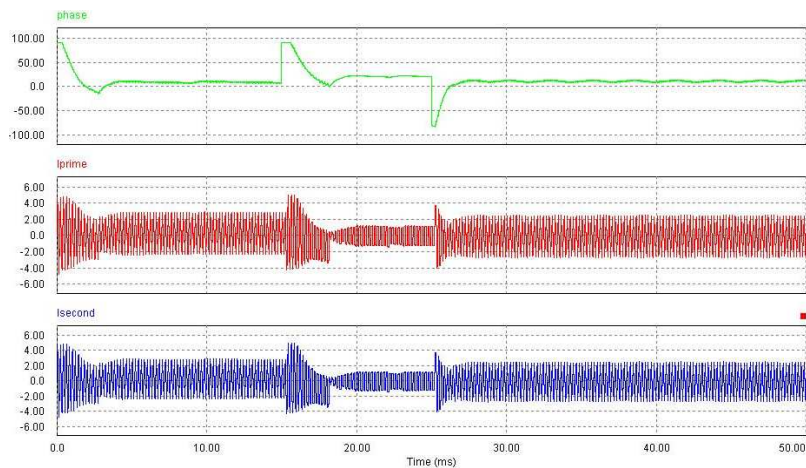
Fig. 15. Current waveform with continuously changing phase difference command (a)phase [degree], (b)I_{prime} [A], (c)I_{second} [A]

D. Gyrator Model Analysis

There is another way to analyze the DAB. Gyrator theory, discussed in [18], can be used in analyzing power converters. It is a very powerful tool. If a switching circuit is a gyrator, it can be easily analyzed and simulated without considering these switches. Also, the description of the circuit gained from gyrator models is valid both in the steady state and transient state. In the following, the gyrator will be briefly described and the DAB will be analyzed by the gyrator theory.

1. Introduction to Gyrator

A gyrator shown in Fig 16 is a realizable network that couples an input port to an output port via a gyrastatic coefficient. It has no losses and no storage, and it transforms one-port network into its dual with its gyration conductance. It can be described by the following equations:

$$i_1 = gv_2 \tag{2.5}$$

$$i2 = -gv_1 \tag{2.6}$$

where g is called the gyration conductance and has the unit $\frac{1}{\Omega}$

If the input power and output power are calculated, we will find they are the same:

$$v_1 i_1 + v_2 i_2 = v_1 i_1 + (\frac{1}{g} i_1)(-gv_1) = 0 \tag{2.7}$$

which means there's no losses and no storage inside the gyrator.

The gyrator converts a network on one port to its dual with respect to the gyrator conductance on the other port. A voltage source on the input port is converted as a
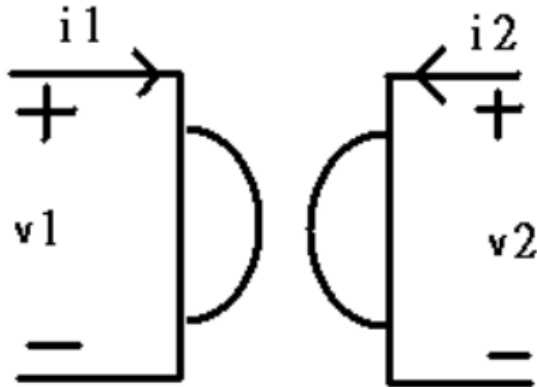
Fig. 16. Symbolic representation of a gyrator

current source on the output port. Capacitors are transformed into inductors. Also, circuits in series on the one port of gyrator are transformed into circuits in parallel on the other port. All of these transformations can be performed in opposite directions.

2. Modeling DAB by Gyrator

Using the gyrator transformation mentioned previously, DAB can be represented with the gyrator model, which is shown in Fig 17. The circuit consists of two full-bridge circuits and the transformer.

Since

$$P = \frac{V_{in}V_{out}}{N\omega L_{lk}}\phi(1 - \frac{|\phi|}{\pi}) \tag{2.8}$$

The input power should be equal to the output power. Therefore

$$P_{in} = V_{in}I_{in} \tag{2.9}$$

$$P_{out} = V_{out}I_{out} \tag{2.10}$$

$$P_{in} = P_{out} = P \tag{2.11}$$

The following is obtained:

$$I_{in} = \frac{V_{out}}{N\omega L_{lk}}\phi(1 - \frac{|\phi|}{\pi})$$

$$= gV_{out}$$

(2.12)

From Equation 2.12, the input current of DAB is the product of a constant and the output voltage. Therefore, the DAB is a gyrator, and the gyrator conductance is

$$g = \frac{1}{N\omega L_{lk}}\phi(1 - \frac{|\phi|}{\pi})$$

(2.13)
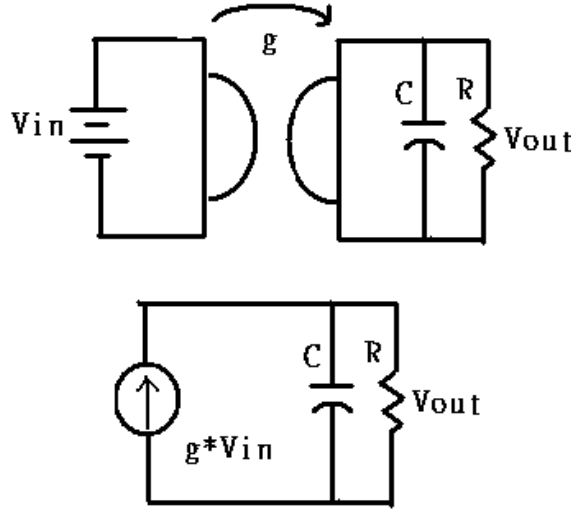
Fig. 17. Gyrator model of the DAB

As seen in Fig. 17, with the gyrator conductance the gyrator model of DAB can be obtained. This circuit is reflected to the load side. The voltage source on the source side is transformed into the current source with gyrator conductance. This model is valid for the steady state and transient state.

In steady state, the capacitor is an open circuit, and all the current from the

source side is flowing into the resistor. The voltage gain will be

$$\frac{V_{out}}{V_{in}} = gR \tag{2.14}$$

In addition to gyrator theory, there is another method to calculate the voltage gain. Since

$$P = \frac{V_{in}V_{out}}{N\omega L_{lk}}\phi(1 - \frac{|\phi|}{\pi}) \tag{2.15}$$

$$= \frac{V_{out}^2}{R} \tag{2.16}$$

Therefore

$$\frac{V_{out}}{V_{in}} = \frac{1}{N\omega L_{lk}}\phi(1 - \frac{|\phi|}{\pi})R = gR \tag{2.17}$$

which is the same as (2.14).

E. Design

In this DAB, some circuit components need to be designed, including switching frequency, turn ratio, leakage inductance of the transformer, filter capacitor, and the voltage rating and current rating of the switches.

First of all, switching frequency f_s needs to be selected. 5 kHz is selected in this work in order to have smaller reactive component size and less switching losses.

If DAB is required to supply 120V AC voltage, an inverter is needed, and the output voltage of DAB needs to be 135V.

From the power equation 2.1

$$P = \frac{V_{in}V_{out}}{N\omega L_{lk}}\phi(1 - \frac{|\phi|}{\pi})$$

the turn ratio, leakage inductance, and the phase difference determine the power

transferred. Usually, the phase difference is kept around 45°, not near 90° because of reactive power issue.

As soon as the input voltage, output voltage, switching frequency, and phase difference are known, the remaining variables are the turn ratio and leakage inductance of the transformer. Since the smaller the leakage inductance, the large the current variation flowing in the transformer. Therefore, it is desirable to have larger leakage inductance. In order to have larger leakage inductance of transformer while maintaining the same level of power transferred, the turn ratio, as seen from the equation, has to be small. Therefore, in this design, turn ratio is chosen to be 1.

Based on the required power transferred, the leakage inductance can be determined according the following equation.

$$L_{lk} = \frac{V_{in}V_{out}}{N\omega P}\phi(1 - \frac{\mid \phi \mid}{\pi})$$ (2.18)

Moreover, the current rating and the voltage rating of these switches can be determined. Since the input voltage of DAB is 100V, the voltage rating of the switches at the input side is 100V. Since the output voltage of DAB is regulated at 135V, the voltage rating of the switches at the output side is 135V. The current in the transformer will flow in these switches. Therefore, the current in the transformer is the current rating of these switches. The magnitude of current will depend on the phase shift, input voltage, and output voltage. The current is maximum when the phase difference is 90°. From the Fig.18, the current in the transformer is changing rapidly from the highest value to the lowest value in half cycle. The magnitude of the current can be calculated with the following equation:

$$\mid I_{prime} \mid = \frac{1}{2}\frac{\left\{ \left(-V_{in} - V_{out}^{\prime}\right) + \left(V_{in} - V_{out}^{\prime}\right) \right\}\frac{T}{4}}{L_{lk}}$$ (2.19)

where T is the switching period= $\frac{1}{f_s}$ and $V_{out}^{\prime}$ is the referred voltage to the primary
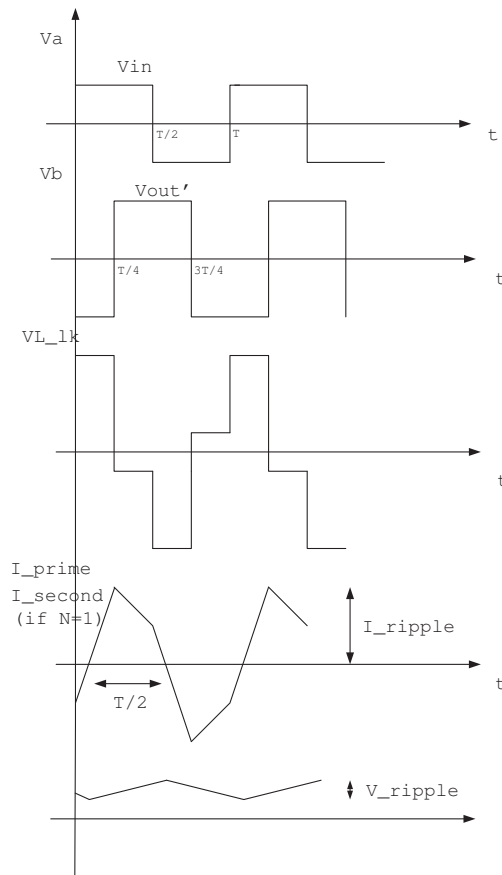
Fig. 18. Current waveform at the primary side of the transformer

side which is $\frac{V_{out}}{N}$.

For the filter capacitor size, it can be simplified by three approximations: 1) the secondary current is like a triangular waveform; 2) all secondary current flows into the filter capacitor; 3) the direction of secondary current and that of the current flowing into the capacitor is the same. With the following equation, the size of the

filter capacitor can be found.

$$Q = C * V \tag{2.20}$$

$$\frac{T}{2} I_{ripple} = C * V_{ripple} \tag{2.21}$$

The designed values of all components in this DAB circuit is summarized in Table I.

Table I. Component values for DAB

component	value
input voltage	100V
output voltage	135V
output power	250W
nominal phase	$\frac{\pi}{4}$
switching frequency	5000Hz
turn ratio	1
current rating	80A
voltage rating at input	100V
voltage rating at output	135V
leakage inductor	0.0011H
filter capacitor	7e-5F

F.   Control

The load voltage is related to the power transferred and the power transferred is related to the phase difference, which can be described as:
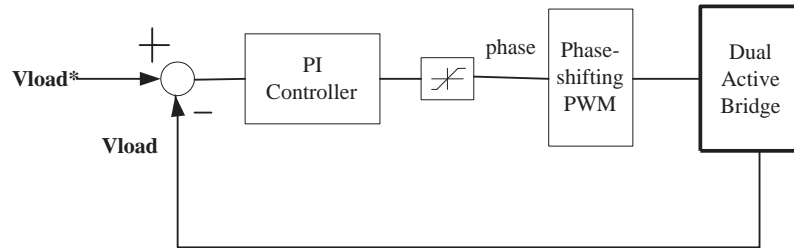
Fig. 19. Feedback control block diagram of DAB

$$P = \frac{V_{in}V_{out}}{N\omega L_{lk}}\phi(1 - \frac{|\phi|}{\pi})$$
$$P = \frac{V_{load}^2}{R}$$

Therefore, the load voltage can be controlled by the phase difference. In this system, a PI controller is used to regulate the output voltage under the influence of dynamic load. In addition to regulating the load voltage, the PI controller can also control the load voltage V_{load} to be different value, no matter the load resistance is changing or fixed.

By using trial and error, the coefficient of the PI controller can be found. Fig 19 shows the block diagram of the feedback system.

G.   Simulation

This work used PSIM to simulate the proposed circuit. The reason is PSIM can incorporate C code into its control circuit with DLL block while in Matlab it is hard to write this kind of program. Moreover, PSIM has higher simulation speed which reduces the simulation time greatly.

In the first simulation shown in Fig 20, the output voltage is controlled at three

levels. The load voltage is first controlled to be 100V, then is changed to 150V at t=0.025sec. At t=0.05, the load voltage is changed back to 100V. The load voltage follows the command, and based on the command load voltage, the phase ϕ changes accordingly. Even if the ϕ is changing continuously, the phase-shifting techniques work very well so that the current in the leakage inductor of the transformer is symmetric, without causing any saturation in the transformer.
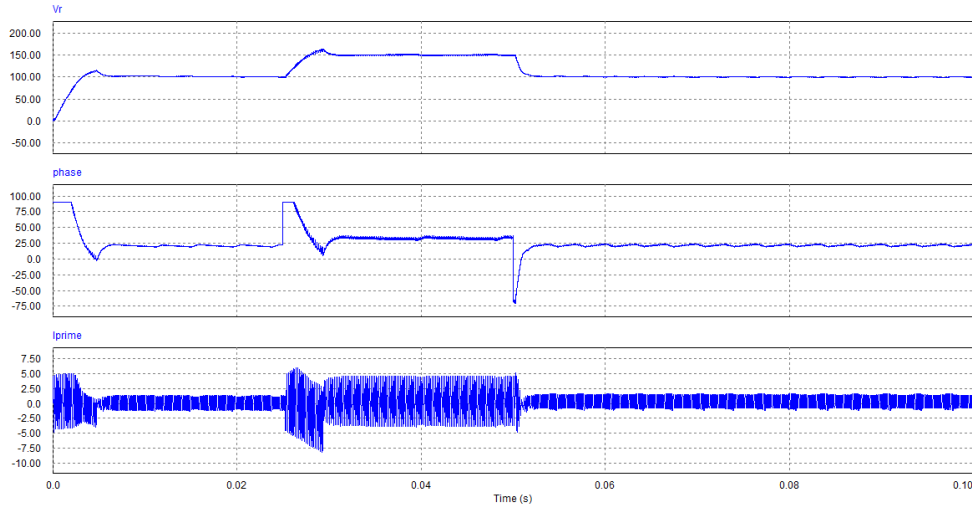
Fig. 20. Voltage control of DAB (a)V_{load} [V], (b)ϕ [degree], (c)$I_{leakage}$ [A]

In the second simulation shown in Fig 21, the voltage is regulated at 135V while the load resistor is changed from 100Ω to 80Ω at 0.5sec. The phase difference is controlled by the PI controller. Since V_{load} is regulated at 135V and the load resistance is decreased, the load power P_{load} increases at 0.5sec. Again, with the phase-shifting technique, the current of the leakage inductor of the transformer is symmetric.

H. Conclusion

In this chapter, the dual active bridge (DAB) was introduced and reviewed. The fundamental principle of operation was described. Gyrator theory was briefly
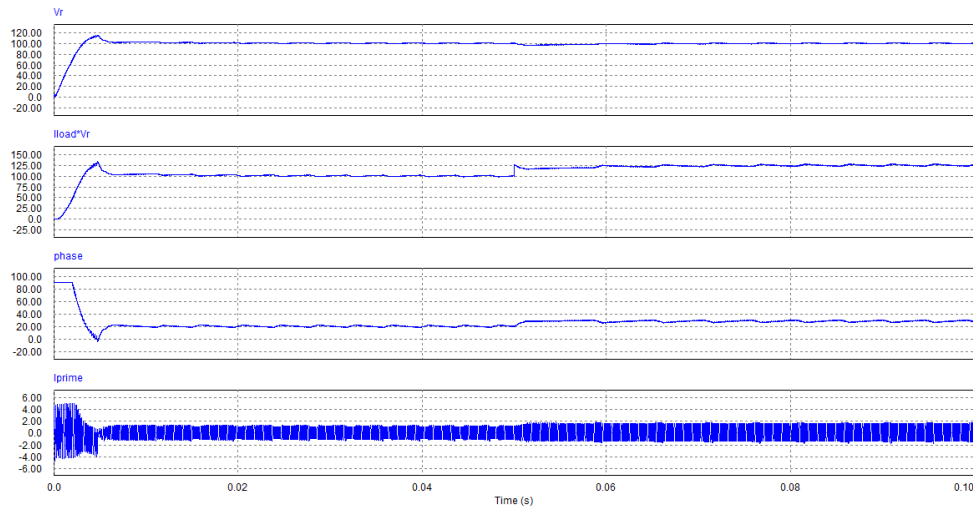
Fig. 21. Voltage regulation of DAB (a)V_{load} [V],(b)P_{load} [W], (c)ϕ [degree], (d)$I_{leakage}$ [A]

introduced and the gyrator model was used to facilitate the analysis of DAB. Also the component designing was performed according to the desired requirement. Finally, the simulation was performed to validate the design. From the result, it is clear that DAB can be used as a fundamental building block in the proposed muiti-port DC-DC converter since it is easy to control the transferred power simply with phase difference between the two ports. Since a transformer is used in DAB, it is easy to expand from the two ports to three ports with three-winding transformers, which will be discussed in the next chapter.

CHAPTER III

REVIEW OF TRIPLE ACTIVE BRIDGE

A. Introduction

Most of electric loads require constant power input or constant voltage input. However, the power from renewable energy sources may be changing with the solar radiation or wind speed. Energy storage is used to provide constant power to the load.

Also if the load requires different power, it takes long time for renewable energy sources to change their output power. It requires energy storage to provide or absorb the power difference between the required load power and supplied power from these sources.

In order to connect energy storage, one way is to use three-port power converter. This converter connects the renewable energy source, energy storage and load. The power converter should be able to satisfy the power demand of the load while maintaining the renewable energy output power constant. By keeping the output power of renewable energy source constant, this renewable energy source can be operated at the optimal operating point, which will have higher efficiency and higher utilization of renewable energy sources. This concept is like hybrid vehicles, where the engine is operated at optimal operating point to generate electricity. With the electricity provided by the engine and the electricity from the storage, the electric motor provides variable power required by the vehicle while the engine is providing constant power.

Fig. 22 shows the system overview. From this figure, the power flow between the power converter and the energy storage has to be bidirectional since the power difference between the renewable energy source and the load is compensated by the
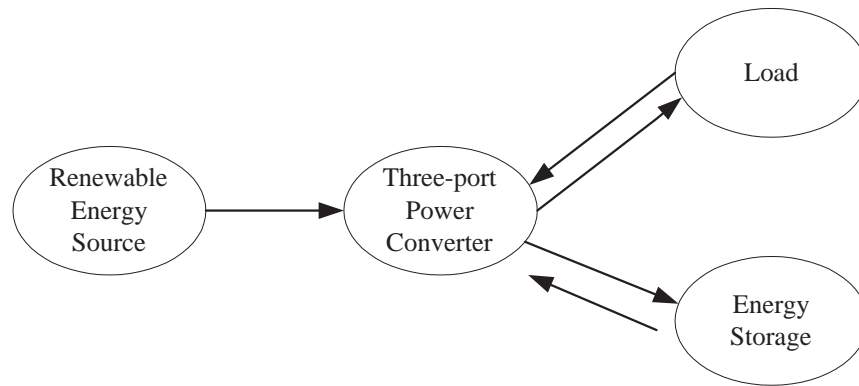
Fig. 22. System overview of three-port power converter

energy storage. If for some reason the load requires less power than the output power from the renewable energy source, this extra power will be absorbed by the energy storage. If the load requires more power than the output power from the renewable energy source, the deficit power will be provided by the energy storage to the load. In this way, even if the load power is changing, the output power of the renewable energy source can remain constant.

The power flow between the power converter and the load can be uni-directional or bi-directional, depending on the application. For some applications, the load will send energy back into the converter, such as in the regenerative braking in hybrid vehicle. In most cases, uni-direction will be sufficient.

In this chapter, two kinds of three-port active bridges will be presented, including full-bridge and half-bridge. Their operation principles will be discussed and some simulations will be made.

B.   Circuit Description of Triple Active Full Bridge

Fig.23 shows a three-port full-bridge converter, which is the extension of dual active bridge, discussed in previous chapter. This circuit supports bi-directional energy flow, so this circuit fulfill the requirement presented in Fig. 22.
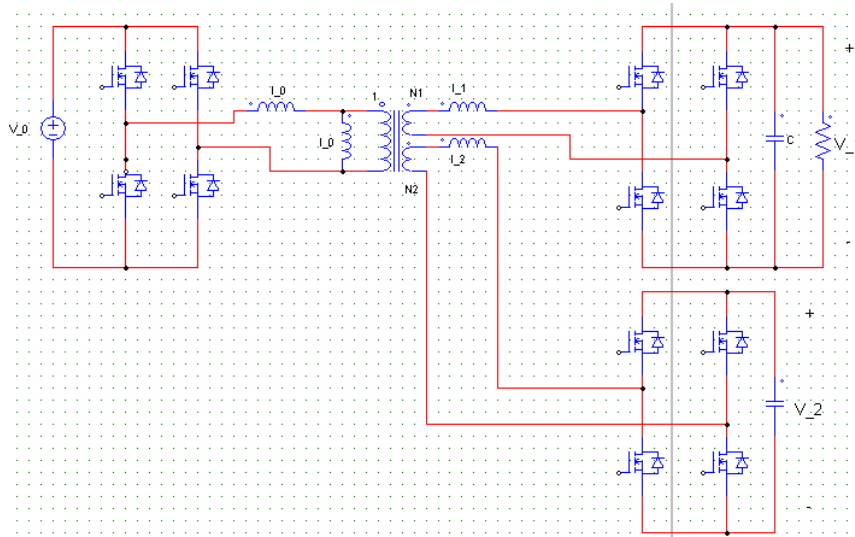
Fig. 23. Circuit representation of TAB

In this circuit, each of the three ports is full-bridge, operating at fixed switching frequency and at fixed 50% duty cycle. It will operate with soft-switching capability under the condition that the voltage on each port remains the same. If the voltage on any one of these three ports changes a lot, there will be no soft-switching. Therefore, in this circuit, there is a range for soft switching. Some literatures [19] and [20] proposed some techniques which change the duty cycle of switches to increase the soft-switching range. In this work, this circuit will be focused on the overall system operation and power management, so the switches of this circuit will be operated at fixed duty cycle.

As in the case in dual active bridge, the power flow between these three ports can be controlled with phase difference. The voltages of these three ports are phase shifted from each other by controlled angles. There are two phases: Φ_{10} and Φ_{20}. The former is the phase difference between the source side and the load side, while the other is the phase difference between the source side and the energy storage side. If the phase is positive, it means the source side is leading. On the other hand, if the phase is negative, the source side is lagging. From the previous chapter, it is seen that the power is flowing from the leading side to the lagging side, just like the power transferred in power systems.

Basically, this circuit can be viewed as a network of inductors, including the magnetizing inductance and the leakage inductance of the transformer. This network of inductors is driven by squared-wave voltages, which have phase differences between each other. To calculate the power flow between these three ports, the inductances between these three ports have to be found. The π-equivalent transformer representation can facilitate this calculation. The equations provided by [21] can be used. Fig 24 shows equivalent circuit.

$$n_1 = \frac{l_3}{l_0 l_3} N_1 \tag{3.1}$$

$$n_2 = \frac{l_3}{l_0 l_3} N_2 \tag{3.2}$$

$$L_{10} = [l_0 + (\frac{1}{l_1} + \frac{1}{l_2} + \frac{1}{l_3})^{-1}][l_1 + (\frac{1}{l_2} + \frac{1}{l_3})^{-1}] * (\frac{1}{l_2} + \frac{1}{l_3})\frac{l_0 + l_3}{l_3} \tag{3.3}$$

$$L_{20} = [l_0 + (\frac{1}{l_1} + \frac{1}{l_2} + \frac{1}{l_3})^{-1}][l_2 + (\frac{1}{l_1} + \frac{1}{l_3})^{-1}] * (\frac{1}{l_1} + \frac{1}{l_3})\frac{l_0 + l_3}{l_3} \tag{3.4}$$

$$L_{21} = [l_1 + (\frac{1}{l_0} + \frac{1}{l_2} + \frac{1}{l_3})^{-1}][l_2 + (\frac{1}{l_0} + \frac{1}{l_3})^{-1}] * (\frac{1}{l_0} + \frac{1}{l_3})\frac{l_0 + l_3}{l_3} \tag{3.5}$$

$$L_{00} = l_0 + l_3 \tag{3.6}$$
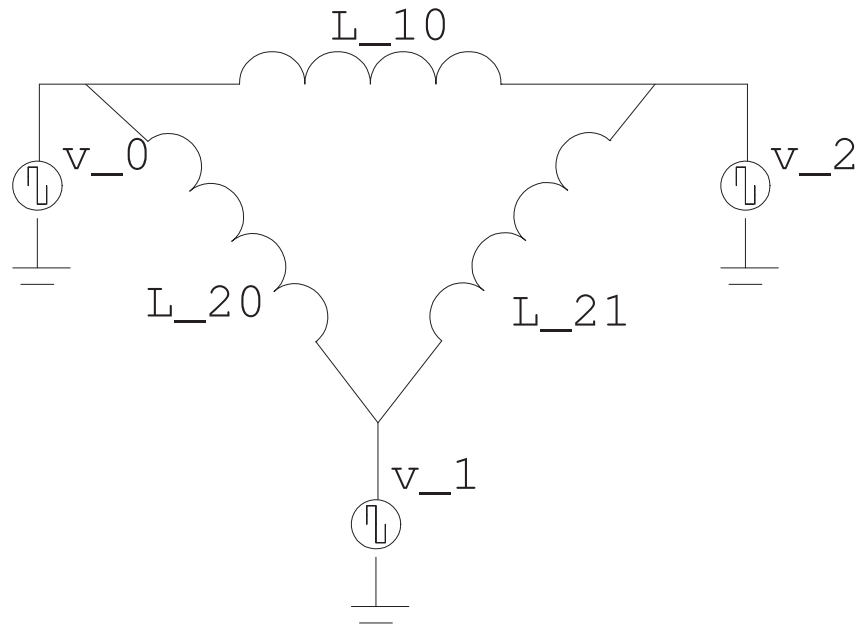
Fig. 24. Primary-referred simplified π-model representation of TAB

where

l_0 is the leakage inductance of the transformer on the source side

l_1 is the leakage inductance of the transformer on the load side

l_2 is the leakage inductance of the transformer on the energy storage side

l_3 is the magnetizing inductance of the transformer

N1 is the turn ratio between source side and the load side

N2 is the turn ratio between source side and the energy storage side

L_{10} is the inductance between the load side and the source side

L_{21} is the inductance between the energy storage side and the load side

L_{20} is the inductance between the energy storage side and the source side

For the design process, usually, L_{10}, L_{20}, and L_{12} are designed. How to convert

these values into l_1, l_2, and l_3 is shown in the following equations.

$$M_0 = L_{00} \tag{3.7}$$

$$M_{01} = \left(\frac{1}{L_{00}} + \frac{1}{L_{10}} + \frac{1}{L_{20} + L_{21}}\right)^{-1} \tag{3.8}$$

$$M_{02} = \left(\frac{1}{L_{00}} + \frac{1}{L_{20}} + \frac{1}{L_{10} + L_{21}}\right)^{-1} \tag{3.9}$$

$$M_1 = n_1^2\left[L_{00} + \left(\frac{1}{L_{10}} + \frac{1}{L_{20} + L_{21}}\right)^{-1}\right] \tag{3.10}$$

$$M_{10} = n_1^2\left[\frac{1}{L_{10}} + \frac{1}{L_{20} + L_{21}}\right]^{-1} \tag{3.11}$$

$$M_{12} = n_1^2\left[\frac{1}{L_{21}} + \frac{1}{L_{10} + \left(\frac{1}{L_{00}+L_{20}}\right)^{-1}}\right]^{-1} \tag{3.12}$$

$$M_2 = n_2^2\left[L_{00} + \left(\frac{1}{L_{20}} + \frac{1}{L_{10} + L_{21}}\right)^{-1}\right] \tag{3.13}$$

$$M_{20} = n_2^2\left[\frac{1}{L_{20}} + \frac{1}{L_{10} + L_{21}}\right]^{-1} \tag{3.14}$$

$$M_{21} = n_2^2\left[\frac{1}{L_{21}} + \frac{1}{L_{20} + \left(\frac{1}{L_{00}+L_{10}}\right)^{-1}}\right]^{-1} \tag{3.15}$$

$$\Delta M_{01} = M_0 - M_{01} \tag{3.16}$$

$$\Delta M_{02} = M_0 - M_{02} \tag{3.17}$$

$$l_3 = \sqrt{\frac{\Delta M_{01} \Delta M_{02}}{1 - \frac{1}{2}\left(\frac{M_{21}}{M_2} + \frac{M_{12}}{M_1}\right)}} \tag{3.18}$$

$$l_0 = M_0 - l_3 \tag{3.19}$$

$$l_1 = M_1\left(1 - \frac{\Delta M_{01}}{l_3}\right) \tag{3.20}$$

$$l_2 = M_2\left(1 - \frac{\Delta M_{02}}{l_3}\right) \tag{3.21}$$

$$N_1 = \frac{\sqrt{\Delta M_{01} M_1}}{l_3} \tag{3.22}$$

$$N_2 = \frac{\sqrt{\Delta M_{02} M_2}}{l_3} \tag{3.23}$$

As soon as the inductances are found, the power transferred between these three ports

can be calculated:

$$P_{10} = \frac{V_0 V_1}{N_1 \omega L_{10}} \phi_{10} (1 - \frac{|\phi_{10}|}{\pi}) \tag{3.24}$$

$$P_{20} = \frac{V_0 V_2}{N_2 \omega L_{20}} \phi_{20} (1 - \frac{|\phi_{20}|}{\pi}) \tag{3.25}$$

$$P_{21} = \frac{V_1 V_2}{N_1 N_2 \omega L_{21}} \phi_{21} (1 - \frac{|\phi_{21}|}{\pi}) \tag{3.26}$$

$$P_0 = P_{10} + P_{20} \tag{3.27}$$

$$P_1 = P_{10} + P_{12} \tag{3.28}$$

$$P_2 = P_{20} + P_{21} \tag{3.29}$$

where

P_0 is the power delivered from the source side

P_1 is the power consumed by the load

P_2 is the power into the energy storage unit

P_{10} is the power delivered from the source side to the load side

P_{20} is the power delivered from the source side to the energy storage unit

P_{21} is the power delivered from the load side to the energy storage unit

From the above equations, there are two variables that can be used to control the power flow. If ϕ_{10} and ϕ_{20} are used as control variables, ϕ_{12} will be determined, which is $\phi_{10} - \phi_{20}$. Therefore ϕ_{10} and ϕ_{20} control the power flow between these three ports.

Fig.25 shows the voltage waveforms imposed on the three terminals of the transformer. These phase differences ϕ_{10}, ϕ_{20}, and ϕ_{12} are shown in this figure.
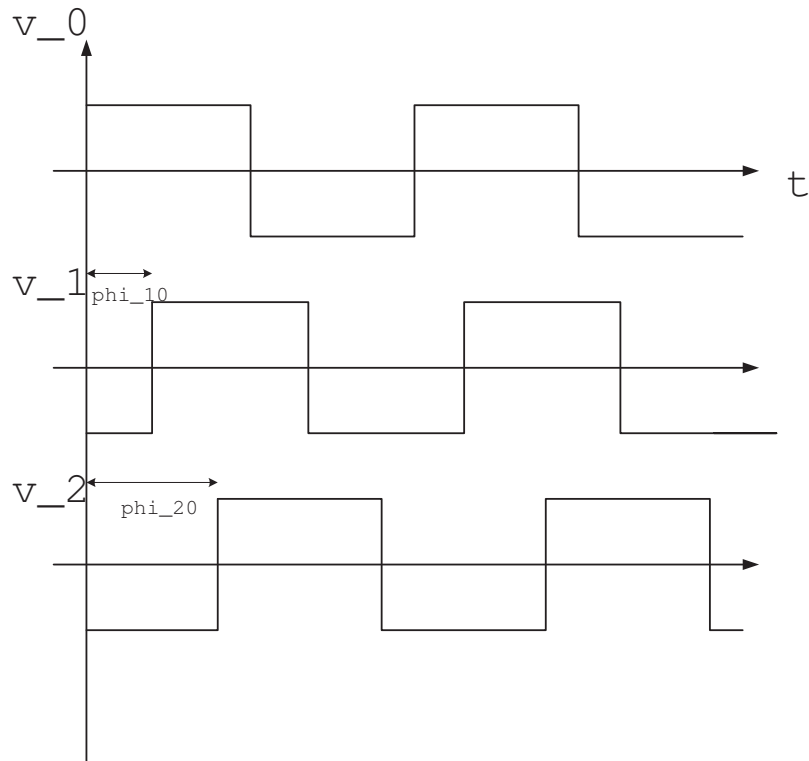
Fig. 25. Voltage generated by the three TAB bridge

C. Circuit Description of Triple Active Half Bridge

The circuit mentioned above is voltage source triple active bridge. The input of this three-port power converter is voltage source. There is another version of triple active bridge which is current source version. In this circuit shown in Fig.26, the source side is current-fed with a boost half-bridge while the load side and the energy storage side are full-bridge. The input voltage source is connected in series with an inductor L_s. The boost half-bridge has two functions. One is to boost the low voltage V_0 of source side to high voltage V_{DC} ($= V_a + V_b$). The other function is to serve as an inverter that produces high frequency ac voltage imposed on the transformer,

whose amplitude is $0.5V_{DC}$.
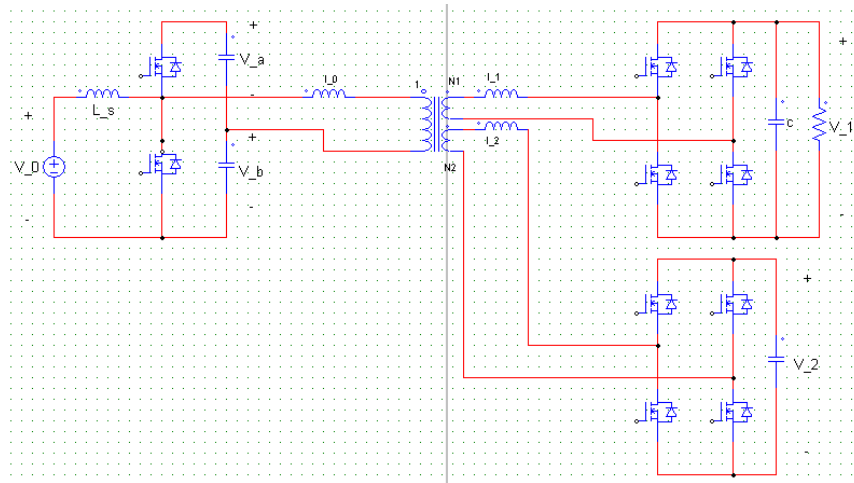
Fig. 26. Triple active half bridge

A three-winding high-frequency transformer is used to link these three bridges. This transformer electrically isolates these three ports. With turn ratio of the transformer, the voltages of the three ports can be of different levels. Moreover, the leakage inductance of the transformer is used as the energy transfer element in the power transferring process.

In order to analyze this circuit, the following assumptions need to be made.

- The inductance of L_s is large enough to maintain the current I_{Ls} to be constant

- All switching devices are ideal

- The output filter capacitors are large enough that V_{DC} is almost constant.

The operation of this circuit is quite similar to the operation of triple active full bridge described in previous section. The voltages imposed on these three terminals of the transformer are square wave with different phases, but with fixed duty-cycle. The

equivalent circuit of half-bridge TAB can be obtained with the same technique shown in (3.1) to (3.6). By using π-representation of transformer, the equivalent circuit can be obtained. The same power equation as (3.24) and (3.29) can be derived. Hence the power flow between these three ports can be controlled by these phase differences, which are ϕ_{10} and ϕ_{20}.

D. Comparison of Full-Bridge and Half-Bridge TAB

Since the number of power devices in full-bridge TAB is higher than that in half-bridge TAB, the cost of full-bridge TAB is higher. However the power rating of the full-bridge TAB is higher than that of half-bridge TAB, since in half bridge version, the high frequency current has to pass through the capacitors. This will be of great concern if the current is high. Therefore, for high power application, full-bridge TAB is more suitable.

However, there is a big advantage for the half-bridge TAB over the full-bridge version. In the half-bridge version, the renewable energy source is connected to the circuit through an inductor. Because of the inductor, the current tends to be constant, provided that the inductor is large enough. With proper design and control, the output current of the renewable energy, which is also inductor current,will have less current ripple than that in the case of full-bridge. In the full-bridge TAB, the output current of the renewable energy source oscillate tremendously, changing from positive value to negative value. This large current ripple is not desirable for renewable energy source. Although this big current ripple can be filtered out by connecting a capacitor in parallel with the renewable energy source, the size of the capacitor will be large if the internal resistance of the renewable energy source is small. Therefore, the half-bridge TAB is suitable for the renewable energy application.

However, there is two major problems in half-bridge TAB. Because the switches SS14 and SS23 are operated with 50% duty cycle, V_{DC}, in the steady state, should be two times of V_0, resulting in less flexibility of V_{DC} choice.

Another problem is about the regulation of V_{DC}. Since there are only two control variables ϕ_{10} and ϕ_{20}, it is impossible to regulate the output power of the renewable energy source P_{in}, the DC bus voltage V_{DC} and the load voltage V_{load} at the same time. If V_{DC} is not regulated, the power from the primary side of the transformer P_0 will consist of two components: the power from the energy source P_{in} and the power from the DC bus capacitor P_C. That is,

$$P_0 = P_{in} + P_C \tag{3.30}$$

Even it is possible to regulate P_0 and V_{load} by controlling ϕ_{10} and ϕ_{20}, the performance of the system will degrade, or even go into unstable region if V_{DC} is off its nominal value. If V_{DC} is not regulated, P_C is not zero. Even P_0 is regulated, P_{in}, which is P_0-P_C, is not regulated. This is undesirable situation since we want to regulate the power from the renewable energy source. In the simulation shown later, it can be found that the performance is not that good because of certain oscillation in P_{in} if V_{DC} is not regulated.

These problems will be solved in the proposed circuit, where the input voltage of the renewable energy source can be flexible and the voltage of DC bus is regulated.

E.   Controller Design

The purpose of control is to regulate the load voltage V_{load} and input power from the renewable energy source P_{in} under the influence of dynamic load. With two variables to control, there should be two control variables. These two control

variables in this system are ϕ_{10} and ϕ_{20}. Since ϕ_{10} and ϕ_{20} both affect the power going into the load and the power coming from the energy source, the system is coupled. That is, ϕ_{10} can affect V_{load} and P_{in}, so can ϕ_{20}. In Hao's paper[19], he derived the mathematical model of TAB and solved the problem of coupling by using two controllers with different bandwidth. The following summarizes the work by Hao.

Since

$$I_0 = \frac{P_0}{V_0} \tag{3.31}$$

$$I_1 = \frac{P_1}{V_1} \tag{3.32}$$

$$I_2 = \frac{P_2}{V_2} \tag{3.33}$$

$$\tag{3.34}$$

The above equations are not linear functions of ϕ_{10} and ϕ_{20}, so they should be linearized at the operating point. They can be derived with partial differentiation:

$$G_{01} = \frac{\partial I_0}{\partial \phi_{10}} |_{\phi_{10_O},\phi_{20_O}} \tag{3.35}$$

$$G_{02} = \frac{\partial I_0}{\partial \phi_{20}} |_{\phi_{10_O},\phi_{20_O}} \tag{3.36}$$

$$G_{11} = \frac{\partial I_1}{\partial \phi_{10}} |_{\phi_{10_O},\phi_{20_O}} \tag{3.37}$$

$$G_{12} = \frac{\partial I_1}{\partial \phi_{20}} |_{\phi_{10_O},\phi_{20_O}} \tag{3.38}$$

where ϕ_{10_O} and ϕ_{20_O} are the operating points. By using the above equations, the change in the current of each port due to the change of these two phase differences can be represented with the following matrix:

$$\begin{bmatrix} \Delta I_0 \\ \Delta I_1 \end{bmatrix} = \begin{bmatrix} G_{01} & G_{02} \\ G_{11} & G_{12} \end{bmatrix} \begin{bmatrix} \Delta \phi_{10} \\ \Delta \phi_{20} \end{bmatrix} \tag{3.39}$$

The equation (3.39) can be shown in Fig.27. From this figure, it can clearly seen that ΔI_0 and ΔI_1 are both influenced by $\Delta \phi_{10}$ and $\Delta \phi_{20}$. When $\Delta \phi_{10}$ is changed to obtain certain ΔI_0, ΔI_1 will also be changed. It seems to be impossible to control ΔI_0 and ΔI_1 by controlling $\Delta \phi_{10}$ and $\Delta \phi_{20}$ independently.
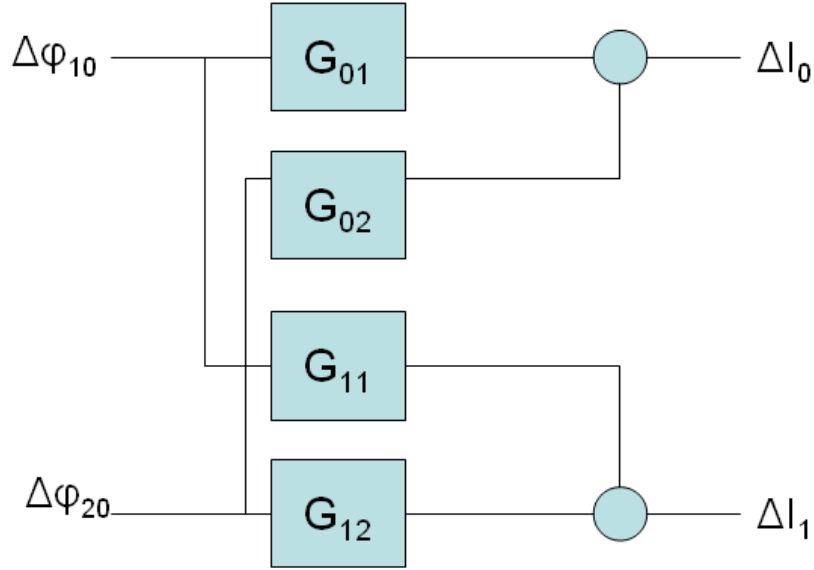
Fig. 27. Transfer function for TAB

In order to solve this problem of coupling, the bandwidth of controllers $G_{c0}(s)$ and $G_{c1}(s)$ are tuned at different values. The bandwidth of $G_{c0}(s)$ is much higher than that of $G_{c1}(s)$ to minimize the interaction between these two control variables. Since $G_{c0}(s)$ has higher bandwidth, which means the system has faster response of the load variation, the controller is called "master". On the other hand, the bandwidth of $G_{c1}(s)$ is lower, which means the system has slower response of the input power regulation. This controller is called "slave".

The work described above was done by Hao. However, he messed up the concept of small signal and large signal. In his paper, he multiplied the output of the transfer functions he derived, ΔI_2 and ΔI_1, with other transfer function to get V_{load} and P_{in},

shown in Fig 28. Because V_{load} and P_{in} are large signals, they can not be found simply by multiplying the small signal ΔI_2 and ΔI_1 with some other transfer functions $H_v(s)$ and $V_{fc} \cdot H_p(s)$.

However, Hao's method of dealing with coupled system with band width difference of the two controllers can be used in the control of the proposed system, shown in next chapter.
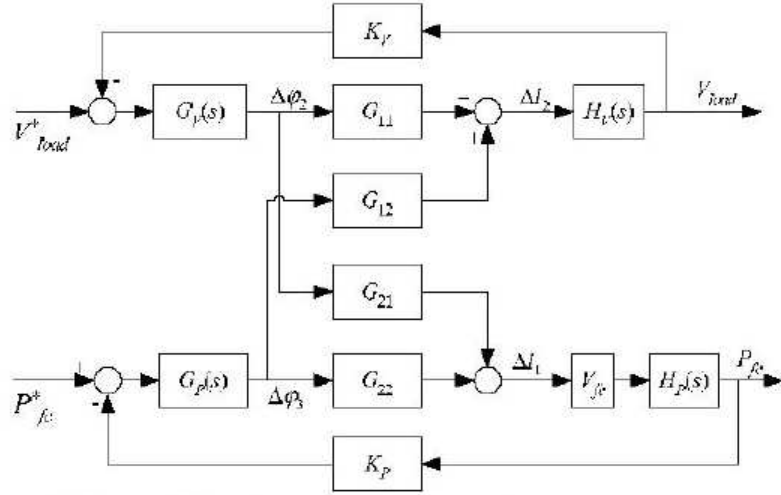
Fig. 28. System block derived by Hao

F. Simulation

In this simulation, the parameters of the two PI controllers were found by trial and error. The purpose was to regulate the load voltage V_{load} and the input power P_{in} under dynamic load by controlling the phase differences ϕ_{10} and ϕ_{20}.

Table II. Component values for full-bridge TAB

input voltage	54V
output voltage	135V
output power	450W
switching frequency	5000Hz
turn ratio n_1	7.6
turn ratio n_2	0.8
leakage inductor	0.000011H
filter capacitor	5e-5F
energy storage capacitor	1F

1. Simulation for Full-Bridge TAB

Table II shows the component value for this circuit. In this simulation, shown in Fig 29 and Fig 30, the load resistance changed from 40Ω to 20Ω at 0.1sec. The load voltage V_{load} and the input power P_{in} were regulated at 135V and 1kW, respectively. The current of the leakage inductor of the transformer, shown in Fig 30 (b), is symmetric, meaning that the phase-shifting technique works. The major drawback of this topology is that the current of the energy source I_{in} is oscillating at a very fast speed. Although the average value I_{in-avg} was the value that gave the average power from the energy source, the large variation of current was not desirable for renewable energy sources.
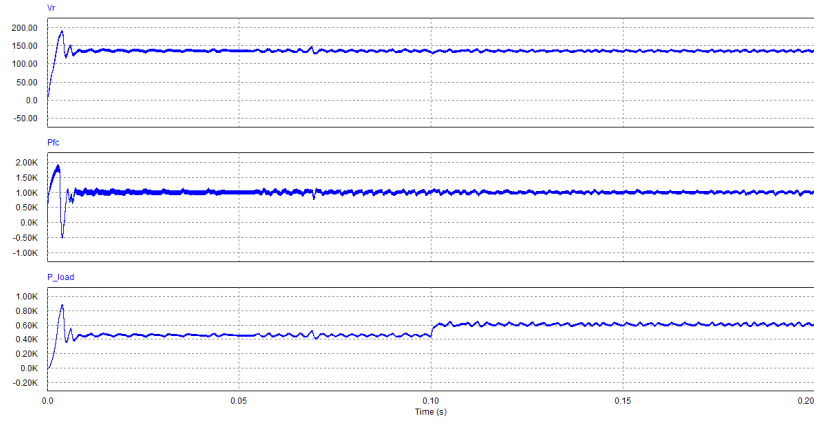
Fig. 29. Simulation of full-bridge TAB (a)V_{load} [V], (b)P_{in} [W], (c)P_{load} [W]
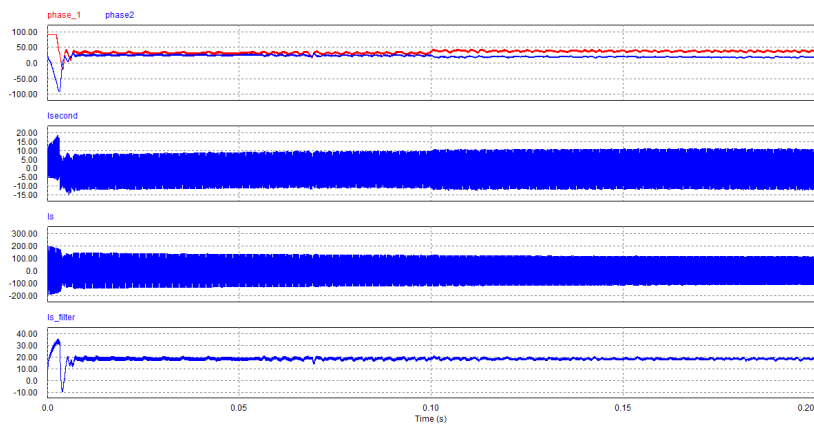
Fig. 30. Simulation of full-bridge TAB (a)ϕ_{10} and ϕ_{20} [degree], (b)$I_{leakage}$ [A], (c)I_{in} [A], (d)I_{in-avg} [A]

2. Simulation for Half-Bridge TAB

Table III. Component values for half-bridge TAB

input voltage	54 V
output voltage	135 V
output power	450 W
switching frequency	5000 Hz
turn ratio n_1	7.6
turn ratio n_2	0.8
input inductor	1 mH
DC bus capacitor	1 mF
leakage inductor	0.000011 H
filter capacitor	5e-5 F
energy storage capacitor	1 F

Table III shows the component value for this circuit. Just like the case for full-bridge topology, in the simulation shown in Fig 31 and Fig 32, the load changed at 0.1sec from 40Ω to 20Ω. The load voltage V_{load} and the input power P_{in} were regulated at 135V and 1kW, respectively. From the results, the oscillation in P_{in} was larger than that in full-bridge case, due to the variation of DC bus voltage V_{DC}, even though the variation was about 10%. Since the DC bus capacitance was not small, even small variation in the voltage of the capacitor caused the power to be provided or absorbed by the DC bus capacitor. This power could not be neglected.

Another interesting point is that the current of energy source I_{in} was not oscillating. It had some current ripple, but not that large. This was desirable for the renewable energy sources.
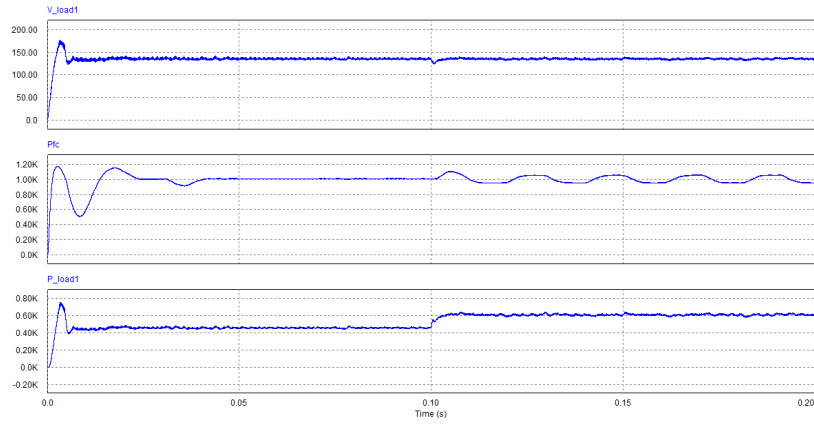
Fig. 31. Simulation of full-bridge TAB (a)V_{load} [V], (b)P_{in} [W], (c)P_{load} [W]
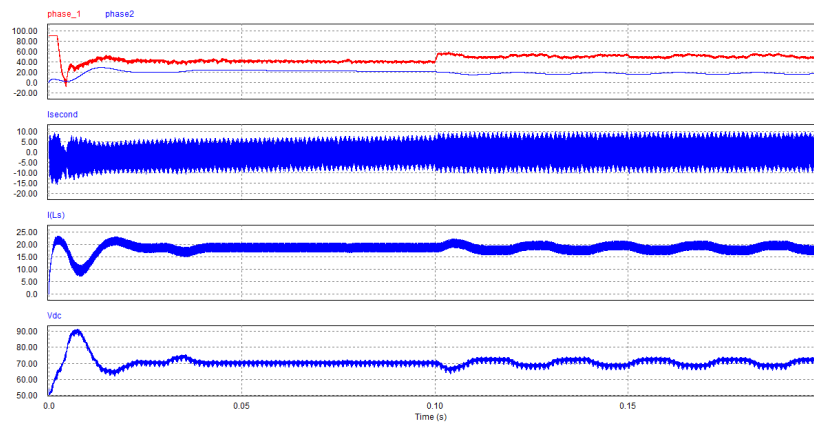
Fig. 32. Simulation of full-bridge TAB (a)ϕ_{10} and ϕ_{20} [degree], (b)$I_{leakage}$ [A], (c)I_{in} [A], (d)V_{DC} [V]

G.   Conclusion

In this chapter, full-bridge and half-bridge TAB were reviewed. The fundamental operating principle was described. The advantages and disadvantages of these two circuits were elaborated. Also how to control the circuit and why the derivation of dynamic equation is wrong in other literature were explained. From the simulation, it can be seen that the concept of TAB is suitable for integrating energy storage in the system, although there are several disadvantages for both full bridge and half bridge. In spite of that, the fundamental operating principle is the backbone of the proposed multi-port DC-DC power converter, which will be discussed in the next chapter. The proposed circuit will solve the problems encountered in TAB.

CHAPTER IV

PROPOSED MULTI-PORT POWER CONVERTER

A. Introduction

The proposed multi-port DC-DC power converter is an improved version of the triple active bridge (TAB). It uses the same operating principle to transfer power as the TAB. It also has some unique features over other similar circuits:

- It can integrate energy storage and multiple sources, whether they are voltage sources or current sources.

- Under the influence of dynamic load, it can regulate and control the output voltage while regulating the output power of the two renewable energy sources.

- The central controller of the circuit will start the circuit without external assistance.

- Power management is performed in this circuit and the state-of-charge of the energy storage is monitored.

- Depending on the current load command, the central controller will change the corresponding controllers to achieve better performance.

- The stability is assured under different operating points.

In this chapter, the operation principles, modeling, analysis, design and control will be elaborated respectively.
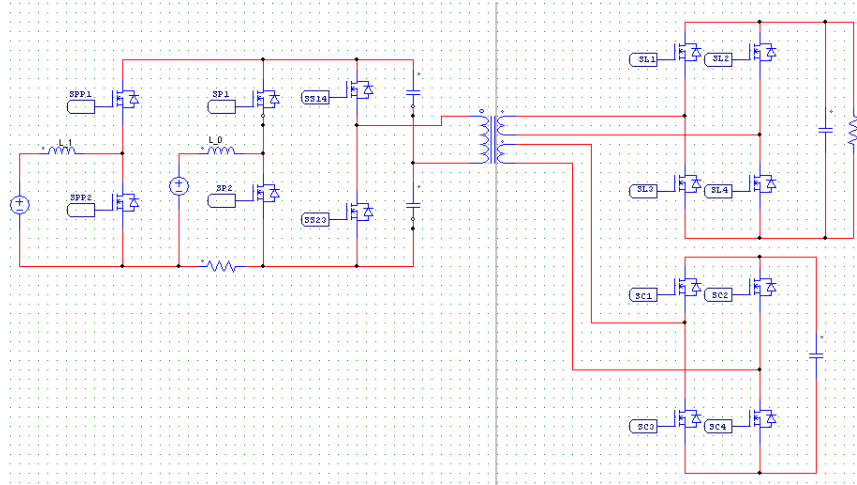
Fig. 33. Proposed multi-port power converter

B. Circuit Description

The proposed multi-port DC-DC power converter is shown in Fig 33. There are three parts in this circuit. The first part has three ports which connect to the source side, the load side and the energy storage side. The source side consists of two DC capacitors and two switches: SS_{14} and SS_{23}. The load side consists of the load R, the filter C_f and four switches. The energy storage side consists of one super-capacitor and four switches SL_1, SL_2, SL_3 and SL_4. This part of the circuit is of vital importance. It is the only part of the circuit that can transfer power from one port to the others. The amount of power transferred can be controlled with the phase difference, ϕ_{10} and ϕ_{20}. The operation principle is the same as that of the DAB or TAB which were discussed in previous chapters. The only difference is that the source side is composed of two DC bus capacitors serving as the energy sources. It is shown in Appendix A that the power equation is the same as that of TAB. The

power equation for this part of circuit is:

$$P_{10} = \frac{V_0 V_1}{\omega L_{10}} \phi_{10} (1 - \frac{\mid \phi_{10} \mid}{\pi}) \tag{4.1}$$

$$P_{20} = \frac{V_0 V_2}{\omega L_{20}} \phi_{20} (1 - \frac{\mid \phi_{20} \mid}{\pi}) \tag{4.2}$$

$$P_{21} = \frac{V_1 V_2}{\omega L_{21}} \phi_{21} (1 - \frac{\mid \phi_{21} \mid}{\pi}) P_0 \qquad = P_{10} + P_{20} \tag{4.3}$$

$$P_1 = P_{10} + P_{12} \tag{4.4}$$

$$P_2 = P_{20} + P_{21} \tag{4.5}$$

where

$V_0 = 0.5 V_{DC}$

V_1 is the referred voltage of the load side to the primary side.

V_2 is the referred voltage of the energy storage side to the primary side.

P_0 is the power delivered from the source side.

P_1 is the power going into the load side.

P_2 is the power into the energy storage side.

P_{10} is the power delivered from the source side to the load side.

P_{20} is the power delivered from the source side to the energy storage side.

P_{21} is the power delivered from the load side to the energy storage side.

The second part of the circuit consists of one voltage source, one inductor, two switches, SP_1 and SP_2, and the DC bus capacitors. The voltage source can be a renewable energy source. The function of this part of the circuit is that by controlling the current of the inductor L_0, the DC bus voltage V_{DC}, which consists of two DC bus capacitors, can be regulated. The reason for this is that the DC bus voltage will decrease while these DC bus capacitors provide energy to the load side and energy storage side. Therefore the voltage source behind the inductor has to provide

the proper amount of energy to support the DC bus voltage such that the DC bus voltage can be kept constant. The reason why DC bus voltage has to be kept constant will be elaborated later.

The third part is exactly the same as the second part, which consists of one voltage source, one inductor L_1, and two switches, SPP_1 and SPP_2. However, the purpose of the third part is that it will integrate another renewable energy source and regulate its output power at a fixed value, which is specified by the central controller. If this renewable energy source is a voltage source, the power from this source can be controlled by controlling the current flowing in the inductor L_1. If the source is a current source, the inductor L_1 has to be removed and the power can be controlled by duty ratio(D) control. The power of the third part can be calculated with the following equations:

$$P_{in1} = V_{in1} \cdot I_{L1} \qquad \text{for voltage source} \qquad (4.6)$$

$$P_{in1} = (DV_{DC}) \cdot I_{in1} \qquad \text{for current source} \qquad (4.7)$$

C. Design of Proposed Multi-port Power Converter

There are several components to be designed, including the transformer turn ratio, the leakage inductor of the transformer, the input inductors, the DC bus capacitor, the energy storage capacitor, the load filter capacitor, and the current rating and voltage rating of the switches.

Table IV shows the specs of the proposed circuit, which is given for the design process.

Table IV. Specs of the proposed circuit

parameter	symbol	value	unit
DC bus voltage	V_{DC}	108	Volt
Primary energy source voltage	V_{in0}	54	Volt
Auxiliary energy source voltage	V_{in1}	50	Volt
Energy storage capacitor voltage	V_C	54	Volt
Switching frequency	f_s	5	KHz
Load Power	P_{load}	1000 ±10%	Watt
Load Voltage	V_{load}	155∼115 (135)	Volt
Primary energy source power	P_{in0}	1000	Watt
Auxiliary energy source power	P_{in1}	500∼50 (300)	Watt

1.   Transformer Turn Ratios

To minimize the current on the leakage inductor of the transformer, the voltage on both side of the leakage inductor should be the same. This can be seen from the derivation in Appendix A. Therefore, the turn ratios are:

$$n_1 \quad = \quad \frac{135}{54} = 2.5 \tag{4.8}$$

$$n_2 \quad = \quad \frac{1}{1} = 1 \tag{4.9}$$

2.   Leakage Inductance of Transformer

Assume that all the load power is provided by the energy source, not from the energy storage capacitor. Therefore, P_{10} will be 1000 W. From Equation (4.1), the smaller the inductor L_{10} ,the greater the power transferred with the same phase ϕ_{10}. However, if the inductor is too small, the current rating of the inductor will be large.

A trade-off has to be made. Therefore, ϕ_{10} is designed to be around 20° when P_{10} is 1000 W. Then L_{10} can be found to be 30 μH. In the same way, L_{20} and L_{12} can be designed. From Eq. 3.7 to 3.21 , the value of l_1, l_1 and l_2 can be calculated.

3.   Output Filter Capacitor

The current flowing into the load side, which is port 1, has DC value and some harmonics. To have a constant load voltage, a filter capacitor needs to be connected in parallel with the load resistor. The conductances of these two components are:

$$G_{C_f} \;=\; -j2\pi f C_f \tag{4.10}$$

$$G_{R_{load}} \;=\; \frac{1}{R_{load}} \tag{4.11}$$

To filter out the harmonic current, G_{C_f} should be large enough at frequency f so that the harmonics of frequency f will flow into the filter capacitor C_f. In this way, there will be DC current flowing in the load resistor, making the load voltage almost constant. Since the switching frequency f_s is 5000 Hz, and R is about 18 Ω when the output power is 1000W, C_f is selected to be 1mF such that the conductance of C_f at the switching frequency is about 500 times the conductance of R.

4.   Input Inductor L_0, L_1

There are two requirements for designing the input inductors. First, the current ripple of inductor current should be small since the inductor current is the output current of the renewable energy sources. It is desirable for renewable energy sources to have small current ripple. However, since the inductor current is also a control variable controlled by the central controller, if the inductance is too large, it takes a longer time to change the inductor current, resulting in slow dynamics. There is a tradeoff to be made.

Since "constant-frequency control with turn-on at clock time" current control method is used, the switching time of the switches is not fixed. It depends on the current in the inductor. Therefore, the worst case design will be performed. The worst case is that the switch SP1 or SPP1 are turned on during the whole period. If the allowable current ripple for I_{L0} is 1A, the following equations is used:

$$\Delta I_{L0} = \frac{V_{in0}}{L_0}(\frac{1}{f_s})$$ (4.12)

The value of L_0 is designed to be 10mH.

The allowable current ripple for I_{L1} is 0.1 A. With the same method, the value of L_1 is 54mH.

5. DC Bus Capacitor C_{DC}

The DC bus voltage should remain at constant value. In triple active bridge, there will be some energy in the DC bus capacitor going into the other two ports, which are the load and the energy storage. In order to maintain the DC bus voltage, the renewable energy source has to provide the necessary energy to the DC bus capacitor. In the control mechanism that regulates the DC bus voltage, discussed in a later section, the energy provided by these energy sources is first stored in the input inductor L_0. Then this energy will be transferred to the DC bus capacitors by resonance. However, the resonance time constant is set much longer that the period of the switching speed of the switch. In this way, the DC bus voltage can be controlled without going through the entire cycle of resonance. The current in the inductor remains almost constant with some ripple while the voltage in the DC bus capacitor is regulated with some ripple. To have a stiff DC bus, the capacitance of the DC bus capacitors should be larger than the inductance of the input inductors. The ripple of the DC bus voltage will be smaller than the ripple of the inductor current. Therefore,

the capacitance of the DC bus capacitors is designed to be 0.1 F.

6. Energy Storage Capacitor

The size of the energy capacitor depends on several requirements: 1) the input power from the two renewable energy sources, 2) the load power, 3) the allowable range of voltage for energy storage capacitors. By using the concept of energy conversation, the size of energy capacitor can be designed.

The time of proper operation for different conditions can be calculated as follows:

$$T = \frac{\frac{1}{2}C(V_{cmax}^2 - V_{cmin}^2)}{P_{input-total} - P_{output} - P_{loss}} \tag{4.13}$$

Table V shows the duration of operation for different conditions, assuming that P_{in0} and P_{in1} are all constant. No central controller is used to control P_{in1}. In the table, if the time T is positive, it means the energy capacitor is being discharged, that is, providing energy. If the time T is negative, it means the energy capacitor is being charged, that is, absorbing energy.

7. Current and Voltage Rating of Switches

Because the inductor current in the energy source side is controlled by the current controller, which will be mentioned in the later section, the current rating of the switches SP1, SP2, SPP1, SPP2 is related to the current command range. The current rating of the switches connected to the transformer depends on the current flowing in the transformer. The current in the transformer depends on the phase differences and turn ratios. If the range of phase differences is known and the turn ratios are designed, the current flowing in the transformer can be found. As for the voltage rating, it depending on the voltage source to which the switches are connected to. Table VI summarizes the rating of all switches.

Table V. Operation time for different conditions

V_{load}=135 V, P_{in0}=1 kW, P_{in1}=100 W		
$P_{load} = 1200W$	$P_{load} = 1000W$	$P_{load} = 856.8W$
T = 7.7088s	T = -18.99s	T = -5.471s
V_{load}=155 V, P_{in0}=1 kW, P_{in1}=100 W		
$P_{load} =1582.7W$	$P_{load} =1318.2W$	$P_{load} = 1129.5W$
T = 2.0961s	T = 4.2252s	T = 15.35s
V_{load}=115 V, P_{in0}=1 kW, P_{in1}=100 W		
$P_{load} = 871.2W$	$P_{load} = 725.6W$	$P_{load} =621.7W$
T = -5.892 s	T = -3.3108 s	T =-2.5222 s

D.   Modeling of Proposed Multi-port Power Converter

The reason why modeling is important is that with the mathematical models, the controller of this power converter can be designed more efficiently, instead of using lots of trial and error. Also, with the mathematical models, some analysis can be done, such as stability issues at different operating points. The issue of stability will be discussed later.

Before modeling the circuit, there is one question we need to ask. What do we do with this circuit? The purpose of this circuit is to integrate two energy sources, one energy storage and one dynamic load. What do we mean by integrate? Here is the problem statement:

Under the influence of dynamic load, the load voltage V_{load} and the output power from the renewable energy sources P_{in0} and P_{in1} are regulated or controlled.

Table VI. Voltage rating and current rating of all switches

	voltage rating (V)	current rating (A)
SP1	V_{DC}	I_{L0}
SP2	V_{DC}	I_{L0}
SPP1	V_{DC}	I_{L1}
SPP2	V_{DC}	I_{L1}
SS14	$0.5\,V_{DC}$	150
SS23	$0.5\,V_{DC}$	150
SL1	V_{load}	60
SL2	V_{load}	60
SL3	V_{load}	60
SL4	V_{load}	60
SC1	V_C	150
SC2	V_C	150
SC3	V_C	150
SC4	V_C	150

This problem can be solved by controlling two variables: ϕ_{10} and ϕ_{20}. Two PI controllers will be used for ϕ_{10} and ϕ_{20}, and the feedback signals are load voltage,V_{load}, and the output power from the source side, P_0. Due to the above requirement, the mathematical models are needed between the V_{load} and ϕ_{10}, and between P_0 and ϕ_{20}.

In power electronics, state space averaging technique is widely used to derive transfer functions. However, in this work it can not be applied because the current of the leakage inductor of the transformer varies substantially. The large variation of current does not meet the requirement of state space averaging technique, where

it requires that all the state variables, including the voltage of capacitors and the current of inductors, should have small variation. Therefore, another method of deriving transfer functions has to be found.

Because the equation is non-linear, which will be seen shortly, the method of perturbation and linearization are used during the derivation of transfer functions.

1. Transfer Function of v_1

The power going into port 1, P_1, can be found as the sum of the power going into port 1 from port 0, P_{10}, and the power going into port 1 from port 2, P_{12}. P_{10} and P_{20} can be expressed as:

$$p_{10} = \frac{v_0 v_1}{\omega L_{10}} \phi_{10} (1 - \frac{\phi_{10}}{\pi}) \tag{4.14}$$

$$p_{12} = \frac{v_1 v_1}{\omega L_{12}} \phi_{12} (1 - \frac{\phi_{12}}{\pi}) \tag{4.15}$$

where v_1 and v_2 are the referred voltages to the primary side of the load voltage v_{load} and the energy storage capacitor voltage v_c.

From this equation, it can be seen that the system is a nonlinear system. In order to find the transfer function, perturbation and linearlization have to be applied.

Assuming that the operating points are:

$$v_0 = V_0$$

$$v_1 = V_1$$

$$v_2 = V_2$$

$$\phi_{10} = \Phi_{10}$$

$$\phi_{20} = \Phi_{20}$$

Now the perturbation signals are added into the above variables. Since v_0 is normally the constant in our application, there is no perturbation in v_0.

$$v_1 = V_1 + \tilde{v}_1$$

$$v_2 = V_2 + \tilde{v}_2$$

$$\phi_{10} = \Phi_{10} + \tilde{\phi}_{10}$$

$$\phi_{20} = \Phi_{20} + \tilde{\phi}_{20}$$

Therefore,

$$
\begin{aligned}
p_1 = p_{10} + p_{12} &= \frac{v_0 v_1}{\omega L_{10}} \phi_{10}(1 - \frac{\phi_{10}}{\pi}) + \frac{v_1 v_2}{\omega L_{12}} \phi_{12}(1 - \frac{\phi_{12}}{\pi}) \\
&= \left[\frac{V_0(V_1 + \tilde{v}_1)}{\omega L_{10}} \cdot (\Phi_{10} + \tilde{\phi}_{10}) \cdot (1 - \frac{\Phi_{10} + \tilde{\phi}_{10}}{\pi}) \right] \\
&\quad + \left[\frac{(V_1 + \tilde{v}_1)(V_2 + \tilde{v}_2)}{\omega L_{12}} \cdot (\Phi_{10} - \Phi_{20} + \tilde{\phi}_{10} - \tilde{\phi}_{20}) \cdot (1 - \frac{\Phi_{10} - \Phi_{20} + \tilde{\phi}_{10} - \tilde{\phi}_{20}}{\pi}) \right] \\
&= \left(\frac{V_0 V_1}{\omega L_{10}} \Phi_{10} + \frac{V_0 V_1}{\omega L_{10}} \tilde{\phi}_{10} + \frac{V_0 \tilde{v}_1}{\omega L_{10}} \Phi_{10} + \frac{V_0 \tilde{v}_1}{\omega L_{10}} \tilde{\phi}_{10} \right] \\
&\quad - \left[\frac{V_0 V_1}{\omega L_{10}} \Phi_{10} + \frac{V_0 V_1}{\omega L_{10}} \tilde{\phi}_{10} + \frac{V_0 \tilde{v}_1}{\omega L_{10}} \Phi_{10} + \frac{V_0 \tilde{v}_1}{\omega L_{10}} \tilde{\phi}_{10} \right] \cdot \frac{\Phi_{10}}{\pi} \\
&\quad - \left[\frac{V_0 V_1}{\omega L_{10}} \Phi_{10} + \frac{V_0 V_1}{\omega L_{10}} \tilde{\phi}_{10} + \frac{V_0 \tilde{v}_1}{\omega L_{10}} \Phi_{10} + \frac{V_0 \tilde{v}_1}{\omega L_{10}} \tilde{\phi}_{10} \right] \cdot \frac{\tilde{\phi}_{10}}{\pi} \right) \\
&\quad + \frac{V_1 V_2 + V_1 \tilde{v}_2 + V_2 \tilde{v}_1 + \tilde{v}_1 \tilde{v}_2}{\omega L_{12}} [\Phi_{10} - \Phi_{20} + \tilde{\phi}_{10} - \tilde{\phi}_{20}] \\
&\quad + \frac{V_1 V_2 + V_1 \tilde{v}_2 + V_2 \tilde{v}_1 + \tilde{v}_1 \tilde{v}_2}{\omega L_{12} \pi} [\Phi_{10} - \Phi_{20} + \tilde{\phi}_{10} - \tilde{\phi}_{20}]^2
\end{aligned}
$$

After simplification and reduction, the following can be found:

$$
\begin{aligned}
\tilde{p}_1 &= \left[(\frac{V_0 \Phi_{10}}{\omega L_{10}} - \frac{V_0 \Phi_{10}^2}{\omega L_{10} \pi}) + (\frac{\Phi_{10} - \Phi_{20}}{\omega L_{12}} + \frac{(\Phi_{10} - \Phi_{20})^2}{\omega L_{12} \pi}) V_2 \right] \tilde{v}_1 \qquad (4.16) \\
&\quad + \left[(\frac{V_0 V_1}{\omega L_{10}} - \frac{2 V_0 V_1 \Phi_{10}}{\omega L_{10} \pi}) + \frac{V_1 V_2}{\omega L_{12}} - \frac{2 V_1 V_2 (\Phi_{10} - \Phi_{20})}{\omega L_{12} \pi} \right] \tilde{\phi}_{10} \\
&\quad + \left[\frac{\Phi_{10} - \Phi_{20}}{\omega L_{12}} V_1 - \frac{(\Phi_{10} - \Phi_{20})^2}{\omega L_{12} \pi} V_1 \right] \tilde{v}_2 \\
&\quad + \left[\frac{-V_1 V_2}{\omega L_{12}} + \frac{2 V_1 V_2 (\Phi_{10} - \Phi_{20})}{\omega L_{12} \pi} \right] \tilde{\phi}_{20} \\
&= a \cdot \tilde{v}_1 + b \cdot \tilde{phi}_{10} + c \cdot \tilde{v}_2 + D \cdot \tilde{\phi}_{20}
\end{aligned}
$$

where

$$a(V_0, V_1, V_2, \Phi_{10}, \Phi_{20}) = (\frac{V_0 \Phi_{10}}{\omega L_{10}} - \frac{V_0 \Phi_{10}^2}{\omega L_{10} \pi}) + (\frac{\Phi_{10} - \Phi_{20}}{\omega L_{12}} + \frac{(\Phi_{10} - \Phi_{20})^2}{\omega L_{12} \pi})V_2 \quad (4.17)$$

$$b(V_0, V_1, V_2, \Phi_{10}, \Phi_{20}) = (\frac{V_0 V_1}{\omega L_{10}} - \frac{2V_0 V_1 \Phi_{10}}{\omega L_{10} \pi}) + \frac{V_1 V_2}{\omega L_{12}} - \frac{2V_1 V_2 (\Phi_{10} - \Phi_{20})}{\omega L_{12} \pi} \quad (4.18)$$

$$c(V_0, V_1, V_2, \Phi_{10}, \Phi_{20}) = \frac{\Phi_{10} - \Phi_{20}}{\omega L_{12}} V_1 - \frac{(\Phi_{10} - \Phi_{20})^2}{\omega L_{12} \pi} V_1 \quad (4.19)$$

$$d(V_0, V_1, V_2, \Phi_{10}, \Phi_{20}) = \frac{-V_1 V_2}{\omega L_{12}} + \frac{2V_1 V_2 (\Phi_{10} - \Phi_{20})}{\omega L_{12} \pi} \quad (4.20)$$

On the other hand, the power going into the load side P_1 can also be expressed as:

$$p_1 = P_1 + \tilde{p}_1 = \frac{(V_1 + \tilde{v}_1)^2}{R} + \frac{d}{dt}(\frac{1}{2}C_f \cdot (V_1 + \tilde{v}_1)^2) \quad (4.21)$$

After simplification, $\tilde{p}_1$ can be expressed as:

$$\tilde{p}_1 = \frac{2V_1}{R}\tilde{v}_1 + C_f V_1 \frac{d}{dt}\tilde{v}_1 \quad (4.22)$$

Using the Laplace transform, the above equation can be written as:

$$\tilde{p}_1 = \frac{2V_1}{R}\tilde{v}_1 + s \cdot C_f V_1 \tilde{v}_1 \quad (4.23)$$

$$= (s \cdot C_f V_1 + \frac{2V_1}{R})\tilde{v}_1$$

From (4.16) and (4.23), $\tilde{v}_1$ can be expressed as:

$$\tilde{v}_1 = \frac{b}{s \cdot C_f V_1 + \frac{2V_1}{R} - a} \cdot \tilde{\phi}_{10} + \frac{d}{s \cdot C_f V_1 + \frac{2V_1}{R} - a} \cdot \tilde{\phi}_{20} + \frac{c}{s \cdot C_f V_1 + \frac{2V_1}{R} - a} \cdot \tilde{v}_2$$

$$(4.24)$$

$$= A \cdot \tilde{\phi}_{10} + B \cdot \tilde{\phi}_{20} + C \cdot \tilde{v}_2 \quad (4.25)$$

2. Transfer Function of P_0

In the similar way, the transfer function of P_0 can be derived as follows:

$$p_0 = p_{10} + p_{20} = \frac{v_0 v_1}{\omega L_{10}} \phi_{10}(1 - \frac{\phi_{10}}{\pi}) + \frac{v_0 v_2}{\omega L_{20}} \phi_{12}(1 - \frac{\phi_{20}}{\pi})$$

$$= [\frac{V_0(V_1 + \tilde{v}_1)}{\omega L_{10}} \cdot (\Phi_{10} + \tilde{\phi}_{10}) \cdot (1 - \frac{\Phi_{10} + \tilde{\phi}_{10}}{\pi})]$$

$$+ [\frac{V_0(V_2 + \tilde{v}_2)}{\omega L_{20}} \cdot (\Phi_{20} + \tilde{\phi}_{20}) \cdot (1 - \frac{\Phi_{20} + \tilde{\phi}_{20}}{\pi})]$$

After the simplification and reduction, we get,

$$\tilde{p}_0 = [\frac{V_0\Phi_{10}}{\omega L_{10}} - \frac{V_0\Phi_{10}^2}{\omega L_{10}\pi}] \cdot \tilde{v}_1 + [\frac{V_0 V_1}{\omega L_{10}} - \frac{2\Phi_{10}V_0 V_1}{\omega L_{10}\pi}] \cdot \tilde{\phi}_{10} \tag{4.26}$$

$$+ [\frac{V_0\Phi_{20}}{\omega L_{20}} - \frac{V_0\Phi_{20}^2}{\omega L_{20}\pi}] \cdot \tilde{v}_2 + [\frac{V_0 V_2}{\omega L_{20}} - \frac{2\Phi_{20}V_0 V_2}{\omega L_{20}\pi}] \cdot \tilde{\phi}_{20}$$

$$= D \cdot \tilde{v}_1 + E \cdot \tilde{\phi}_{10} + F \cdot \tilde{v}_2 + G \cdot \tilde{\phi}_{20}$$

where

$$D(V_0, V_1, V_2, \Phi_{10}, \Phi_{20}) = \frac{V_0\Phi_{10}}{\omega L_{10}} - \frac{V_0\Phi_{10}^2}{\omega L_{10}\pi} \tag{4.27}$$

$$E(V_0, V_1, V_2, \Phi_{10}, \Phi_{20}) = \frac{V_0 V_1}{\omega L_{10}} - \frac{2\Phi_{10}V_0 V_1}{\omega L_{10}\pi} \tag{4.28}$$

$$F(V_0, V_1, V_2, \Phi_{10}, \Phi_{20}) = \frac{V_0\Phi_{20}}{\omega L_{20}} - \frac{V_0\Phi_{20}^2}{\omega L_{20}\pi} \tag{4.29}$$

$$G(V_0, V_1, V_2, \Phi_{10}, \Phi_{20}) = \frac{V_0 V_2}{\omega L_{20}} - \frac{2\Phi_{20}V_0 V_2}{\omega L_{20}\pi} \tag{4.30}$$

In (4.24) and (4.26), there are two points worthy of attention. First, the relationship between $\tilde{v}_{load}$ and $\tilde{\phi}_{10}$ and the relationship between $\tilde{p}_0$ and $\tilde{\phi}_{20}$ are not simple. They are coupled. $\tilde{\phi}_{20}$, $\tilde{v}_2$ have effect on $\tilde{v}_1$. Also, $\tilde{\phi}_{10}$, $\tilde{v}_1$ and $\tilde{v}_2$ also have impact on $\tilde{p}_0$. Fig 34 shows the coupling between the variables.

Secondly, the coefficients in (4.24) and (4.26) depend on the operating points V_0, V_1, V_2, Φ_{10} and Φ_{20}. These coefficients change as the operating points change. In
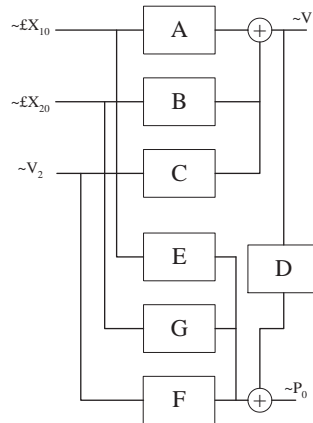
Fig. 34. Transfer function of the system

order to use these transfer functions, the operating points have to be found first.

3.   How to Find the Operating Point

In normal operation, the power from port 0 will be equal to the power into port 1. In other word, the power into the energy storage C from the source side will be equal to the power into the load side from the energy storage C. The net power of C is zero. The above condition can be expressed as follows:

$$P_1 = P_0$$

$$P_{20} = P_{12}$$

We can see from Fig 35 that P_1 consist of two part: one is P_{10}, the other is P_{12}. We have to find out the ratio of P_{10} to P_{12} so that the operating point Φ_{10} and Φ_{20} can be calculated.

The given value will be P_1 and we need to find the ratio Q. First, we set the ratio
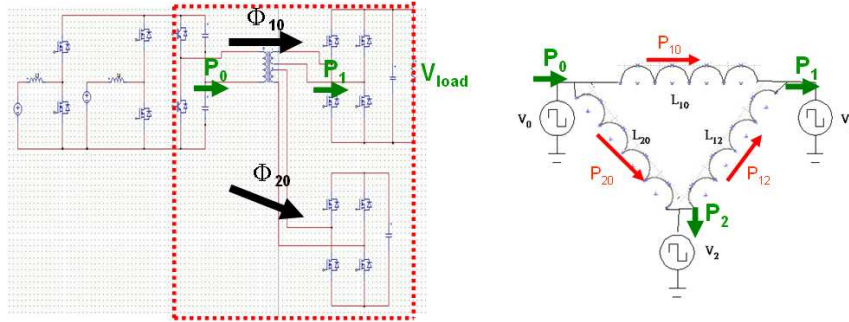
Fig. 35. Power flow between 3 ports

Q as 1. Then P_{10} can be found as:

$$P_{10} = P_1 \cdot Q = \frac{V_0 V_1}{\omega L_{10}} \Phi_{10}(1 - \frac{\Phi_{10}}{\pi})$$

Φ_{10} can be solved.

As soon as Φ_{10} is found, Φ_{20} can be solved from the following equation:

$$P_{20} = P_{12}$$

$$\frac{V_2 V_0}{\omega L_{20}} \Phi_{20}(1 - \frac{\Phi_{20}}{\pi}) = \frac{V_1 V_0}{\omega L_{12}}(\Phi_{10} - \Phi_{20})(1 - \frac{\Phi_{10} - \Phi_{20}}{\pi})$$

When both Φ_{10} and Φ_{20} are known, P_1 can be calculated from:

$$P_{1-cal} = P_{10} + P_{12}$$
$$= \frac{V_0 V_1}{\omega L_{10}} \phi_{10}(1 - \frac{\phi_{10}}{\pi}) + \frac{V_1 V_2}{\omega L_{12}} \phi_{12}(1 - \frac{\phi_{12}}{\pi})$$

Compare P_{1-cal} and P_1. If the error is not within the limit, decrease the ratio Q and do the above procedure again till the error is within the satisfactory range. The flow chart of finding the operating point is shown in Fig 36.
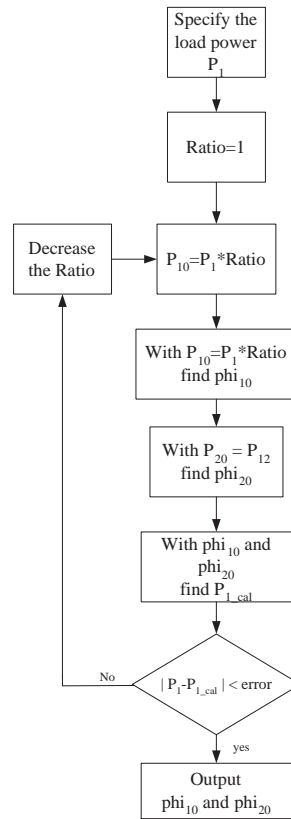
Fig. 36. Flow chart for finding operating point: Φ_{10} and Φ_{20}

E. Control of Proposed Multi-port Power Converter

After the model of the system is obtained, the controllers can be designed. In this proposed circuit, there are several things to be controlled. The purpose of the control is, under the influence of dynamic load, to 1) regulate or control the load voltage V_{load} and 2) regulate or control the input power from these two renewable energy sources. To achieve this purpose, there are several controls that need to be done. The first one is to use ϕ_{10} and ϕ_{20} to control the load voltage, V_{load}, and the input power from the primary side, P_0. The second one is to regulate the DC bus voltage, V_{DC}. The third one is to control the current, I_{L0} and I_{L1}, flowing in the two

energy sources. How to design the controller for ϕ_{10} and ϕ_{20}, how to regulate V_{DC}, and how to control I_{L0} and I_{L1} will be discussed in the section.

1. Controller Design for ϕ_{10} and ϕ_{20}

The transfer functions of ϕ_{10} to V_{load} and of ϕ_{20} to P_0 were found in the previous section. However, the transfer functions are complicated. They are coupled, and their coefficients depend on the operating points. It seems like the system is hard to control.

However, if the operation points are found according to the normal operation, where V_{load} is 135V, P_0 is 1000 W, the coefficient of these transfer functions can be found. Fig. 37 shows the transfer functions when the system operates at normal operation.
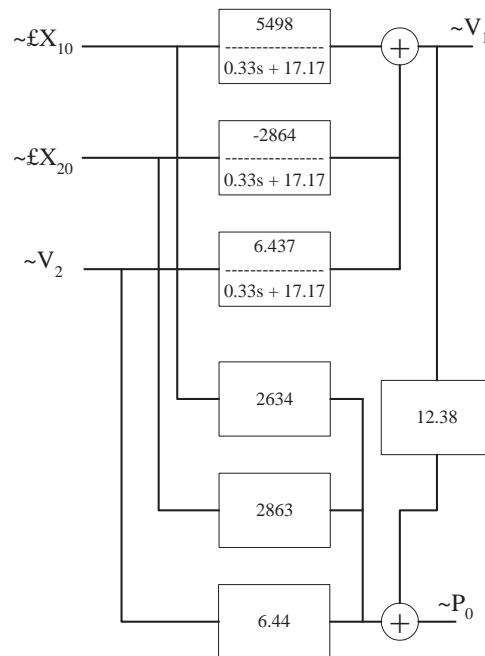
Fig. 37. Transfer function of TAB under normal condition

From this graph, it can be seen that some coefficients are much larger than other coefficients. Therefore, it is logical to say some variables are more influential than some other variables. In this case, the coefficient of the transfer function from $\tilde{v}_2$ to $\tilde{v}_1$ is much smaller than that from $\tilde{\phi}_{10}$ to $\tilde{v}_1$ and from $\tilde{\phi}_{20}$ to $\tilde{v}_1$. Also, the coefficient of the transfer function from $\tilde{v}_2$ to $\tilde{p}_0$ and from $\tilde{v}_1$ to $\tilde{p}_0$ is much smaller than that from $\tilde{\phi}_{10}$ to $\tilde{p}_0$ and from $\tilde{\phi}_{20}$ to $\tilde{p}_0$. Therefore, the impact of $\tilde{v}_2$ on $\tilde{v}_1$ and $\tilde{p}_0$ can be ignored. The above arguments simplified the transfer functions of the system as shown in Fig 38.
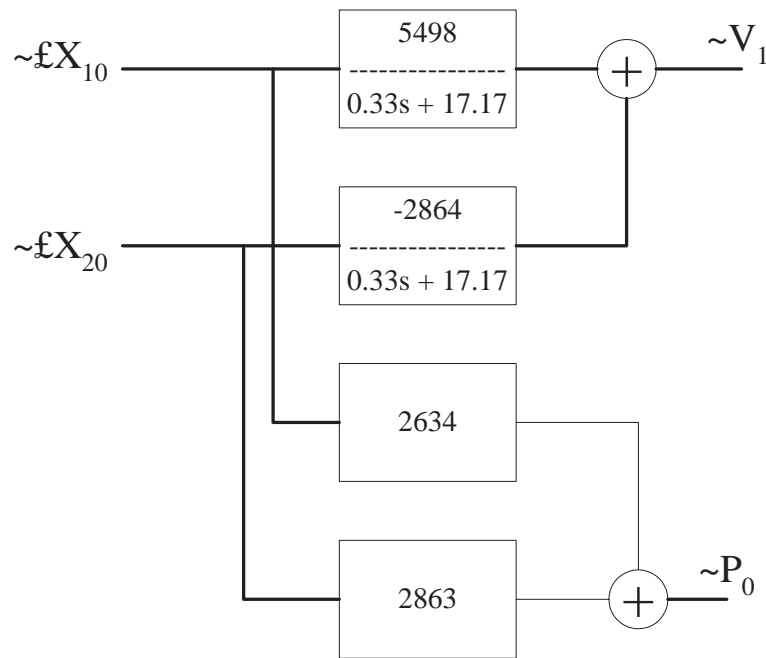
Fig. 38. Simplified transfer function of TAB

Since the simplified transfer functions are obtained, it is possible to design the controllers to meet certain performance requirements. However, due to the coupling, it is hard to design controllers by using conventional methods. Most designing methods are for single-input-single-output systems. There are many literatures on how

to design controllers for multi-input-multi-output coupled systems. In this work the method, proposed by He, Mao-Jun [22], is adopted. The procedure for this method is shown in Fig 39. The concept is simple. In this method, the controllers are designed, first, without considering the effect of coupling. Then, depending on the effects of coupling between variables, the procedure detunes the parameters of these controllers to make the system stable. The effects of coupling between variables are measured by the matrix called dRI. This method ensures this feedback system be stable.

Fig. 39. Design procedure for coupled systems

Due to the conservativeness of this method, the performance of the system is not optimal. Therefore, several fine-tunings have to be done. In conclusion, this method is used to get the approximate value of the parameters of these controllers, which will

facilitate the design process.

2. Current Control

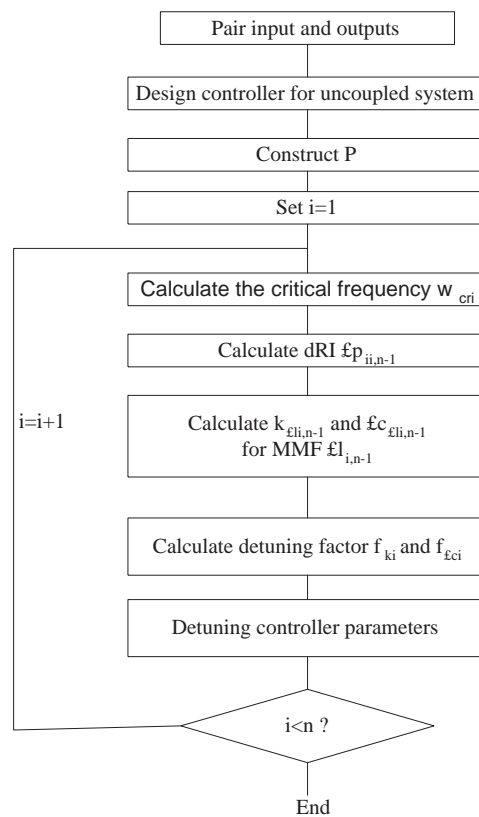There are several methods to control the current flowing in the inductors, including:

- Tolerance band control,

- Constant-off time control,

- Constant-frequency control with turn-on at clock time.

The method adopted in this work is constant-frequency current control. The benefits is that the operation frequency is fixed, which makes designing the filter easier compared to the other methods of current control. [23]

When the time is at clock time, the switche, SP2 or SPP2, is turned on. As soon as the current reaches the specified value, the switche, SP2 or SPP2, is turned off and switche, SP1 or SPP1, is turned on. This will result in the decrease of the current. This will last during the rest of the period. Till the time is at clock time, SP1 or SPP1 is turned off and SP2 or SPP2 is turned on again. Then the procedure repeats.

Fig. 40 shows the circuit when switches are turned on and off. Fig. 41 shows the current waveform during the current control, and Equation 4.31 and 4.32 describe the mathematical equations for these two different configurations.

$$\frac{dI_L}{dt} = \frac{V_{in}}{L} \qquad \qquad \text{when SP2 or SPP2 are turned on} \qquad (4.31)$$

$$\frac{dI_L}{dt} = \frac{V_{in} - V_{DC}}{L} \qquad \qquad \text{when SP1 or SPP1 are turned on} \qquad (4.32)$$
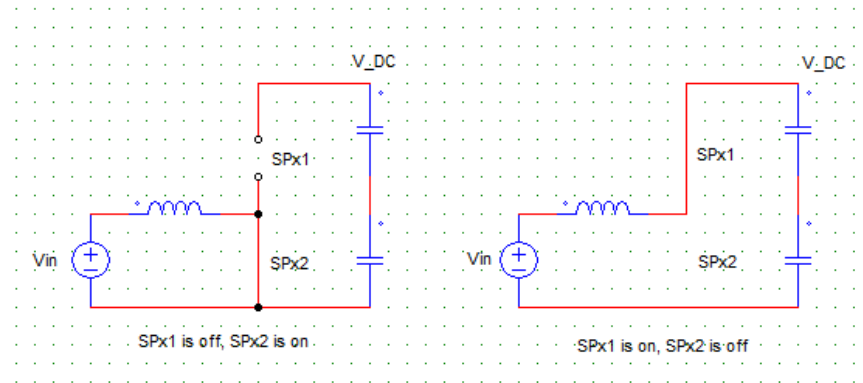
Fig. 40. Inductor circuit during different time period
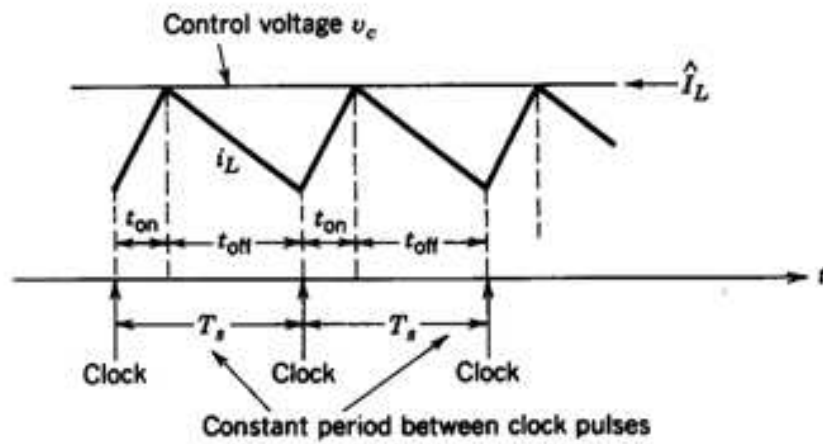
Fig. 41. Current waveform during the current control [23]

3. DC Bus Voltage Regulation

To regulate the DC bus voltage, the proposed system uses the switches, SP1 and SP2, on the primary energy source. In this part of the circuit, shown in Fig. 42, there are one voltage source, one inductor, two switches and two DC bus capacitors. There are two ways to regulate the DC bus voltage. One is to use duty ratio control. The other is to use current control. For duty ratio control, the DC bus voltage can be regulated by controlling the duty ratio of the switches. From the analysis of power
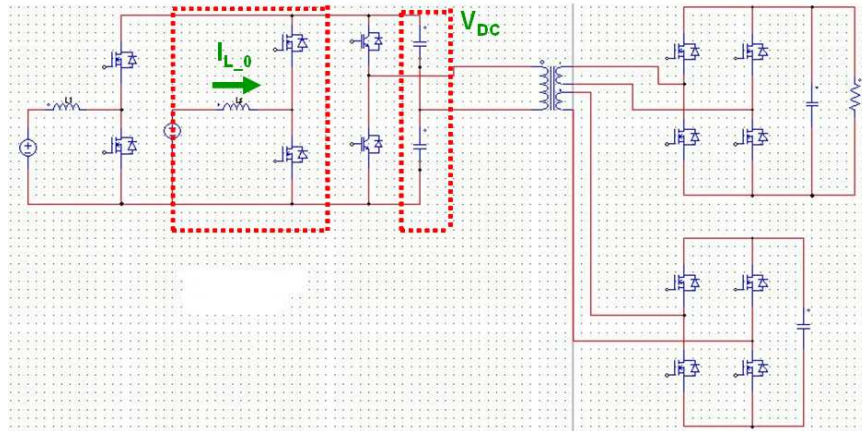
Fig. 42. DC regulation circuit

electronics, the voltage gain for this circuit can be expressed as follows:

$$\frac{V_{DC}}{V_{in1}} = \frac{1}{1 - D} \qquad (4.33)$$

where D is the ratio of time to the period when SP2 is on.

With the feedback signal of V_{DC}, one PI controller is used to give the duty ratio command D to regulate the DC bus voltage. However, there are several shortcomings for this method. The dynamic response is slow compared to the current control method. Another shortcoming is that the current in the inductor may be large, depending on the value of D. If the dynamics of PI is fast to strictly regulate the DC bus voltage, the inductor current may be large, which is undesirable.

Another way to regulate the DC bus voltage is to use current control. The inductor current is controlled by the method of constant-frequency control with turn-on at clock time, as discussed in previous section. The current command is given by the PI controller whose input signal is the reference DC bus voltage, and the feedback signal of the PI controller is the DC bus voltage. After the PI controller, a limiter is inserted before the current command goes into the current controller. With the

limiter, the peak inductor current can be confined. This method has better dynamic performance, and ensures the current be within the allowable range as well. Fig. 43 shows the block diagram for the DC bus regulation.
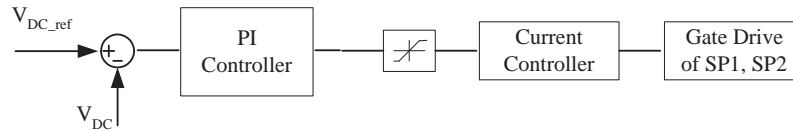
Fig. 43. Block diagram for DC voltage regulation

4. Control Strategy for Different Set of Switches

There are 14 switches in the proposed circuit. The switches on the load side are SL1, SL2, SL3, and SL4. The switches on the energy storage side are SC1, SC2, SC3, and SC4. The switches on the source side can be categorized into three groups: SS14 and SS23 connecting the DC bus capacitor with the transformer; SP1 and SP2 connecting the primary energy source; and SPP1 and SPP2 connecting the auxiliary energy source.

The control variables ϕ_{10} and ϕ_{20} control the gating signals of SS14, SS23, SL1, SL2, SL3, SL4, SC1, SC2, SC3 and SC4. The hysteresis control of input power P_{in1} controls the gating signals of SPP1 and SPP2. But what control strategy is applied to SP1 and SP2?

From the transfer functions of the proposed circuit, the feedback signal for ϕ_{20} control loop should be the signal of P_0. However, the value of P_0 can not be measured easily. Since the current flowing in the primary side of the transformer is oscillating tremendously, it will be hard to find the average value of this current, which means it will be hard to find the average power from the primary side. Even if it is possible to measure the exact P_0 and by feedback control, ϕ_{20} is controlled such that P_0 is

regulated, it is possible that P_{in0} is not regulated. Since

$$P_0 = P_{in0} + P_{in1} + P_c \tag{4.34}$$

If the DC bus voltage is not regulated, the value of P_c depends on the DC bus voltage and its rate of change. This can be seen from the energy and power of the DC bus capacitors:

$$E_c = \frac{1}{2}C \cdot V_{DC}^2 \tag{4.35}$$

and

$$P_c = \frac{d}{dt}E_c = C \cdot V_{DC} \cdot \frac{dV_{DC}}{dt} \tag{4.36}$$

Therefore, the proposed control strategy will control the switch SP1 and SP2 to regulate the DC bus voltage, V_{DC}, such that P_c is almost zero. That is

$$P_c \cong 0 \tag{4.37}$$

Also, the input power of the auxiliary source, P_{in1} is regulated at constant value K by hysteresis control.

$$P_{in1} = K(\text{constant}) \tag{4.38}$$

Therefore, P_0 can be expressed as follows:

$$P_0 = P_{in0} + K \tag{4.39}$$

From the above equation, it can been seen that P_{in0} can be controlled by P_0. Since P_0 is controlled by ϕ_{20}, P_{in0} can be indirectly controlled by ϕ_{20}. This is the reason why the proposed control strategy uses P_{in0} as the feedback signal for the ϕ_{20} control loop.

Table VII. The dependence of switches

Switches	Dependence
SS14, SS23 , SL1, SL2, SL3, SL4	ϕ_{10}
SC1, SC2, SC3, SC4	ϕ_{20}
SP1, SP2	DC bus voltage regulation
SPP1, SPP2	input power P_{in1} regulation

Table VIII. The feedback signal for different control variables

Feedback signal	Controller
V_{load}	ϕ_{10}
P_{10}	ϕ_{20}

Table VII summarizes the control of all switches, and Table VIII lists the feedback signal for ϕ_{10} and ϕ_{20}.

5. Benefits of PI Controller

In this work, the operating points are found at first and, based on the operating points, the controllers are designed. Because perturbation and linearlization are used to derive the transfer functions of the system, the signal input for these transfer functions should be small signals, namely, $\tilde{v}_{load}$ and $\tilde{p}_{10}$.

However, the input to the phase shifting controllers is the whole signal, consisting of the DC signal and the small signal. The DC signals are Φ_{10} and Φ_{20} while the small signals are $\tilde{\phi}_{10}$ and $\tilde{\phi}_{20}$. The DC signals have to be derived first from the operating points and then are added with small signals to produce the whole signals for the phase shifting controllers.

There are two interesting points in the actual implementation of control. Since it is impossible to get the small signals, which are $\tilde{v_{load}}$ and $\tilde{p_{10}}$, as the feedback signals. The feedback signals are the whole signals, which are v_{load} and p_{10}. Therefore, the reference signal to the feedback controller should be the reference DC signal, not 0. This is shown in Fig. 44.
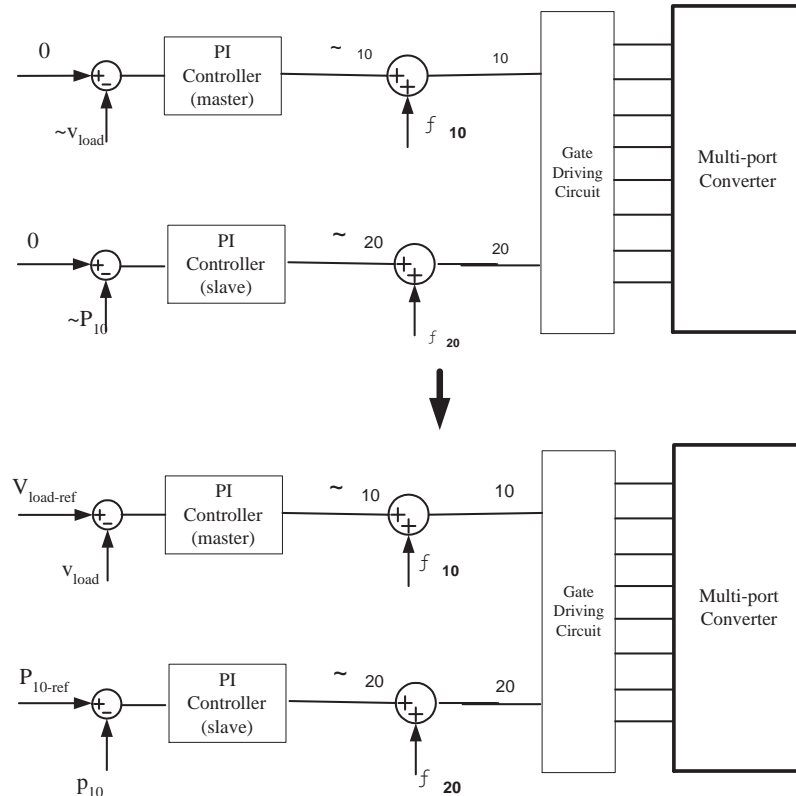
Fig. 44. Signals for the feedback system

Another point worth mentioning is that Φ_{10} and Φ_{20} do not have to be calculated precisely. Because of the integrator in the PI controllers, the PI controllers produce proper value such that the whole signals ϕ_{10} and ϕ_{20} are correct for current operating points. Because of the PI controllers, it is possible to go from one operating point to another. Even though the value Φ_{10} and Φ_{20} are not correct for these different

operating points, the PI controllers will adjust $\tilde{\phi}_{10}$ and $\tilde{\phi}_{20}$ such that these two signals contain certain DC values to give the correct whole signals for these different operating points.

The only difference between having correct or incorrect value of Φ_{10} and Φ_{20} is the time to reach steady state. If Φ_{10} and Φ_{20} are correct, it takes less time to reach steady states. While Φ_{10} and Φ_{20} are incorrect, it takes longer time to reach steady states.

F. Central Controller

In addition to the controller that controls the phases, ϕ_{10} and ϕ_{20}, there is a central controller in the proposed system. The central controller does the following tasks.

- Gives control signal during the start-up process of the circuit

- Gives the power command to the auxiliary energy source

- Selects the controller for different load voltages

1. Starting of the Circuit

Before the circuit enters the normal operation, the circuit has to be started first. During the start-up of the circuit, the central controller controls ϕ_{10} and ϕ_{20} to determine the power flow among the three ports. Also the central controller will send the gating signals to the switches of the proposed circuit. By controlling these switches, we can open or close some of the ports, which is very important during the starting procedure.

There are two cases for starting. In the first case, some energy storage components have been energized, including the DC bus capacitors and the energy storage

capacitor. This scenario may be encountered when the circuit is connected to the grid, and there are some external circuits that pre-charge these capacitors. In the second case, all the energy storage components are relaxed. No energy is stored in these components. This scenario may be encountered when the circuit is stand-alone. All the energy is provided by renewable energy sources, and no external energy sources or charging circuits exist.

Some components are energized

Before the circuit is started, the voltage of the DC bus capacitors, V_{DC}, and the voltage of the energy storage capacitor, V_C, are set up, which is easily done by first charging these capacitors to specified voltages by external circuits and connecting these capacitors to the proposed circuit. Except the above components, all other components are relaxed. These components including the filter capacitor, C_{load}, the input inductors, L_0 and L_1, the leakage inductance of the transformer, $L_{leakage}$. The following shows the state before starting the circuit.

$$V_{DC} = 108 \text{ V}$$

$$V_C = 54 \text{ V}$$

$$V_{load} = 0 \text{ V}$$

$$I_{L0} = 0 \text{ A}$$

$$I_{L1} = 0 \text{ A}$$

$$I_{leakage} = 0 \text{ A}$$

During the starting of the circuit, ϕ_{10} is set at 40° and the switches on the energy storage side are all open. The above setting lets the power go from the energy source

side into the load side, charging the load capacitors. This value is constant, since ϕ_{10} is constant.

Because the inductor currents, I_{L0} and I_{L1}, are zero at the beginning, the current controllers of these two inductor currents close the switches SP2 and SPP2 to increase these two inductor currents linearly. During this period, the DC bus voltage decreases. This is because there is no energy supply from energy source and the two DC bus capacitors supply the energy to the load side, charging the load capacitor. As soon as the inductor currents reach the specified values, the hysteresis control of current will begin to be executed.

When the capacitor on the load side is charged to specified value, the starting process ends and this circuit enters the normal state. The PI controllers, which control ϕ_{10}, ϕ_{20} and I_{L0-cmd}, begin to function and the circuit of the energy storage side gets connected back to the system.

Fig. 45 shows the procedure during the starting of the circuit.

No components are energized

For an isolated power system, it is more practical to assume that all the components are relaxed in the beginning. There is no charger to charge the capacitors. Therefore, the energy sources of the proposed circuit have to charge these capacitors first before the circuit begins the normal operation.
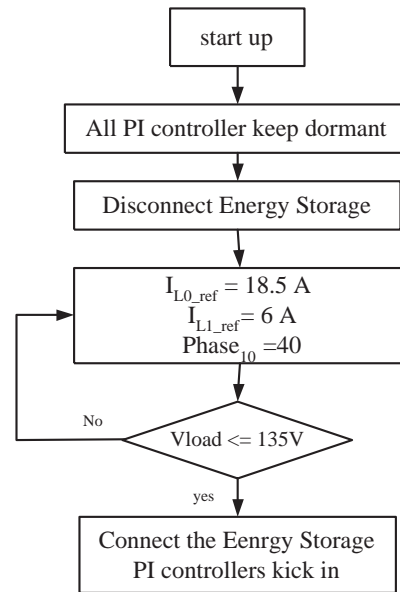
Fig. 45. Flow chart for starting the circuit

The following shows the state at the beginning.

$$V_{DC} = 0 \text{ V}$$

$$V_C = 0 \text{ V}$$

$$V_{load} = 0 \text{ V}$$

$$I_{L0} = 0 \text{ A}$$

$$I_{L1} = 0 \text{ A}$$

$$I_{leakage} = 0 \text{ A}$$

First, assume that the voltages of the renewable energy sources are rising linearly with time in the beginning. After these voltages rise to certain value, they are constant afterward. This is more practical since it takes time for renewable energy sources to warm up. During the increase in the voltage of the renewable energy sources, the

inductor currents are also increasing due to current control. This step is quite similar to the previous case. During this period, DC bus capacitors are also being charged because the current of the inductors will flow into the DC bus capacitors.

As soon as the DC bus voltage reaches the specified level, the energy storage capacitor begins to be charged. During this period, ϕ_{20} is set at certain value and the secondary side of the transformer, which is connected to the load port, is shorted. The reason for shorting the secondary side of the transformer is that even though the gating signals for all IGBTs on the load side are open, there will be small current flowing into the load side via these diodes. This part of the circuit is like a current source rectifier, consisting of four diodes and a current source. As soon as the current flows into the load side, some power goes into the load side, which greatly increase the time required to charge the energy storage capacitors. There are two ways of shorting the secondary side of the transformer. One way is to use a bidirectional current switch, which is shown in Fig. 46. During charging the energy storage capacitor, this switch is conducting. The current flowing on the secondary side of the transformer will flow though this switch without providing power to the load side. Another method is by closing the switches SL1 and SL2 or SL3 and SL4. In this way, the current on the secondary side of the transformer will flowing in these two switches, without providing power to the load. In this way, the time to charge the energy storage capacitor will be greatly decreased.

There is another problem left. What is the value of ϕ_{20}? The value is hard to determine because when the energy storage capacitor is being charged, the power provided by the renewable energy sources, which is related to the inductor current, I_{L0} and I_{L1}, is flowing into the energy storage side. Since the power absorbed by the energy storage capacitor varies with the voltage of the energy storage capacitor V_c, it is impossible to find a constant value ϕ_{20} such that the power provided by
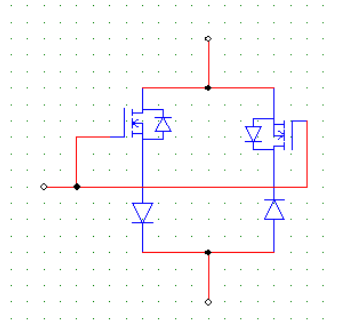
Fig. 46. Bidirectional current switch connected on load side

the renewable energy sources is equal to the power absorb by the energy storage capacitor. The power difference will cause the voltage fluctuation in the DC bus. That is, the power difference will go into the DC bus capacitor. This is not desirable. The constant voltage of DC bus is preferred for the proper operation of the proposed circuit.

To solve this problem,a PI controller is used to find ϕ_{20}. The feedback signal is the DC bus voltage, and output signal is ϕ_{20}. Since the larger ϕ_{20} is, the more power will go from the source side to energy storage side, which will decrease the DC bus voltage. Due to this relation, the coefficient of the PI controller needs to be negative. This will make the variation of DC bus voltage small during the charging of the energy storage capacitor.

As soon as the voltage of the energy storage capacitor reaches the specified level, the energy storage capacitor is disconnected from the proposed circuit by opening all the switches connecting the energy storage capacitor. ϕ_{10} is set at 40° to charge the filter capacitor on the load side. After the filter capacitor is charged, this circuit will enter the normal state. All PI controllers kick in and the energy storage capacitor is connected back to the circuit.

Fig. 47 summarizes the starting procedure.

```
┌─────────────────────┐
│      start up       │
└─────────────────────┘
           │
           ▼
┌─────────────────────────────┐
│ All PI controller keep dormant │
└─────────────────────────────┘
           │
           ▼
┌─────────────────────────────┐
│   Disconnect the load side   │
└─────────────────────────────┘
           │
           ▼
┌─────────────────────────────┐
│    Increase inductor currents │
│    Charge DC bus capacitor    │
└─────────────────────────────┘
           │
           ▼
┌───────────────────────────────────┐
│ Charge the energy storage capacitor │
└───────────────────────────────────┘
           │
           ▼
┌─────────────────────────────┐
│    Charge the load capacitor  │
└─────────────────────────────┘
           │
           ▼
┌─────────────────────────────┐
│  Connect the Eenrgy Storage  │
│   PI controllers kick in     │
└─────────────────────────────┘
```
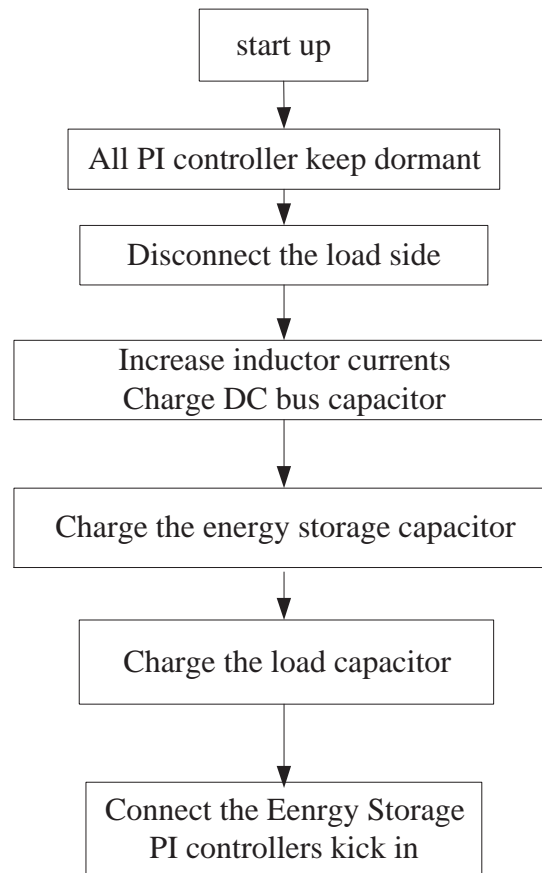
Fig. 47. Flow chart for starting the circuit with all components relaxed

2. Power Management

According to the voltage of the energy storage capacitor, V_C, the central controller will give the corresponding power command to the auxiliary energy source. If V_C is too high, the central controller will decrease the power command of the auxiliary energy source to decrease the total input power, discharging the energy storage capacitor. If V_C is too low, the central controller will increase the power command of the auxiliary energy source to increase the total input power, charging the energy storage capacitor.

There are three levels of the power command for auxiliary energy source: 500W,

300W and 50W. The ranges of V_C are 45-50, 50-60 and 60-65V. Intuitively, the corresponding input power command should be 500W(P_{max}), 300W (P_{normal}) and 50W (P_{min}) respectively. However, if we determine input power command just depending on what V_C is, there will be oscillation when the V_C is closed to the turning point. To solve this problem, not only the value of V_C, but also the current input power command have to be considered. For different current input and different power command for the auxiliary energy source, the new input power command will be different even if the V_C range is the same. Fig. 48 shows the corresponding input power command under different conditions.
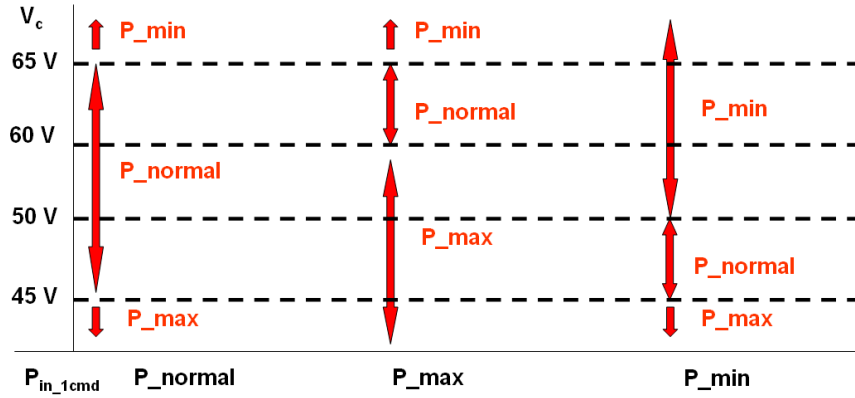

Fig. 48. Input power command P_{in1} for different conditions

3.   Controller Scheduling

The last thing the central controller does is to select the corresponding controller, depending on the load voltage, V_{load}. This is called "controller scheduling."

Up to this point, the control purpose of the proposed circuit is to regulate the load voltage, V_{load}. Is it possible that the load voltage can be controlled to be different value? This problem will be controlling problem, instead of regulating problem.

If the stability analysis, which will be discussed in the next section, is performed,

it can be seen that the stability is good for a range of V_{load}. If we sweeping the V_{load}, from 135V to 155V, the poles of the closed loop system will be on the left half plane. Therefore, the designed controller is able to control the load voltage without being unstable. However, because the controller is designed with the normal load voltage, which is 135V, the performance for different load voltage will be not as good as that for the case where load voltage is 135V.

In order to improve the performance for different load voltages, the concept of "controller scheduling" is used in this work. There are three sets of controller, which control the value of ϕ_{10} and ϕ_{20}. These three sets of controllers are designed for each different load voltage. Table IX shows the corresponding controller for each load voltage.

Table IX. Controller scheduling

Load voltage command	Controllers
115 V	C_{11}, C_{21}
135 V	C_{12}, C_{22}
155 V	C_{13}, C_{23}

The central controller will choose the corresponding controller, depending on the load voltage command. In this way, the dynamics for each load voltage command will be better. Fig 49 shows the block diagram for controller scheduling.

G. Stability Analysis

From (4.24) and (4.26), the coefficients depend on the operating points. For the dynamic load, the value of R is changing, resulting the change of the coefficients. Also, during the operation, the voltage of the energy storage capacitor, V_C, changes,
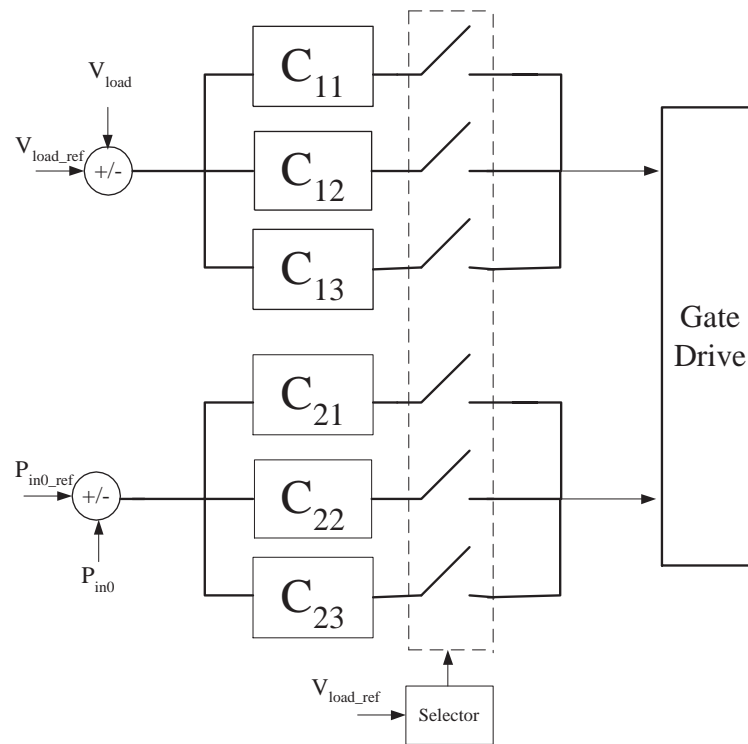
Fig. 49. Block diagram for controller scheduling

depending on the power difference between the source and the load. The question regarding the stability of the system arises. Will the change of R due to the dynamic load let the system be unstable?

Because of the cross-coupling of the transfer function, the traditional way to determine the stability due to the change of coefficient, such as Nyquist plot, Bode plot is not practical. Fortunately, with the power of modern computer technology, the poles of the system can be solved directly.

First, the transfer function of the coupled system need to be derived so that we can use the traditional method to determine the stability of the system

The coupled system is represented in Fig. 50. The system can be represented by Fig. 51. The function of g_1 and g_2 can be found by the following method.
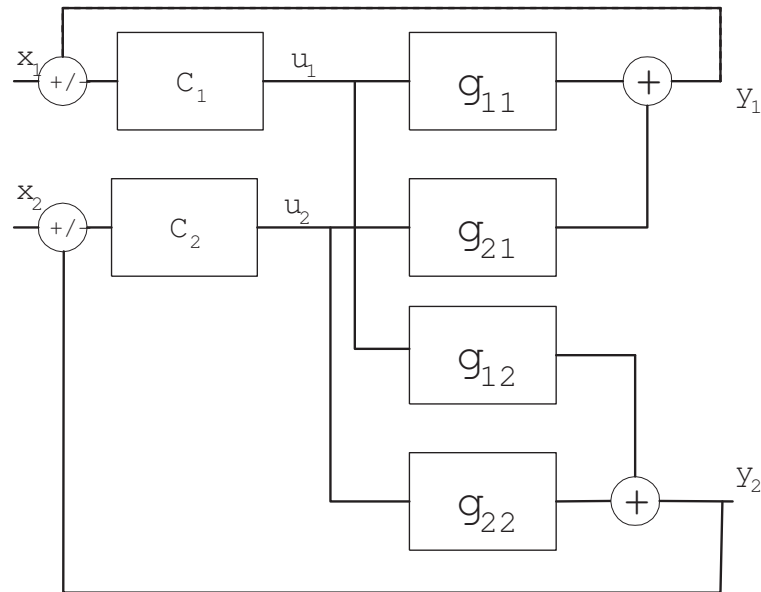
Fig. 50. Transfer functions of coupled system

Since

$$y_1 = u_1 \cdot g_{11} + u_2 \cdot g_{12} \tag{4.40}$$

$$y_2 = u_2 \cdot g_{22} + u_1 \cdot g_{21} \tag{4.41}$$

and

$$u_2 = -c_2 \cdot y_2 = -c_2 \cdot (u_2 \cdot g_{22} + u_1 \cdot g_{21})$$

Therefore,

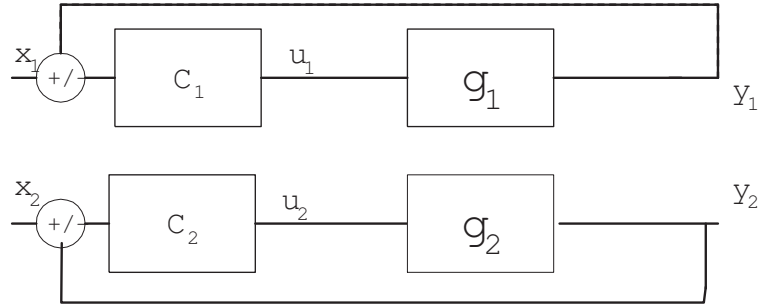$$u_2 = \frac{-c_2 \cdot g_{21}}{1 + c_2 \cdot g_{22}} \cdot u_1 \tag{4.42}$$

Fig. 51. Simplified transfer function of coupled system

Combining (4.40) and (4.42), we get

$$y_1 = (g_{11} + \frac{-c_2 \cdot g_{21} \cdot g_{12}}{1 + c_2 \cdot g_{22}})u_1 \tag{4.43}$$

$$= g_1 \cdot u_1$$

where

$$g_1 = g_{11} + \frac{-c_2 \cdot g_{21} \cdot g_{12}}{1 + c_2 \cdot g_{22}} \tag{4.44}$$

In the same way, we can found that

$$g_2 = g_{22} + \frac{-c_1 \cdot g_{21} \cdot g_{12}}{1 + c_1 \cdot g_{11}} \tag{4.45}$$

As soon as g_1 and g_2 are calculated, the characteristic equation of the feedback system can be found as:

$$\Phi_1(s) = 1 + c_1 \cdot g_1 = 0 \tag{4.46}$$

$$\Phi_2(s) = 1 + c_2 \cdot g_2 = 0 \tag{4.47}$$

The roots of the characteristic equations are the poles of the two feedback systems, which are for the load voltage regulation and for the input power regulation. In order

to be stable, these poles have to have negative real part.

During the operation of the circuit, the operating points changes. It is necessary to make sure that the system is stable during the operation. With the powerful calculation capability of modern computers, it is easy to find all the poles for this system by sweeping some variables. These variables include ϕ_{10}, ϕ_{20}, V_2, and R. By sweeping these variables in certain range, which depends on the actual operation, we can find the stability of the system. Fig. 52 shows the poles of the closed loop, where the sweep range for the variables are shown in Table X. In this graph, it can be seen that all poles are on the left half plane. Therefore, the system is stable even though the operating points changes during the operation of the circuit.

Table X. Sweeping range for variables

Variable	Sweeping Range
ϕ_{10}	0∼15 (Degree)
ϕ_{20}	0∼15 (Degree)
V_2	45∼65 (V)
R	15∼20 (Ω)

H.   Integration of Current Source

Some renewable energy sources have the characteristic of current sources. They will provide constant current while their output voltage varies. One example of renewable energy sources that has current source characteristics is photovoltaic cells.

The proposed circuit can integrate current source with little modification. Fig 53 shows the modified circuit. Assume that the current source provides I_{in1} current.
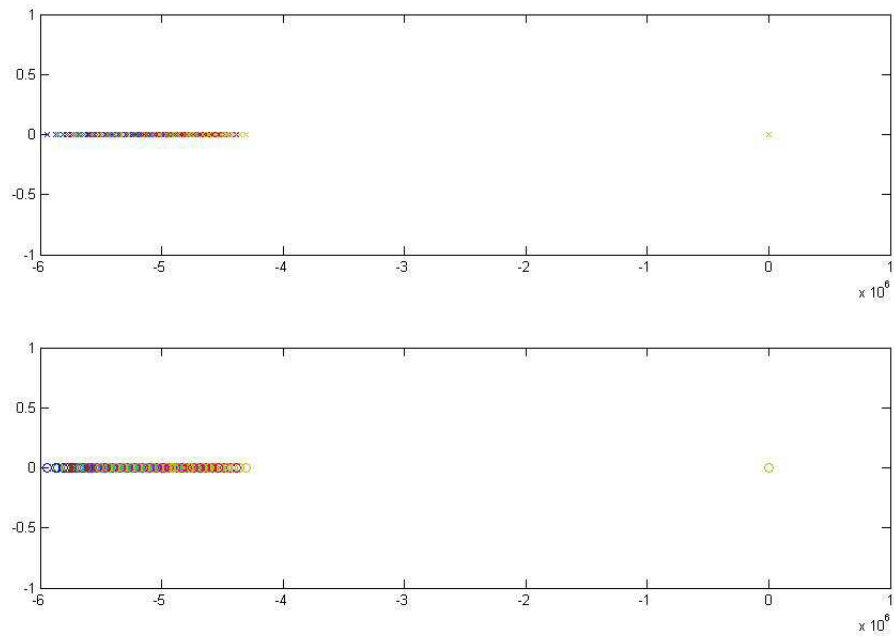
Fig. 52. The poles of closed loop transfer functions under the sweeping of variables

The power provided by the current source can be controlled by the duty ratio of SPP1 and SPP2. If the duty cycle is defined as the on time of SPP1, then the power from the current source can be expressed as:

$$P_{in1} = D \cdot I_{in1} \cdot V_{DC} \tag{4.48}$$

Since I_{in1} and V_{DC} are constant, the only way to control the power P_{in1} is to control D. Based on different power requirement, a table can be built to give the corresponding D. To improve the control dynamics, a PI controller can be used, whose feedback signal is power, while the output is duty ratio D. The block diagram is shown in Fig 54.
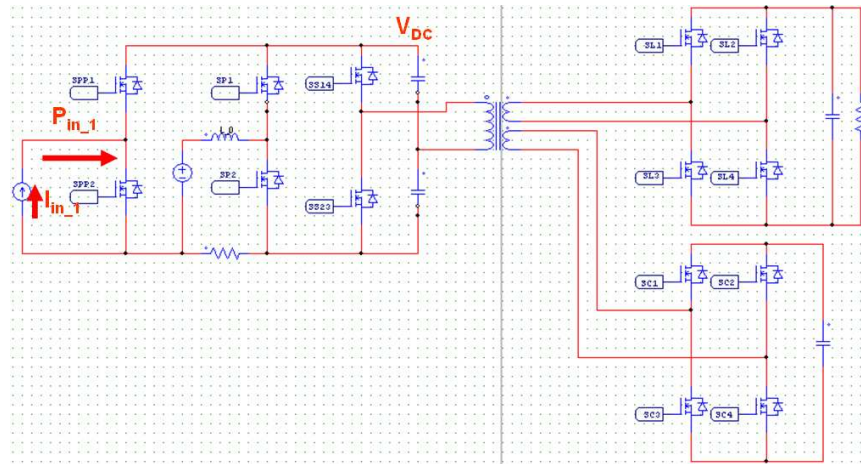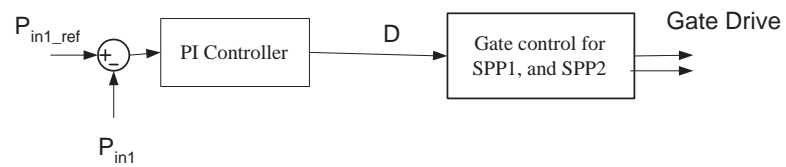
Fig. 53. Modified circuit to integrate current source

Fig. 54. Block diagram of P_{in1} control for current source

CHAPTER V

SIMULATION AND DISCUSSION

This chapter will present several simulations and discussion under different scenarios encountered in real application. In these simulations, the component values are the values designed in the previous chapter. The input voltage of the renewable energy source are 54V for V_{in0} and 50V for V_{in1}. The nominal output load voltage V_{load} is 135V and nominal input power, P_{in0}, is 1000W. The other input power, P_{in1}, is controlled by the central controller to charge or discharge the energy capacitor.

A. Starting of the Circuit

If some energy storage components are initialy energized, the starting procedure is easier. The initial voltage of the energy capacitor is 54V and the DC bus voltage is 108V. With the starting procedure described in the previous chapter, V_{load} increase, shown in Fig 55 (c). As soon as V_{load} reaches 135V, the starting process stops, and the two PI controllers kick in, shown by the two phase values ϕ_{10} and ϕ_{20} changing from constant values to varying values at time=9ms. Also at the same time, the energy storage is also connected back to the system, shown in the gating signal SC14. Fig 55 and Fig 56 show the simulation for this case.
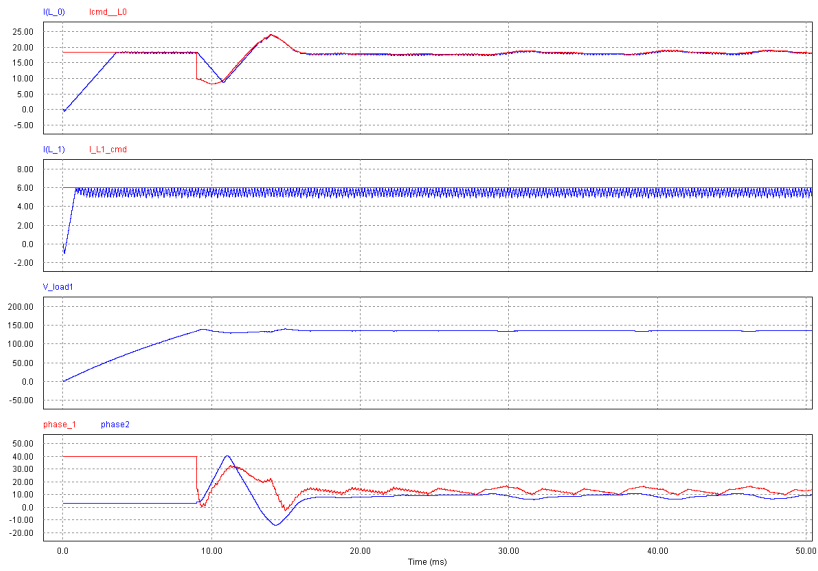
Fig. 55. Starting with some component energized (a)I_{L0} and I_{L0-cmd} [A], (b)I_{L1} and I_{L1-cmd} [A], (c) V_{load} [V], (d) ϕ_{10} and ϕ_{20} [degree]
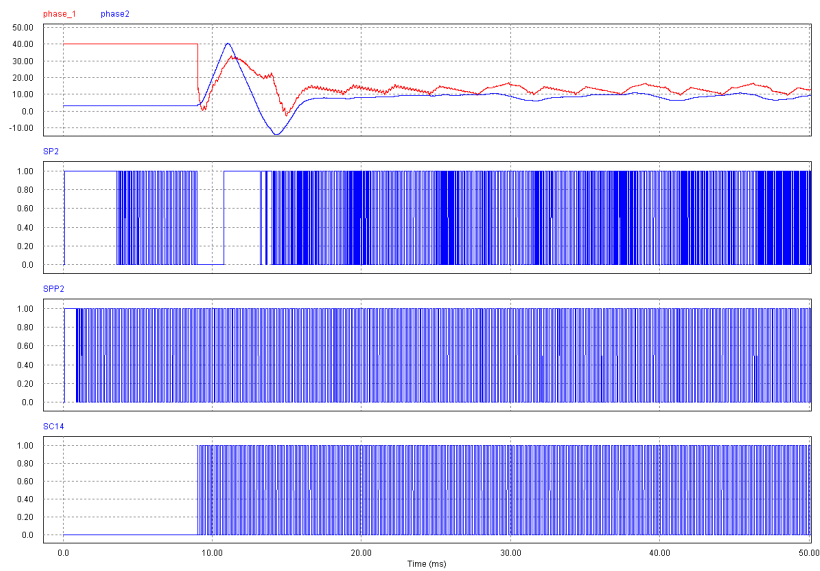

Fig. 56. Starting with some component energized (a) ϕ_{10} and ϕ_{20} [degree] , (b)SP_2, (c) SPP_2, (d)SC_{14}

Another case for starting this circuit is that all components are relaxed. The simulation results are shown in Fig 57 and Fig 58. In addition to charging the output filter capacitor, the circuit has to charge the DC capacitors, the energy storage capacitor. In the starting procedure expressed in Fig.47, the DC bus capacitor is first charged to 108V with $control_{SS}= control_{SL}= control_{SC}=0$ and then energy storage capacitor is charged to 54V with $control_{SS}=1$, $control_{SL}=0$, $control_{SC}=1$. Then the output filter capacitor is being charged to 135V with $control_{SS}=1$, $control_{SL}=1$ and $control_{SC}=0$. After that, the system exits the starting procedure and enters the normal operation.
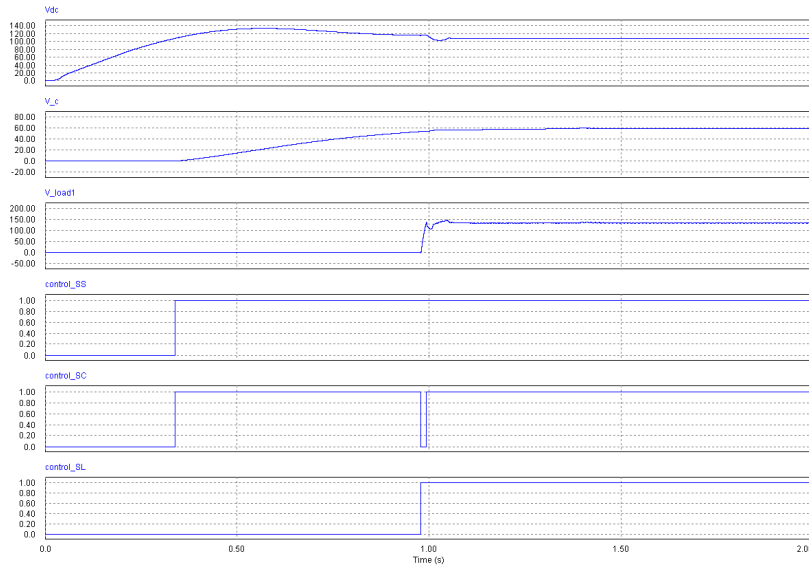

Fig. 57. Starting with all components relaxed (a)V_{DC} [V], (b) V_C [V], (c)V_{load} [V], (d)$control_{SS}$, (e)$control_{SC}$, (f)$control_{SL}$
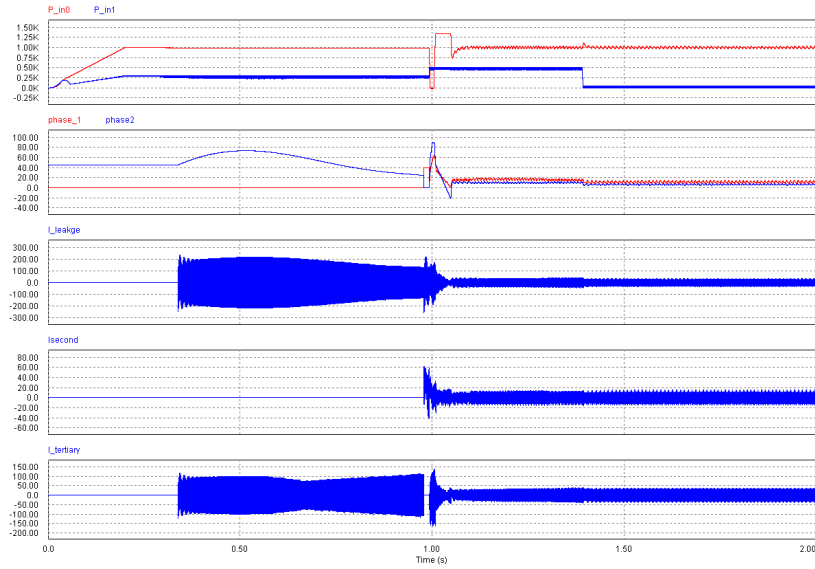
Fig. 58. Starting with all components relaxed (a)P_{in0}, P_{in1} [W], (b)ϕ_{10} and ϕ_{20} [degree], (c)$I_{leakage}$ [A], (d)I_{second} [A], (e)$I_{tertiary}$ [A]

B. Dynamics in Load

In this section, the load is changed at different time by changing the load resistor. In Fig 59 and Fig 60, it can be seen that there are three levels of load, which are 1200W, 1000W and 800W. The controllers control the proposed circuit such that the output voltage, V_{load}, is regulated and the input power from the renewable energy sources, P_{in0} and P_{in1}, remain constant regardless of the change of the load. The difference of the input power, sum of P_{in0} and P_{in1}, and load power, P_{load} is absorbed by the energy storage capacitor. The voltage of energy storage capacitor shows that there are some power going into and out of the energy storage capacitor. Also, from the Fig. 60 (c) the current in the leakage inductor of the transformer is symmetric due to the proper phase-shifting techniques.
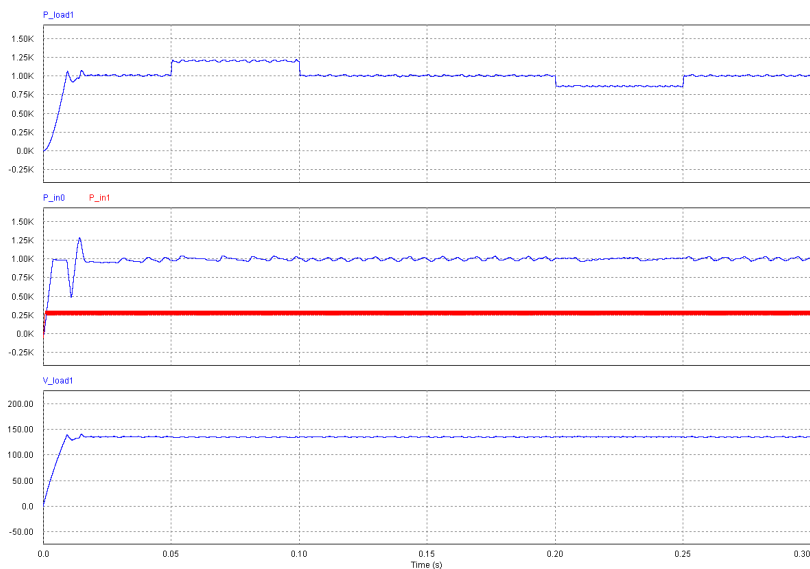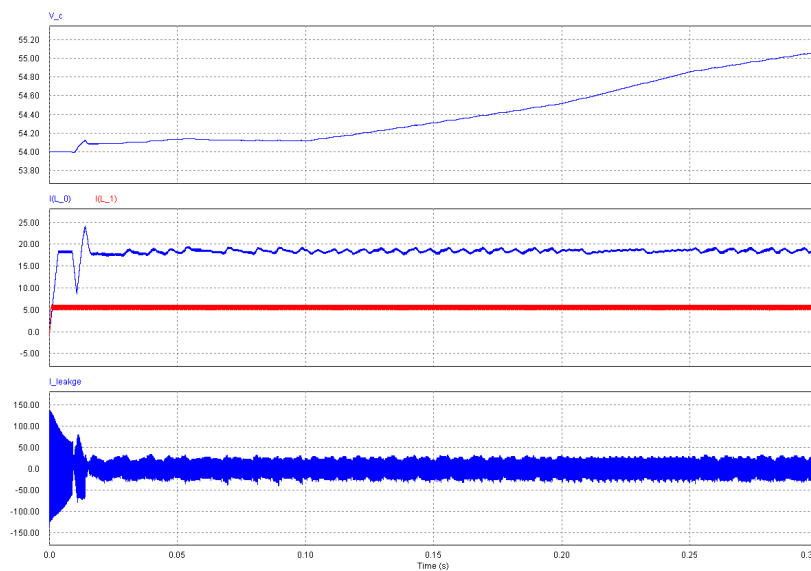
Fig. 59. Simulation of dynamic load (a) P_{load} [W], (b) P_{in0} and P_{in1} [W], (c) V_{load} [V]

33

Fig. 60. Simulation of dynamic load (a) V_C [V], (b) I_{L0} and I_{L1} [A], (c) $I_{leakage}$ [A]

C.   Large Dynamics in Load

Instead of small change in the load, in the following simulations, the load changes tremendously. The load changes from normal load to two times of the load, changes from normal load 1kW to 100W, change from normal load to 0W. The above cases may be encountered in the stand-alone application, where short time over-ride or short time no load are possible.

In Fig 61 and Fig 62, the load is increased from 1kW to 2kW at t=0.05 sec. Before t=0.15, the regulation of V_{load} and P_{in0} are quite good. Because the load power increase to 2kW while the total input power is about 1.5kW, the deficit 500W is supplied by the energy storage capacitor. Therefore, the voltage V_C decreases very fast. The function of control works fine until V_C is too small. When V_C is 0V at t=0.18 sec, P_{in0} tries to supply whole power required by load.
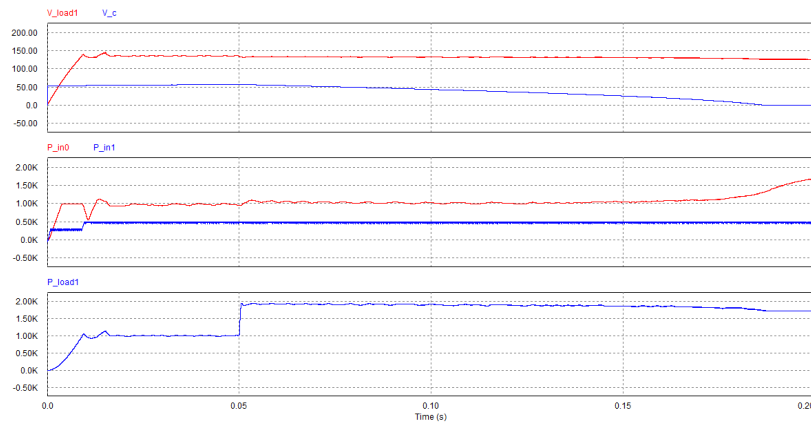

Fig. 61. Large increase in load power (a)V_{load} and V_C [V], (b)P_{in0} and P_{in1} [W], (c)P_{load} [W]
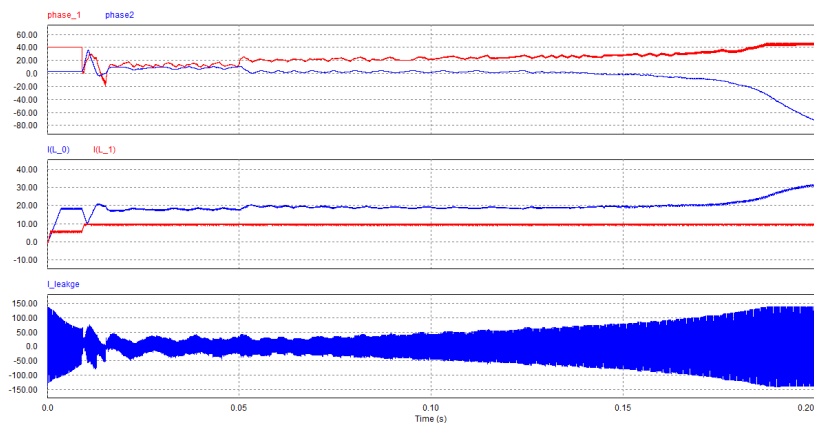
Fig. 62. Large increase in load power (a)ϕ_{10} and ϕ_{20} [degree], (b)I_{L0} and I_{L1} [A], (c)$I_{leakage}$ [A]
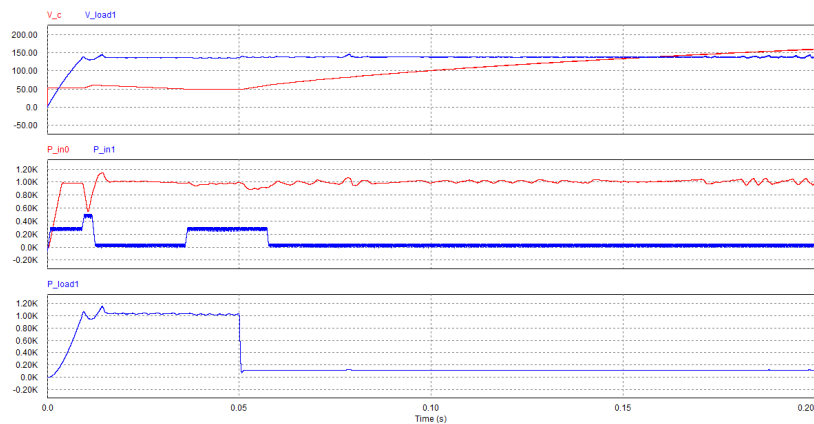

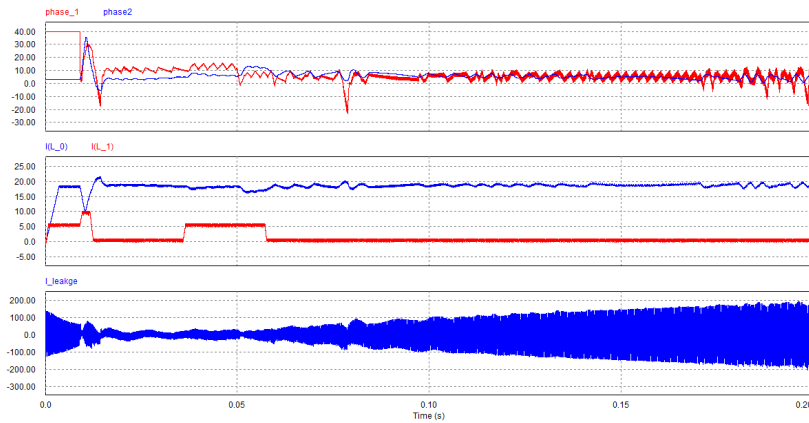Fig. 63. Large decrease in load power (a)V_{load} and V_C [V], (b)P_{in0} and P_{in1} [W], (c)P_{load} [W]

Fig. 64. Large decrease in load power (a)ϕ_{10} and ϕ_{20} [degree], (b)I_{L0} and I_{L1} [A], (c)$I_{leakage}$ [A]

In Fig 63 and Fig 64, the load is decreased from 1kW to 100W at t=0.05 sec. Before t=0.15, the regulation of V_{load} and P_{in0} are quite good. Because the load power decrease to 100W while the total input power is about 1.5kW, the extra 1400W is absorbed by the energy storage capacitor. Therefore, the voltage V_C increases very fast. The function of control works fine even V_C is way above the limit. But this is not desirable. Extra large voltage can destroy the energy capacitor. Therefore there exists limited time of operation for very low small load power.

Even the load power is reduced to 0W, the circuit works fine for short period of time. From Fig 65 and Fig 66, the load power is reduced to 0W at 0.05sec. The voltage V_C increases very fast while V_{load} and P_{in0} are kept at constant.
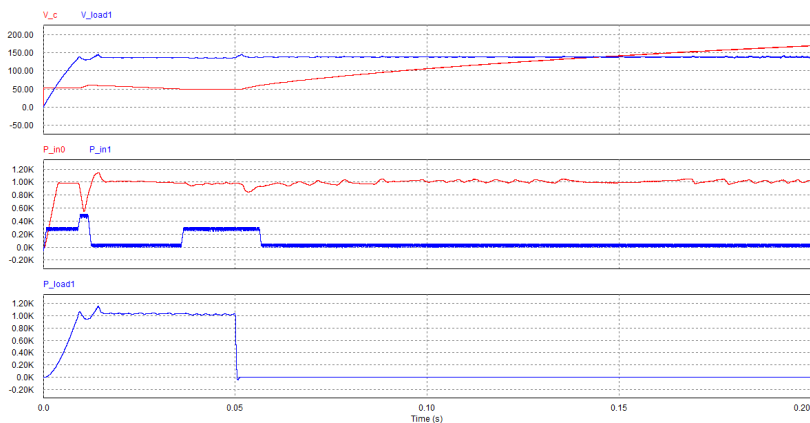
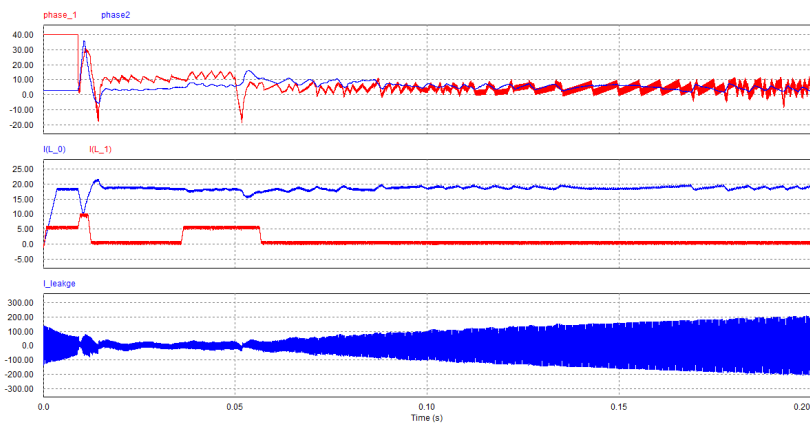Fig. 65. Large decrease to no load (a)V_{load} and V_C [V], (b)P_{in0} and P_{in1} [W], (c)P_{load} [W]

Fig. 66. Large decrease to no load (a)ϕ_{10} and ϕ_{20} [degree], (b)I_{L0} and I_{L1} [A], (c)$I_{leakage}$ [A]

D.   Control of Load Voltage

With controller scheduling, the system can be operated at different operating points. The simulation shown in Fig 67 and Fig 68 shows that the load voltage can be control to be different values with quite good dynamic performance. These values of output voltage are 155V, 135V and 115V. Because the output resistance is constant, the output power is related to the output voltage. The regulation of P_{in0} and P_{in1} is quite good except for some overshoot and some oscillation in P_{in0}. The variation of V_C shows the energy absorbed or released by the energy storage capacitor. Again, the current in the leakage inductor of the transformer is symmetric, ensuring the proper operation of the circuit.
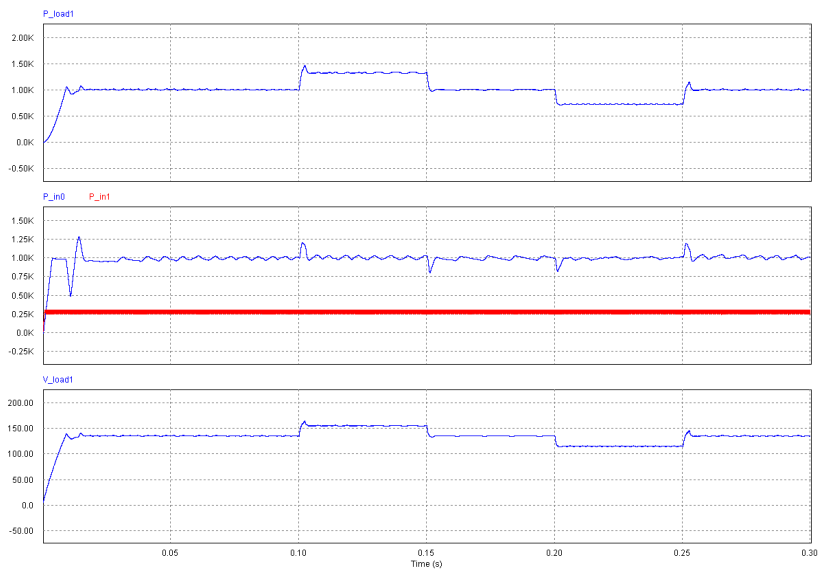
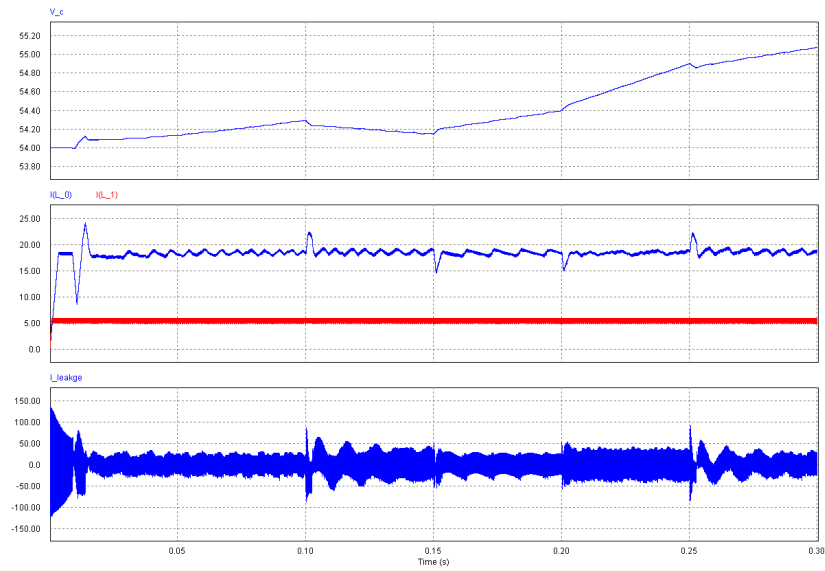Fig. 67. Output voltage control (a)P_{load} [W], (b)P_{in0} and P_{in1} [W], (c) V_{load} [V]

Fig. 68. Output voltage control (a)V_C [V],(b)I_{L0} and I_{L1} [A], (c)$I_{leakage}$ [A]

E.   Dynamics in Source

For renewable energy sources, the output power from these sources depends on several factors, such as the wind speed, solar radiation, ambient temperature. The proposed circuit shows the capability to make the output power constant under the variation of input power of the input energy source. The difference of power is supplied or absorbed by the energy storage capacitor. In Fig 69, the input power increases from 1 kW to 1.5 kW while the load voltage and load power remain constant. The extra power goes into the energy storage capacitor, resulting the increasing of V_C. In Fig 70, the input power decreases for 1 kW to 400 W while the load voltage and load power also remain constant. The deficit power is supplied by the energy storage capacitor. Therefore, the voltage of the capacitor V_C is decreasing.
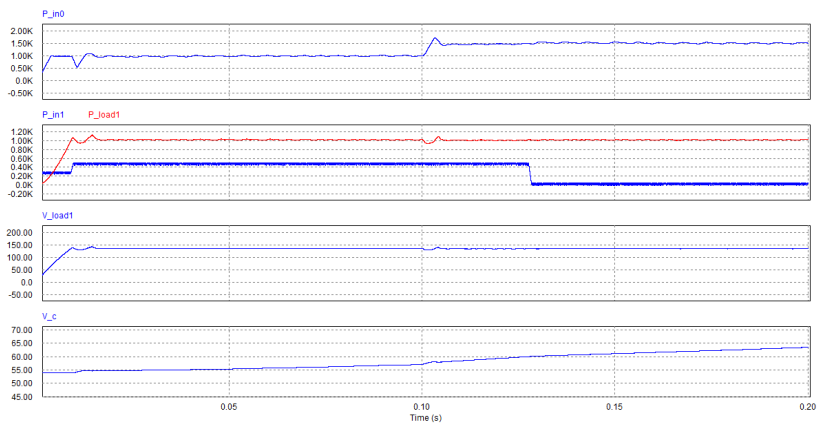
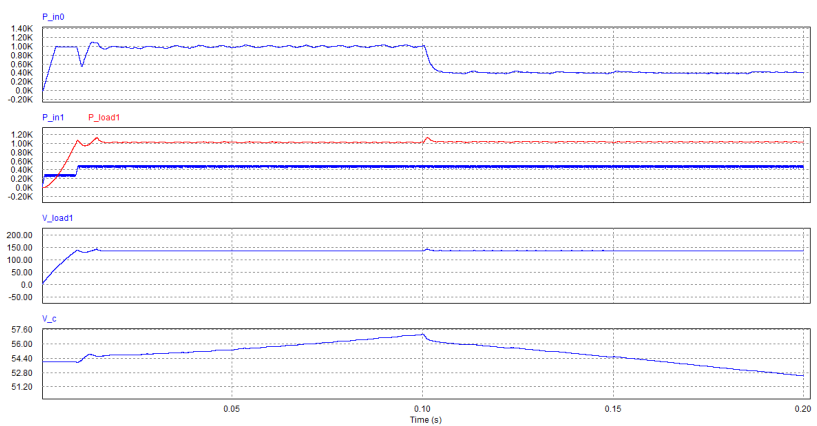Fig. 69. P_{in0} increases (a)P_{in0} [W], (b)P_{load} and P_{in1} [W], (c)V_{load} [V], (d)V_C [V]

Fig. 70. P_{in0} decreases (a)P_{in0} [W], (b)P_{load} and P_{in1} [W], (c)V_{load} [V], (d)V_C [V]

F.   Integration of Current Sources

In this simulation shown in Fig 71, the auxiliary energy source is a current source. The power from the current source P_{in1} is controlled at different values: 300W, 150W and 350W. In this simulation, the load is changed at 0.075 second to 1.25kW and changed back to 1kW at t=0.15 second. During the change of load, the P_{in0} and V_{load} are regulated at 1kW and 135V, respectively. This simulation shows that with the integration of current source type energy source, the control of the circuit still works, whose intend is to regulated load voltage V_{load} and primary input power P_{in0}.
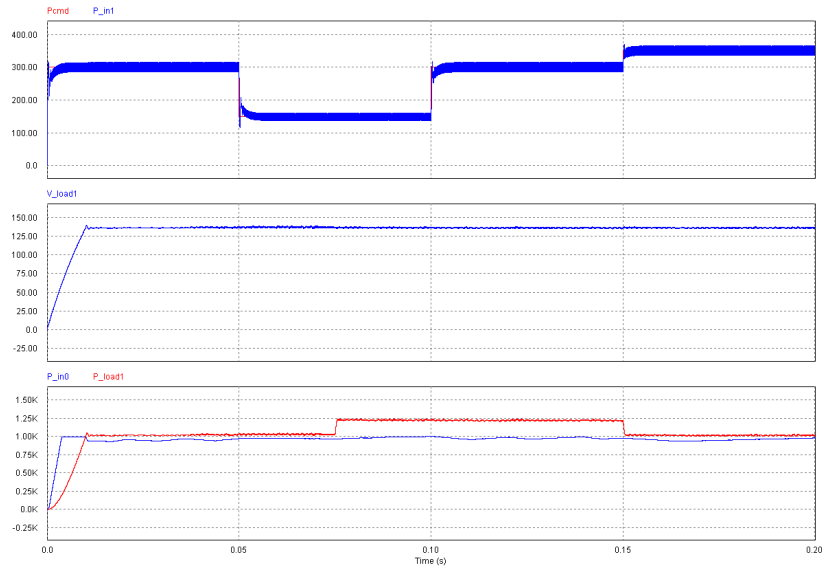
Fig. 71. Different input power from current source (a)P_{in1} and $P_{in1-cmd}$ [W], (b)V_{load} [V], (c)P_{load} and P_{in0} [W]

G.   Power Management

One of the roles of the central controller is to control the input powerP_{in1} from the auxiliary energy source so that the voltage of energy storage capacitor V_C remains within a certain range.   In this simulation in Fig 72, the capacitance of the energy

storage is reduced ten times so that it is easier to notice the voltage change of the energy storage capacitor. When V_C is below 45V, P_{in1} is changed to 500W. When V_C reaches 60V, P_{in1} is reduced so that V_C won't increase above the limit. At the same time, the load power is changing at three levels, but the control requirements are still met, which is to keep V_{load} and P_{in0} at constant.

Fig. 72. Control of P_{in1} (a)$Pload$ [W], (b)P_{in0} and P_{in1} [W], (c)V_{load} [V], (d)V_C [V]

CHAPTER VI

CONCLUSION AND FUTURE WORK
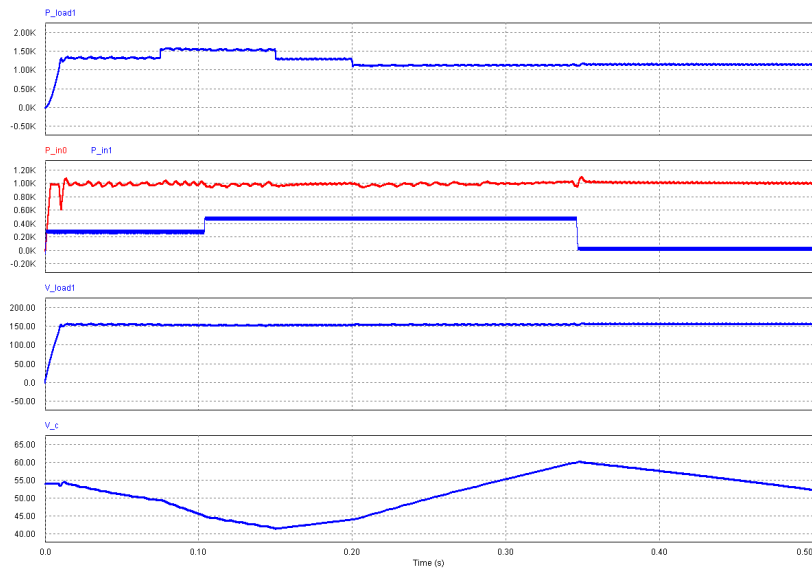
A. Conclusion

In recent years, numerous investment and research have been put in renewable energy. Because of inherent intermittent characteristics and slow response of renewable energy, energy storage has to be used in the system to provide the energy when the energy from these renewable energy sources is low and supply when the energy from these energy sources is high. In order to reduce the requirement of energy storage, different kinds of renewable energy have to be integrated.

To integrate different renewable energy sources and energy storage devices, a new multi-port DC-DC power converter is proposed because of the better performance, lower cost, higher efficiency and system-level control.

The proposed circuit can integrate different renewable energy sources of different voltage levels efficiently. Also the transformer in the circuit provides electrical isolation between the source and the load. There are several desirable features of the proposed circuit. This circuit can integrate voltage source type and current source type of renewable energy sources effectively without any clamping circuits. Also under wide range of different operating points, including normal load, large load, small load, even no load, the system can remain stable and controlled. Furthermore, under the fluctuation of power from the renewable energy sources, the load voltage can be remained at constant.

This work first reviewed the previous work on "Dual Active Bridge" and "Triple Active Bridge" to get some insight of the proposed circuit. In chapter four, the description of fundamental operating principle was made. Design and Modeling were

made and based on the obtained transfer functions, the controllers were designed accordingly. In addition to the low level control, central controller is used to deal with various issues, including starting the circuit, maintaining the "state-of-charge" of the energy storage capacitor and selecting different controller for different operating points. Also the stability and the robustness of the system were studied.

After simulations for different scenarios encountered in real application and some dynamic stability test, it is shown that the proposed circuit is able to integrate renewable energy sources and energy storage economically and efficiently. Therefore the proposed circuit will be an effective solution to the problem due to the intermittent nature and slow response of the renewable energy.

B. Future Work

Because of the powerful capability of the proposed circuit, several applications and extensions can be made. First, at the input side of the circuit, where renewable energy sources are connected, some kinds of maximum power tracking techniques can be done with the help of the central controller. By intelligently switching, based on some maximum power tracking algorithm, the maximum power tracking can be made for wind turbine and photovoltaic cells.

Another extension is to extend from three-port circuits to four-port or even five-port circuits. Different ports are connected to different kinds of renewable energy sources, whose voltage levels are different. Because there will be many phase differences between these multiple ports, the interaction between these ports will be complicated. How to deal with the interaction between ports and how to control the power flow are challenging. With the technique of shorting of one port, used in the starting procedure in this work, the interaction between different ports may be

reduced and can be controlled easily.

Another extension is to replace the energy storage capacitor with load. In this topology, there will be two loads. With phase control, the two voltages at two different outputs can be controlled independently, which may be of practical use for multi motor drive application.

Instead of another load, another source can replace the energy storage capacitor in this circuit. By controlling the phases, the power from source A to the load and the power from source B to the load can be controlled independently as well. This application is useful for load sharing application.

Therefore, the proposed circuit is suitable not only for the renewable energy application, but also for the application of multi-source and multi-load application, with little modification.

REFERENCES

[1] REN21 Steering Committee, (2007, June), "REN21 Renewables 2007 Global Status Report," Available: http:www.ren21.netdefault.asp

[2] U.S. Department of Energy, (2008, September), "Renewable Energy Data Book," Available: http:www1.eere.energy.govbapbadata_books.html

[3] F. A. Farret and M. G. Simes, *Integration of Alternative Sources of Energy*, New York: Wiley, 2006.

[4] P. Nema; R. K. Nema; S. Rangnekar, "A current and future state of art development of hybrid energy system using wind and PV-solar: A review," *Renewable and Sustainable Energy Reviews*, vol.4, no.2, pp. 157-175, 2000.

[5] M. Ehsani; Y. Gao; S. E. Gay, *Modern Electric, Hybrid Electric, and Fuel Cell Vehicles: Fundamentals, Theory, and Design*, Boca Raton, Florida: CRC, 2004.

[6] S. Jain; V. Agarwal, "An integrated hybrid power supply for distributed generation applications fed by nonconventional energy sources," *IEEE Trans. Energy Conversion*, vol.23, no.2, pp.622-631, June 2008.

[7] A. D. Napoli; F. Crescimbini; S. Rodo; L. Solero, "Multiple input dc-dc power converter for fuel-cell powered hybrid vehicles," *Proc. IEEE Power Electronics Specialist Conf.*, vol.4, pp.1685-1690, 2002.

[8] L. Solero; F. Caricchi; F. Crescimbini, O. Honorati; F. Mezzetti, "Performance of a 10kW power electronic interface for combined windPV isolated generating systems," *Proc. IEEE Power Electronics Specialist Conf.*, pp.1027-1032, June 1996.

[9] Y.M. Chen; Y.C. Liu; F.Y. Wu "Multi-input dc/dc converter based on the multi-winding transformer for renewable energy application," *IEEE Trans. Ind. Appl.*, pp.1096-1104, 2002.

[10] R. D. Doncker; D. M. Divan; M. H. Kheraluwala, "A three-phase soft-switched high-power-density DC/DC converter for high-power applications," *Industry Applications, IEEE Transactions on*, vol.27, no.1, pp.63-73, Jan/Feb 1991.

[11] F. Z. Peng; H. Li; G-J Su; J. S. Lawler, "A new ZVS bidirectional DC-DC converter for fuel cell and battery application," *Industry Applications, IEEE Transactions on*, vol.27, no.1, pp.63-73, Jan/Feb 1991.

[12] M. Michon; J. L. Duarte; M. Hendrix, "A three-port bi-directional converter for hybrid fuel cell systems," *IEEE Power Electronics Specialists Conf.*, pp.4736-4742, June 2004.

[13] D. Liu; H. Li, "A ZVS bi-directional DC-DC converter for multiple energy storage elements," *IEEE Trans. Power Electronics*, pp.1513-1517, Sept. 2006.

[14] R. L. Steigerwald; M. H. Kheraluwala, "High-frequency resonant transistor DC-DC converters," *Industrial Electronics, IEEE Transactions on*, vol.IE-31, no.2, pp.181-191, May 1984.

[15] O. D. Patterson; D. M. Divan, "Pseudo-resonant full bridge DC/DC converter," *Power Electronics, IEEE Transactions on*, vol.6, no.4, pp.671-678, Oct 1991.

[16] K-H Liu, R. Oruganti, F-C Lee, "Resonant switches-topologies and characteristics ," presented at the 1998 IEEE Power Electron. Special Conf., Toulouse, France.

[17] M. Ehsani, R. L. Kustom, *Converter Circuit for Superconductive Magnetic Energy Storage*, College Station, Texas: Texas A&M Press, 1988.

[18] S. Singer, "Gyrators in power processing circuit," *Ind. Electron, IEEE Transactions on*, vol.IE-34, no.3, pp.313-318, Aug. 1987.

[19] H. Tao; A. Kotsopoulos; J. L. Duarte; M.A.M. Hendrix, "Design of a soft-switched three-port converter with DSP control for power flow management in hybrid fuel cell systems," presented at the 2005 European Conf. on Power Electronics and Applications, Dresden, Germany.

[20] D. Xu; C. Zhao; H. Fan, "A PWM plus phase-shift control bidirectional DC-DC converter," *Power Electronics, IEEE Transactions on* , vol.19, no.3, pp. 666-675, May 2004.

[21] M. Michon; J. L. Duarte; M. Hendrix; M.G. Simoes, "A three-port bi-directional converter for hybrid fuel cell systems," presented at the 2004 Power Electronics Specialists Conf., Aachen, Germany.

[22] M-J He; W-J Cai; B-F Wu, "Design of decentralized IMC-PID controller based on dRI analysis," *AlChE Journal*, vol.52, no.11, pp. 3852-2863, Oct 2006.

[23] N. Mohan; T. M. Undeland; W. P. Robbins;, *Power Electronics: Converter, Applications, and Design*, Boston: Wiley, 2002.

APPENDIX A

DERIVATION OF POWER EQUATION OF DAB AND TAB

In the DAB, the power equation can be found by averaging the current flowing in the source side and the load side, because the voltage on the source side is DC value while the voltage on the load side is almost constant with some ripple. The following will show how to derive the power equation of DAB. There is one thing worth of attention. The power derived here is the averaged power during the switching period, which is a running average.

In the following derivation, V_1 is assumed to be larger than V_2 and the gating signals of the load side lags that of the source side by ϕ. Fig 73 shows the waveform of the circuit.

In order to find the average of input current, the time X needs to be find where the current is crossing zero from negative to positive. The slope of the current when the switch SS1 and SS4 are on is

$$m_1 = \frac{V_1 + V_2}{L} \tag{A.1}$$

and the slope of the current when the switch SS2 and SS3 are on is

$$m_2 = \frac{V_1 - V_2}{L} \tag{A.2}$$

The amplitude of the cuurent i_x can be found as

$$\Delta i_x = \frac{1}{2}[m_1 \cdot \phi + m_2 \cdot (\pi - \phi)] \cdot \frac{T}{2\pi} \tag{A.3}$$
$$= \frac{T}{4\pi L}(2V_2\phi + V_1\pi - V_2\pi)$$

We have to solve the following equation to get time X:

$$-\Delta i_x + m_1 \cdot X = 0 \tag{A.4}$$

$$X = \frac{2V_2\phi + (V_1 - V_2)\pi}{2(V_1 + V_2)} \frac{T}{2\pi}$$

The length of y_1 and y_2 can be found as:

$$y_1 = (\phi - X) \cdot m_1 \cdot \frac{T}{2\pi} \tag{A.5}$$

$$y_2 = (\pi - \phi) \cdot m_1 \cdot \frac{T}{2\pi} + y_1 \tag{A.6}$$

The area of area 1, 2, 3 can be found as:

$$Area_1 = \frac{1}{2}(\phi - X) \cdot y_1 \cdot (\frac{T}{2\pi})^2 \tag{A.7}$$

$$Area_2 = \frac{1}{2}(\pi - \phi) \cdot (y_1 + y_2) \cdot (\frac{T}{2\pi})^2 \tag{A.8}$$

$$Area_3 = \frac{1}{2}X \cdot y_2 \cdot (\frac{T}{2\pi})^2 \tag{A.9}$$

Total area will be:

$$Area_{total} = Area_1 + Area_2 + Area_3 \tag{A.10}$$

$$= \frac{1}{2}\big(\phi y_1 - Xy_1 + y_1\pi + y_2\pi - \phi y_1 - \phi y_2 - Xy_2\big) \cdot (\frac{T}{2\pi})^2$$

$$= \frac{1}{2}\big((\pi - X)y_1 + (\pi - \phi - X)y_2\big) \cdot (\frac{T}{2\pi})^2$$

Substitude y_1, y_2 and X, we will get the total area as:

$$Area_{total} = \frac{V_2}{L}\pi\phi(1 - \frac{\phi}{\pi})(\frac{T}{2\pi})^2 \tag{A.11}$$

Therefore, the average current will be

$$< I_x > = \frac{Area_{total}}{\frac{T}{2}} \tag{A.12}$$
$$= \frac{V_2}{\omega L}(1 - \frac{\phi}{\pi})$$

The power going out of the source port will be

$$< P >= V_1 \cdot < I_x >= \frac{V_1 V_2}{\omega L}(1 - \frac{\phi}{\pi}) \tag{A.13}$$

For the case of triple active bridge(TAB), the power equation can be derived similarly with the use of superposition theory.

For the proposed circuit, the power equation is the same as the ordinary TAB. The only difference will be the V_1 will be replaced by $V_{DC}/2$.
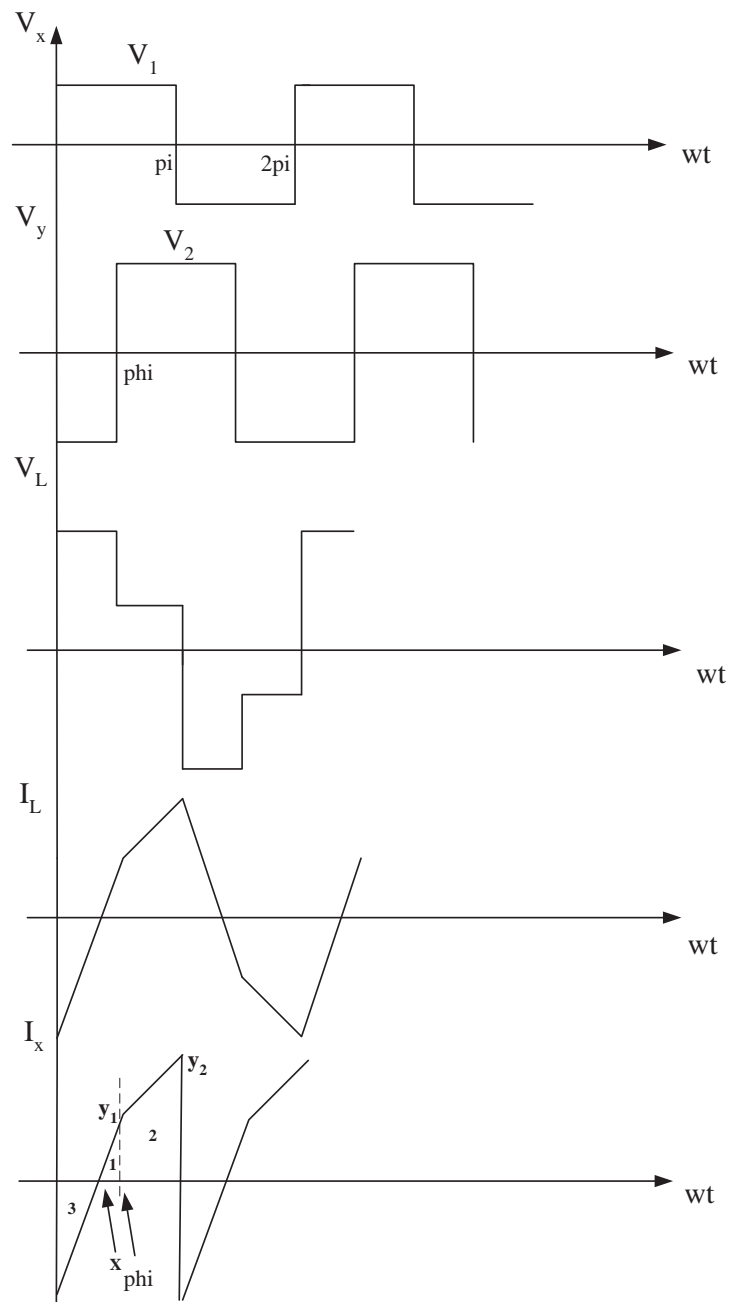
Fig. 73. Waveform of dual active bridge

VITA

Hung-ming Chou received his Bachelor of Electrical and Control Engineering from National Chiao Tung University, Taiwan in 2004. After two years of military service, he entered the graduate program in the Department of Electrical and Computer Engineering at Texas A&M University and graduated in 2009. His research interests include FACTS, HVDC, doubly-fed wind turbine, renewable energy integration, variable speed drive.

He can be reached at homing93@gmail or through his advisor Dr. M. Ehsani, Power Electronics Laboratory, Department of Electrican and Computer Engineering, Texas A&M University, College Station, Texas 77843-3128.